UNIVERSIDAD DE ANTIOQUIA

FORMATION OF HOMOGENEOUS NANOTUBES ON TITANIUM C.P. BY ANODIZING TECHNIQUE FOR BIOMEDICAL APPLICATIONS

Robinson Aguirre Ocampo

Universidad de Antioquia

Facultad de Ingeniería, Departamento de Ingeniería de Materiales

Medellín, Colombia

2020

CC BY NC ND

Formation of homogeneous nanotubes on titanium c.p. by anodizing technique for biomedical applications.

Robinson Aguirre Ocampo

Tesis de doctorado para optar al título de:
Doctor en Ingeniería de Materiales

Asesor:
Félix Echeverría Echeverría Ph.D.

Línea de Investigación:
Biomateriales
Grupo de Investigación:
Centro de Investigación, Innovación y Desarrollo de Materiales – CIDEMAT

Universidad de Antioquia
Facultad de Ingeniería, Departamento de Ingeniería de Materiales
Medellín, Colombia
2020

Centro de Investigación, Innovación y Desarrollo de Materiales CIDEMAT

Sede de Investigación Universitaria – SIU

Universidad de Antioquia

Cr 53 # 61 – 30

Medellín, Colombia

Derechos de autor de R. Aguirre Ocampo 2019. Todos los derechos reservados

Abstract

The nanostructures and within them, the titanium dioxide nanostructures have had an investigative awakening because they have a large surface area, allowing ion exchange processes and possible photocatalytic activity. One of the structures that have attracted more the attention of researchers is nanotubular because it presents unique geometric properties that allow it to be applied as a catalyst in reactions that employ radiation for removing water contaminants, like the sensor of chemical compounds present in the air, and in medicine as a biomedical device. Although there are several methods of producing titanium dioxide nanotubes, one that has gained strength because of its easy implementation and simplicity is the anodizing process. Titanium is a material used in many engineering fields due to its high mechanical and corrosion resistance properties, but to further enhance the above features, anodizing is presented as a viable option for surface improvement, because it can produce nanotubes with higher organization and orientation that with other techniques could not be obtained. This project aim was obtained homogeneous TiO_2 nanotubes on c.p Ti using aqueous electrolytes. For that purpose, an anodizing protocol was established to get geometrically homogeneous nanotubes by modifying different parameters of the anodizing process. Then the best coatings were selected and were characterized by SEM, TEM, AFM, XRD, and micro-Raman, correlating the obtained with the nano-tubular coating characteristics, after that, it was analyzed the effect of the above on biocompatibility and antibacterial capacity of coatings by bioassays.

Acknowledgments

I would like to thanks to many people who were there in one way or another, including my family, who allowed me to grow personally every day, supporting me in each of the difficulties presented along this path. On the other hand, I also wish I would like to thank my study center at “Universidad of Antioquia,” which through many of its excellent teachers were able to contribute to my training process, through their guidance, advice, knowledge, and experiences.

I would like to particularly thank the CIDEMAT research group, which welcomed me so pleasantly, offering me a wide range of knowledge that served as input for this research project; I especially thank the professor Ph.D. Félix Echeverría E., for their dedication in each of their advice that allowed me to carry out this research. Furthermore, I would like mainly thanks to professor Ph.D. Sara Robledo in the PECET research group.

I would like to thanks to my dear friend and laboratory partner Ph.D. Mónica Echeverry Rendón for her advice, tutorial, and accompaniment, since the beginning of my process as an undergraduate student until finish the current process.

I am pleased to acknowledge the financial assistance of the “Departamento Administrativo de Ciencia, Tecnología e Innovación – COLCIENCIAS” through the “Fondo Francisco José de Caldas” with the contract 124-2017 and “Convocatoria Doctorados Nacionales 2015-Convocatoria No 727”.

I am pleased to acknowledge the financial assistance for the internship to “Convocatoria 2018-2 del Fondo Sapiencia Posgrados Internacionales”, “Programa

de becas de la Plataforma de movilidad estudiantil y académica de la Alianza del Pacífico 11ª edición México" through "becas de excelencia otorgadas por el gobierno de México, a través de la Agencia Mexicana de Cooperación Internacional para el Desarrollo" and "COLCIENCIAS".

Last but not least, I would like to acknowledge to the professor Ph.D. Facundo Ruiz and the Ph.D. Idania De Alba-Montero for their support, advice and suggestions during the internship at "Laboratorios de Materiales de la Facultad de Ciencias en la Universidad Autónoma de San Luis Potosí."

Table of Contents

List of Figures

List of Tables

List of Acronyms & Abbreviations

Ti	Titanium
TiO_2	Titanium Dioxide
SEM	Scanning Electron Microscope
FESEM	Field Emission Scanning Electron Microscope
TEM	Transmission Electron Microscope
HRTEM	High Resolution Transmission Electron Microscope
AFM	Atomic Force Microscope
SAED	Selected Area Electron Diffraction
XRD	X-ray diffraction
GPA	Geometric Phase Analysis
nm	Nanometer
V	Volt
m^2	Square meter
mJ	Millijoule
Ra	Roughness Average
Rsm	Mean width of the profile elements
Rz	Maximum height of profile
Rq	Root mean squared
ºC	Celsius scale
CFU	Colony Forming Unit
mL	Milliliter
mm^2	Square millimeter
CMC	Carboxymethyl cellulose
MRSA	Methicillin Resistant *Staphylococcus Aureus*
N/m	Newtons per meter
Hz	Hertz
Ir	Iridium

Research Output

Published papers

Formation of nanotubular TiO2 structures with varied surface characteristics for biomaterial applications.
Robinson Aguirre Ocampo, Mónica Echeverry-Rendón, David Quintero, Juan Guillermo Castaño, M.C. Harmsen, Sara Robledo, Félix Echeverría Echeverría. Journal of Biomedical Materials Research - Part A. 106 (2018) 1341-1354.
https://doi.org/10.1002/jbm.a.36331

Effects of fluoride source on the characteristics of titanium dioxide nanotubes.
Robinson Aguirre Ocampo, Félix Echeverría Echeverría.
Applied Surface Science 445 (2018) 308–319.
https://doi.org/10.1016/j.apsusc.2018.03.139

Effect of the anodization parameters on TiO_2 nanotubes characteristics produced in aqueous electrolytes with CMC.
Robinson Aguirre Ocampo, Félix Echeverría Echeverría.
Applied Surface Science 469 (2019) 994–1006.
https://doi.org/10.1016/j.apsusc.2018.11.097

Effect of surface characteristics on the antibacterial properties of TiO2 nanotubes produced in aqueous electrolytes with carboxymethyl cellulose.
Robinson Aguirre Ocampo, Mónica Echeverry-Rendón, I. DeAlba-Montero, Sara Robledo, Facundo Ruiz, Félix Echeverría Echeverría.
Journal of Biomedical Materials Research Part A. (2020) 1– 18.
https://doi.org/10.1002/jbm.a.37010

TiO2 nanotubes produced on curved titanium surfaces using aqueous electrolytes with carboxymethyl cellulose.
Robinson Aguirre Ocampo, Félix Echeverría Echeverría.
Physica E: Low-dimensional Systems and Nanostructures, vol.125, January 2021
https://doi.org/10.1016/j.physe.2020.114391

Published paper as co-author in related subjects

Modification of titanium alloys surface properties by plasma electrolytic oxidation (PEO) and influence on biological response.
Mónica Echeverry-Rendón, Oscar Galvis, Robinson Aguirre Ocampo, Sara Robledo, Juan Guillermo Castaño, Félix Echeverría Echeverría.
Journal of Materials Science: Materials in Medicine (2017) 28:169.
https://doi.org/10.1007/s10856-017-5972-x

Submitted papers

TiO_2 nanotubular structures for biomedical applications.
Robinson Aguirre Ocampo, Félix Echeverría Echeverría.
Journal of Engineering Science and Technology Review

Congress

Robinson Aguirre Ocampo, Mónica Echeverry-Rendón, Sara Robledo, Félix Echeverría Echeverría. The 46th International Conference on Metallurgical Coatings and Thin Films (ICMCTF 2019). TiO_2 nanotubes produced in aqueous electrolytes with CMC for biomaterials application. San Diego-USA.

Introduction

The titanium is a material with low density, high corrosion resistance, high mechanical strength, and bio-compatibility; this allows its use in aerospace, automotive and biomedical applications [1]–[3]. Titanium has the capacity to naturally form a passive layer of titanium oxide (TiO_2); this layer provides it with corrosion resistance by inhibiting the release of ions and allows its use in biomedical applications [4], [5]. However, to enhance its possible application as bio-implant, it is necessary to modify the characteristics of this passive layer in both morphology and thickness, transforming, thus, the surface properties of the material [6], [7]. Among the possible morphologies that can be obtained with TiO_2, the nanotube morphology has had a great surge in the research field because this geometry has a big specific surface that allows their applications in catalysis, solar cells, and biomedical devices, etc. [8], [9]. The formation of titanium oxide nanotubes has been carried out mainly through techniques such as sol-gel, hydrothermal processes, and anodizing [10].

Anodizing as surface modification technique has gained attention in the scientific community because of its easy use, versatility, and low cost compared to other types of surface treatments [11]–[14]. Besides the above features, the anodizing process allows modifying the titanium, whereby the nanotube TiO_2 layer grows tidily with regular diameter and normal to the surface, in contrast with the other techniques mentioned above in which nanotubes are obtained in free form and with a lower degree of order [15], [16]. Furthermore, during the anodizing process, it is also possible to vary the nanotube morphology through the control of the process

parameters. Nanotubes produced in aqueous electrolytes have size uniformity problems, in contrast with the nanotubes produced in organic electrolytes, especially the ethylene glycol based, which have a higher uniformity [17]–[20]. However, this organic electrolyte has a higher cost, higher toxicity, lower yield and needs a more complicated protocol for his final disposition compared with aqueous electrolytes; this last part could be a problem when the process is carried out at industrial scale. Therefore, the titanium surface control during anodizing process by using affordable electrolytes is one of the main requirements for nanotubes production at industrial scale.

The first reports of nanotubes formation are attributed to Zwilling et al [21] in 1999, but over the years, those first nanotubes, which had a low degree of organization and less than a micron of length, have evolved into highly ordered nanotubes hundreds of microns thick [18], [22]. The first electrolytes used to produce nanotubes were aqueous solutions with HF, those electrolytes generated disorganized and short nanotubes; however, the use of organic electrolytes allowed highly ordered nanotubes and lengths higher than 200 μm [18], [22], [23]. Because of the characteristics that offers the nanotubes produced in organic media, the research work related with them has increased notably [24]–[26]. Although, it is necessary to consider that those electrolytes are more expensive and less environmentally friendly in contrast to the aqueous electrolytes. Thus, this generates a research opportunity to increase the organization of the nanotubes produced in aqueous electrolytes. To achieve the last aim, sodium carboxymethylcellulose (CMC) was used as additive in an aqueous electrolyte. CMC is a cheap, no toxic and

environmental friendly reactive widely used in food, cosmetics, and drugs [27]–[30]. To the best of our knowledge, the reports of use of aqueous electrolytes that contains CMC are few [31], [32]; furthermore, in those research works only one experimental condition was analyzed. In this experimental work, it has been studied various anodization parameters such as electrolyte temperature, fluoride concentration, electrolyte aging, anodizing time, pH and CMC concentration with the aim to increase the organization of nanotubes produced in aqueous electrolytes. To measure the nanotubes organization, a quantitative Fast Fourier Transformation (FFT) analysis was made by using SEM images of the nanotubes surfaces.

On the other hand, implants have been used to replace osseous tissues that were damaged as a consequence of degenerative diseases, accident trauma or injuries among others; allowing to the affected patients to remain active and productive for a lengthier period of time [2]. Depending of the location, the implants often get rejected which causes their subtraction and replacement leading to a high cost for the medical insurances, a higher hospitalization time and patient annoyance [33], [34]. The lack of bone bonding is one of the major causes of implant rejection [35]; this is caused by the deficiency of interaction between the peri-implant bone and the implant. In the recent years, some experimental works have been highlighted the importance of the surface modification of the implants with nanostructures [35]–[39]. The main reason to carry out those kind of surface modifications is mainly increasing the bone cell proliferation, adhesion and differentiation around the implant producing new bone tissue which results in a successful osseointegration [40], [41]. Titanium has been widely used in implantology due to their properties as biocompatibility,

strength and corrosion resistance [24], [42], [43]; however, through their surface modification an increase of those properties can be achieved. Due to the Titanium features, this material could be anodized producing TiO_2 with various morphologies on their surface [1] [2]. One of most promissory structures is the nanotubular, due to their high surface area, that allows titanium an easy interaction with bone cells that finally permits new bone growth [36]. However, bacterial infection is one of the main issues that implantable devices must tackle. In fact, bacterial infections on different implantable devices derive on implants removal from patients [33], [44], [45]. In the first step of the bacteria colonization process, bacteria adhere to the surfaces of biomaterials, afterwards the bacteria proliferate and finally the biofilms appear; as a consequence of biofilm formation, the bacteria become more resistant to treatment with systemic antibiotics [34], [46], [47]. Depending on the biomaterial, the infecting microorganisms can vary, for instance, Staphylococcus aureus and Staphylococcus epidermidis are the most common detected pathogens in implants, as well as the Gram-negative microorganism Pseudomonas aeruginosa [33], [45], [48]. Due to this kind of risks, nanotechnology has been used for improving the implants rate of success [49]. By using surface modification is possible to reduce the bacteria adhesion and proliferation; two important steps before the bacteria biofilm formation [34], [44]. Thus, with the aim to reduce bacteria colonization, titanium surfaces have been modified with acid etch, alumina blast, smooth machined, anodizing, among others. Anodizing has been used to modify the titanium surface due to their low cost, versatility, and easy operability [1]. Anodizing allows to produce nanotubular coatings on titanium; the nanotube structures could improve the surface properties and modify the interaction with external agents (bacteria, cells, fungi etc.) [43], [48],

[50], [51]. Kunrath et al reports that although there are studies about the relationship between the TiO_2 nanotubes surface characteristics and the biological behavior (bacteria /cells), this is not completely clarified [52]. The propose of producing nanotubes with different diameters and various heat treatments was to correlate the nanotube characteristics (morphology, internal diameter, phase composition and surface properties) and the antibacterial properties against both Staphylococcus Aureus and Pseudomonas Aeruginosa strains. To achieve this, in this investigation nanotubular coatings produced at various conditions (as-anodized, heat and UV treated) have been characterized by Raman spectroscopy, XRD (X-ray Diffraction), SEM (Scanning Electron Microscopy), TEM (Transmission Electron Microscopy), Geometric Phase Analysis (GPA), HRTEM (High Resolution Transmission Electron Microscopy), SAED (Selected Area Electron Diffraction) and Atomic Force Microscope (AFM); all combined with antimicrobial activity and bacterial adhesion essays. In the same way, the effect of nanotubes with different diameters, various heat treatments and UV irradiation, looking to correlate the nanotube characteristics (morphology, internal diameter, phase composition and surface properties) with the adhesion, proliferation and mineralization of osteoblast cells.

This research confronted the challenge to increase the uniformity of nanotubes in the anodic coatings produced in aqueous electrolytes by modifying the parameters of the anodizing process (pH, electrolyte composition, electrolyte aging, voltage, current, electrolyte temperature and anodizing time) to further correlate the morphological and physicochemical properties with biological properties in terms of cell adhesion and antibacterial ability.

Hypothesis

¿Is it possible to improve the homogeneity of the nanotubes produced in aqueous solutions for potential biomedical applications?

General Objective

To study the formation of homogeneous nano-tubular structures of titanium dioxide by anodizing of commercially pure titanium in aqueous electrolytes and to evaluate the effect of nanotube diameter, heat treatment and photocatalytic activation on the osseointegration and infection resistance for biomedical applications.

Specific Objectives

To systematically analyze the effect of the different variables involved in the formation of nanotubes of TiO_2, namely: pH, electrolyte composition, electrolyte aging, voltage, current, electrolyte temperature and anodizing time in the characteristics of the formed structures, seeking to establish the anodizing conditions that allows obtaining nano-tubular coatings with a homogeneous geometry.

To study the effect of geometrical characteristics (internal and external diameter and spacing) of the more homogeneous samples obtained, as well as of heat treatment and photo-catalytic activation on wettability and other surface properties e.g. roughness, surface charge and surface energy.

To evaluate the biological properties of uniformly anodized surfaces, using cytotoxicity tests such as MTT and osteoblast interaction in terms of adhesion and proliferation.

To study the antibacterial behavior of uniformly anodized surfaces with and without both heat treatment and photo-catalytic activation, by bacteria adhesion tests.

Materials and Methods

Samples anodization and coatings characterization

Square samples of c.p titanium grade 2 (ASTM F-67), with an area of 2 cm^2 and 1 mm of thickness were mechanically polished with SiC paper up to grade 2500, and finally cleaned in acetone in an ultrasonic bath for 20 minutes.

Then after, the samples were prepared at voltages of 20, 15 and 10 V in 200 mL of an aqueous solution containing sodium carboxymethylcellulose (CMC) and NaF, the electrolyte pH was adjusted using H_3PO_4. The anodic coatings were obtained using a DC power supply (Kepco BHK 500-0.4 MG) and the current data was recorded during 5 hours. The configuration used in the anodization was composed by two electrodes, the titanium sample was the anode and a platinum mesh were the cathode. When the anodization was completed, the samples were extracted from the anodized solution and cleaned with deionized water and dried in cold air. The temperatures used to the heat treatments were 200, 350 and 600 ° C, the ramp used at each temperature will be shown at further sections, after the heat treatment the samples were allowed to slowly cool inside the oven. The UV treatment consisted of irradiaton of the anodic coatings using a high intensity UV lamp with a wavelength of 435 nm for 30 minutes, the distance between the samples and the lamp was 2.5 cm, and the UV dose was 3.44 mJ/cm^2.

The morphology of the coatings was observed by Scanning Electron Microscope (SEM) using a JEOL JSM 6940 LV instrument and a Field Emission Scanning Electron Microscope (FESEM) (TESCAN MIRA3 SEM). The coating thickness

measurements were made by scratching the surface sample and then tilting the sample holder to get the SEM images. The FFT analysis were made using the WSxM 5.0 software [53] and other measurements as internal diameter and coating thickness were made using the public domain software Image J

The Transmission Electron Microscope (TEM) used was a Tecnai G2 F20 S-Twin TMP equipment, with a field emission source, resolution of 0.1 nm at 200 kV, maximum magnification in TEM 1.0 MX and, GATAN camera US 1000XP-P. HRTEM and SAED images were analyzed using the Digital Micrograph software with the Difftools script [54] and CrysTBox [55], [56]. Pdf files (rutile (01-088- 1172), anatase (01-089-4921), and the work of Bowden [57] were used to identify the crystal phases comparing d-spacings.

For X-ray diffraction (XRD) analysis, the instrument used was a PANanalytical EMPYREAN model with Cu Kα radiation and 2θ scan from 5 to 100 degrees. For micro-Raman spectroscopy was employed a Labram High Resolution Jovin Yvon Horiba spectrometer.

The Atomic Force Microscope (AFM) used was an MFP-3D AFM (Asylum Research), and the AFM images were processed with the open-source software Gwydion [58] and the ARgyle light software. For the surface roughness measurements, a Dektak XT profilometer was used. Five measurements were thru along 500 μm in various sample positions. Roughness parameters (Ra, Rsm, Rz, and Rq) were calculated based on this data. Surface potential measurements where made using an Asylum Research MFP-3D AFM (Oxford Instruments) using a dual-pass technique. Topography was mapped using tapping-mode AFM during the first

pass, which is then traced at a set lift height above the surface performing the surface potential measurement. During the second pass of Kelvin probe force microscopy (KPFM), the mechanical drive of the cantilever is disabled and an alternating current bias voltage (Vac = 1 V) is applied to the probe at the mechanical resonance of the cantilever. Vac causes the cantilever to oscillate due to the attractive and repulsive electrostatic interaction between the probe and the sample. A feedback loop monitors and keeps constant the amplitude of the cantilever oscillations by applying a compensating direct current bias voltage to the probe to cancel the probe−sample electrostatic forces. The tips used were silicon Ti−Ir coated (Asyelec-01) with a nominal spring constant of 2.89 N/m and resonance frequency of 71.7 kHz. The scan size was 5 μm at a scan rate of 0.5 Hz [59].

The contact angle measurements were executed using a Goniometer/Tensiometer Ramé-hart Model 250 Standard using water as probe liquid. The samples used for the contact angle measurements at 30 and 60 days were stored in the dark. The surface free energy (SFE) calculations were carried out using the Neumann method, whose equation is:

$$cos\,\theta = 2\left(\frac{\gamma_S}{\gamma_L}\right)^{0.5} exp[-\beta(\gamma_L - \gamma_S)^2] - 1 \quad \textbf{(1)}$$

where β = 0.0001247 (m^2/mJ)^2, γ_L =72.8 mJ/m^2, θ the contact angle measured for each sample and γ_S the surface free energy. The Neumann equation was solved using numerical methods.

Antimicrobial activity

The determination of antibacterial activity against both Gram-positive (*Staphylococcus Aureus*, (ATCC ® 29213™)) and Gram-negative (*Pseudomonas Aeruginosa*, (ATCC® 27853™)) strains, were performed by the disk diffusion assay (Kirby-Bauer) [60]. Both strains were aerobically cultured at 37ºC for 24 h on Müeller-Hinton agar plate to proceed with the inoculum adjusting the bacterial suspension turbidity to a 0.5 McFarland Standard, comparable to a bacterial suspension of $1.5x10^8$ UFC/ml. The strains were inoculated onto each plate; then, the samples were placed and incubated at 37ºC for 24 h. All the samples (0.49 mm^2) were sterilized by dry heat, placed into a muffle furnace (Barnstead/Thermolyne) at 170 ºC for one hour previously to the essay; and, the UV treated samples were used in this essay 1.5 months after irradiation. All the assays were replicated three times.

Bacterial Adhesion

Adhesion of bacteria on the different surfaces was evaluated by using *S. aureus* (ATCC ® 29213™) and *P. aeruginosa* (ATCC® 27853™), strains. With this purpose, both bacteria suspensions were individually incubated and seeded on agar for 24 hours at 37°C to expand the culture. Posteriorly, one isolated colony was resuspended in 3 mL of PBS, and the concentration of bacteria was determined by using the McFarland turbidity standards and adjusted to 1 to 2 x 10^8 CFU / mL. The same protocol used to sterilize the samples in the antimicrobial activity essay was used here. Then, the samples were placed in 24 well plates, and 20 uL of each inoculum was seeded on the surface of each material and incubated at 37ºC. After one hour, samples were washed five times with PBS and fixed with 4% formaldehyde

for 30 min. Next, cells were dehydrated by using a series of ethanol concentrations in PBS (30%, 50%, 70%, 80%, 90%, and 100%), each dilution during 15 min. Finally, samples were air-dried and covered with gold and observed by SEM.

Proliferation assay

Cell proliferation was determined by Alamar Blue assay (Invitrogen). For this purpose, human osteoblast-like cell line (SaOS-2, ATCC® HTB-85™) were seeded at a concentration of 10,000 cells/cm^2 on the top of the nanotubular anodic coatings and incubated at 37 °C with 5% CO_2. Quantification of the cell grow was performed every 24h during 4 days. For that, the quantity of viable cells was measured by addition of Alamar Blue solution (Thermo Scientific) to the culture medium at a 1:10 ratio. Then, cells were incubated at 37°C during 90 min, after that, medium was transferred to a new plate and fluorescence was measured in a spectrophotometer (Biotek FL-600) at an excitation wavelength of 530 nm with an emission wavelength of 590 nm. Fluorescence values were corrected in relation to the average blank. After each measurement new medium was added to the samples and incubated until next time point. Assays were performed in three independent experiments.

Cell-Material Interaction

Osteoblasts were seeded at a density of 10.000 cell/cm^2 on the nanotubular anodic coatings and incubated at 37 °C with 5% CO_2. After 1h and 48h, cells were washed with phosphate buffered saline (PBS) and fixed with 2.5% glutaraldehyde at 4 °C (overnight). Afterward, specimens were washed three times with PBS and dehydrated in each of the following concentrations: 30, 50, 70, 80, 90 and 100%; during 15 min each. Finally, Samples were dried in a critical point dryer (Samdri-

795), sputter coated with gold (Dentom Vacuum Desk IV) and analyzed using SEM (SEM, JEOL JSM-6490LV). Pictures at 600x and 3000x magnifications were taken.

Mineralization

SaOS-2 osteoblasts were seeded at a concentration of 10.000 cell/cm^2 directly on the nanotubular anodic coatings in presence of differentiation medium consisted of McCoy (Invitrogen), 10% FBS, 1% penicillin streptomycin, 50mg/ml L- ascorbic acid, 1mM b-glicerophosphate (Sigma) and 0.01μM Dexamethasone (Sigma). Medium was changed every two days. Cells growing in the culture plate without differentiation medium were used as negative control. After 7 and 14 days cells were fixed with ethanol and stained with alizarin red to detect mineralization zones by using light microscopy (Nikon Eclipse E200). Pictures at 10x, 20x and 50x magnifications were taken.

1.Chapter 1
TiO_2 nanotubular structures for biomedical applications

Several parts of the text and figures have been taken from:

TiO_2 nanotubular structures for biomedical applications.
Robinson Aguirre Ocampo, Félix Echeverría Echeverría.
Journal of Engineering Science and Technology Review
Submitted for Publication

Abstract

Titanium dioxide nanotubes combined the geometrical properties of a tubular structure with the physicochemical properties of TiO_2, and these ordered nanotubes improve the surface characteristics of a material such as titanium, with high mechanical resistance, and low density, enhancing its use for biomedical devices, thanks to the improved interaction between cells and the nanostructured surface. In this chapter, we discuss various aspects of the anodizing technique when used to obtain ordered nanotubes and how the process parameters can be controlled to obtain highly ordered TiO_2 nanotubes. Besides, we review the biological activity of TiO_2 nanotubes, the effect of nanotube size on this bioactivity, the antibacterial effect of TiO_2 nanotubes without doping and finally novel applications of TiO_2 nanotubes employed as a biomaterial are discussed.

1.1 The anodization technique for producing self-ordered TiO_2 nanotubes

Anodic oxidation is an electrolytic process that generates a layer which could be used for decorative purposes or protection against corrosion. The piece to be anodized is submerged in a conductive solution and connected to a direct current source at the positive pole, i.e. the anode of the circuit. On the other hand, the cathode is a piece usually made of platinum or some material that conducts electricity and with low or none reactivity in the anodizing solution. To produce nanotubes using the anodizing technique, the applied potentials used are between 1-30 V for an aqueous electrolyte and 20-100 V for non-aqueous electrolytes. The content of fluoride ions generally used is from 0.4 to 2.0% in weight; if the amount of fluoride ion is too low, only a barrier coating is formed, but if it is too high, the titanium sample is electropolished.

Although the TiO_2 formation mechanism is under discussion, few models have been proposed for TiO_2 nanotubes formation, such as “plastic flow” [61], and “oxygen bubble mold” [62]; however, the classic mechanism reported for the majority of authors is based in field assisted oxidation and dissolution [63]–[66]. **Figure 1** shows the typical curve of current density vs. time for nanotube formation processes under potentiostatic control, where five stages of formation are described (S1 to S5 in **Figure 1**). In the first step, an oxide barrier layer is formed and therefore, the current density decreases (**equation 2**), water molecules are divided in O^{2-} and H_2 assisted by the electric field (**equation 3 and equation 4**) and O^{2-} ions travel through the barrier layer and reacts with Ti^{4+} ions produced by titanium oxidation (**equation 2 and equation 5**). In the second stage, the number of bites and cracks increases,

acting as nucleation sites for the pores that begin their formation process due to the presence of the fluoride ion (**equation 6 and equation 7**). that forms $[TiF_6]^{2-}$ ions by reaction with TiO_2 in the barrier layer surface, or reacting with Ti^{4+} ions that travel outwards across the barrier layer. This process generates an increase in current density until it reaches a maximum density of pinholes and cracks. In the third stage, the current density begins to decrease when the thickness of the porous structure increases. As the process progresses over time, the porous structure begins to transform into a nanotubular structure due to an equilibrium between field assisted oxidation and field assisted dissolution (**equation 2, equation 6 and equation 7**). This change in the structure is part of step 4. In step 5, the previous transformation is completed and the nanotube already has its final form.

$$Ti + 2H_2O \rightarrow TiO_2 + 4H^+ + 4e^- \quad \textbf{(2)}$$

$$H_2O + 2e^- \rightarrow H_2 + O^{2-} \quad \textbf{(3)}$$

$$2O^{2-} \rightarrow O_2 + 4e^- \quad \textbf{(4)}$$

$$Ti \rightarrow Ti^{4+} + 4e^- \quad \textbf{(5)}$$

$$Ti^{4+} + 6F^- \rightarrow [TiF_6]^{2-} \quad \textbf{(6)}$$

$$TiO_2 + 6F^- \rightarrow [TiF_6]^{2-} \quad \textbf{(7)}$$

In the literature, four generations have been identified for TiO_2 nanotubes formation using the anodizing technique. Each generation have a different sort of electrolyte, in the first generation strong acids were used accompanied of HF in aqueous solutions; the nanotubes produced in this generation had a length equal or lower than 500 nm due to the high oxide dissolution rate. Besides, these nanotubes had unions between them similar to “ribs”, and the organization was low [16], [67], [68]. In the second generation, HF was replaced by fluoride salts and buffered solutions

or weak acids replaced the strong acids; the nanotubes lengths were close to 1 μm and the organization was better than the nanotubes produced in the first generation [69], [70]. In the third generation the aqueous solutions were replaced by organic solutions with fluoride salts. In this generation the nanotubes do not show ribs but had a smooth wall surface; nevertheless, in some cases those nanotubes growth up in coral reef structures with different condition of packing along the surface [71]–[73]. Some discrepancies are found in the literature about the fourth generation, some authors reported that in the fourth generation fluoride free electrolytes were used [74]–[77], other authors reported that in the fourth generation organic solutions were used, but with a precise anodizing parameters control to produce highly packed and organized TiO_2 nanotubes [17], [20], [22], [78].

1.2 Factors affecting the nanotubes growth

Many factors affect the nanotubes growth such as: anodizing time, pH, electrolyte reuse, anodic coating removal and re-anodization, and applied potential [20], [79], [80]. **Table 1** shows the effect of electrolyte composition and fluoride source on the internal diameter and growth rate. Organic electrolytes, specially, the ethylene glycol based solutions have a higher growth rate compared with aqueous electrolytes; this behavior can be attributed to the more aggressive conditions of dissolution of the aqueous electrolytes compared with the organic electrolytes [79]. However, using additives in aqueous electrolytes thicker nanotubes could be produced [3]. In **Figure 2**, the effect of the electrolyte nature (keeping voltage, and anodizing time constant

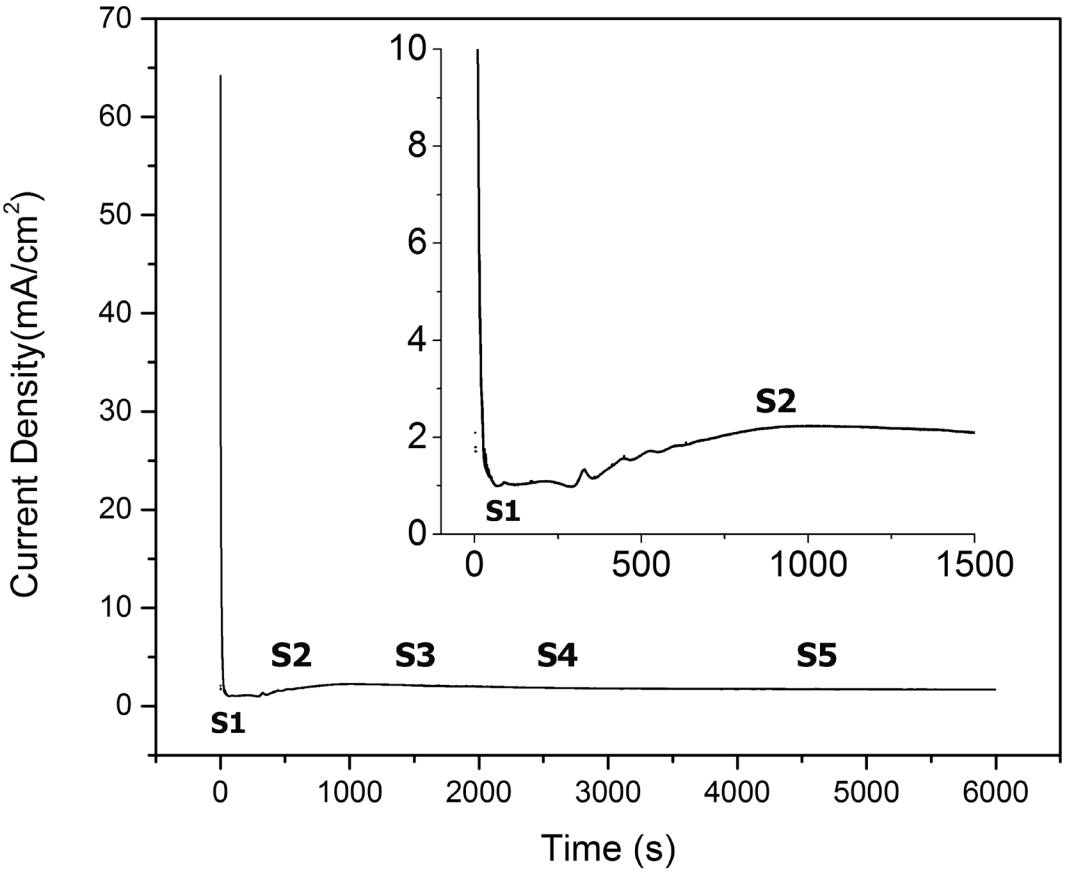

Figure 1. Typical current density vs. time response for anodic formation of a nanotube TiO_2 coating.

for both experiments) on the nanotubes coating thickness is showed. From this figure it is clear that the nanotube length in the organic electrolyte (ethylene glycol) is almost 3 times higher compared to the aqueous electrolyte.

Table 1. Effect of anodizing parameters on the characteristics of TiO_2 nanotubes.

Electrolyte	Fluoride Source	Growth rate (nm/min)	Applied potential (V)	Internal diameter (nm)	Ref.
Dimethyl sulfoxide	HF	4.51	20	70	[81]
Dimethyl sulfoxide	HF	11 22	40 60	120 150	[73]

Ethylene glycol, 2 vol. % H_2O	NH_4F	216	60	110	[18]
Ethylene glycol, 3 vol. % H_2O	NH_4F	135	50	119	[82]
Ethylene glycol	HF	290	120	70	[22]
Ethylene glycol, 10 vol. % H2O	NH_4F	-------	60 90 120 150 180	150 260 360 470 570	[83]
Ethylene glycol	NH_4F	41	60	100	[84]
Ethylene glycol, Lactic acid, 5 vol. % H_2O	NH_4F	2467	120	100	[85]
Ethylene glycol, 3 vol.% H_2O	NH_4F	308	60	140	[86]
Glycerol	NH_4F	13	20	90	[86]
Glycerol	NH_4F	7.91	30	130	[87]
H_2O	HF	12.5	20	60	[16]
H_2O, H_3PO_4	HF	6.66 9.16 13.33 16.66	10 15 20 25	50 70 100 120	[88]
H_2O, H_3PO_4	HF	------	1-20	15 20 30 50 70 100	[89] [90]

H_2O, Na_2SO_4	NaF	25 16.66 9.16 6.66	20	100	[69]

In any case, for the best of our knowledge, the higher growth rate reported is for a mixture of ethylene glycol, lactic acid and water with a value of about 2467 nm·min-1 [45] whereas the lower is for dimethyl sulfoxide, about 4.51 nm·min-1 [8]. Regarding the nanotube internal diameter the higher and lower values are about 570 nm [83] and 10 nm [3], respectively.

1.2.1 Electrolyte pH

The electrolyte pH has a direct effect in the chemical dissolution control; thus, it affects the geometric characteristics (uniformity) and the length principally. Besides, the pH value controls the amount of OH^- and H^+ ions in the electrolyte; therefore, it influences the oxidation rate [91]. Wei Lai et al. [92] produced nanotubes with glycerol and NH_4F varying the pH value from 1 to 7; the authors found that the length was higher when the pH value was 7. Besides, the nanotubes were more uniform at higher pH values compared with lower pH values. The authors explained those results based on the chemical reactions; in acidic conditions, the amount of H^+ ions is high, affecting the H_2O hydrolysis (**equation 2 and equation 3**), reducing the amount of oxygen present, thus the layer formed will be less dense and consequently, the chemical dissolution process increases, restraining oxide growth. Besides, at lower pH values the nanotubes were shorter due to the high chemical etching at the tip of the tubes as a consequence of high H^+ and $[\boldsymbol{TiF_6}]^{2-}$ ion

concentrations; similar results were found by Sreekantan et al. [91].The pH value has an effect in the TiO_2 nanotubes uniformity, nanotubes produced in acidic aqueous solutions (pH value: 1-2) have lower uniformity [16], [42], [88], [93], [94], compared with nanotubes produced in organic solutions (pH value: 5-7) [22], [84], [85]. The explanation of the last phenomena is mainly based on the fact that the pH value directly controls oxide growth rate (O^{2-} concentration depends on pH value [94]) and chemical dissolution rate [3], [91], [92], thus controlling the coating morphological characteristics.

1.2.2 Electrolyte reuse

Many authors had been reported the anodizing of dummy samples to “get older” the electrolyte before anodization of the sample of interest [17], [95], [96], with the aim of increasing uniformity and self-organization. Zhu et al. [95] found that the use of aged electrolytes increases the adhesion the nanotube layer to the titanium surface. The author attributes this phenomenon to changes in the dissolution rate that allow a decrease in the internal stresses in the barrier layer and the titanium surface interface. Sopha et al [97] evaluated the electrolyte aging effect on the nanotubes morphology and found that the nanotubes growth rate was slower and the diameter increases after electrolyte aging; the author reported that such variations in the nanotubes, can be attributed to the changes in viscosity, pH and fluoride ion concentration, when the electrolyte was aged.

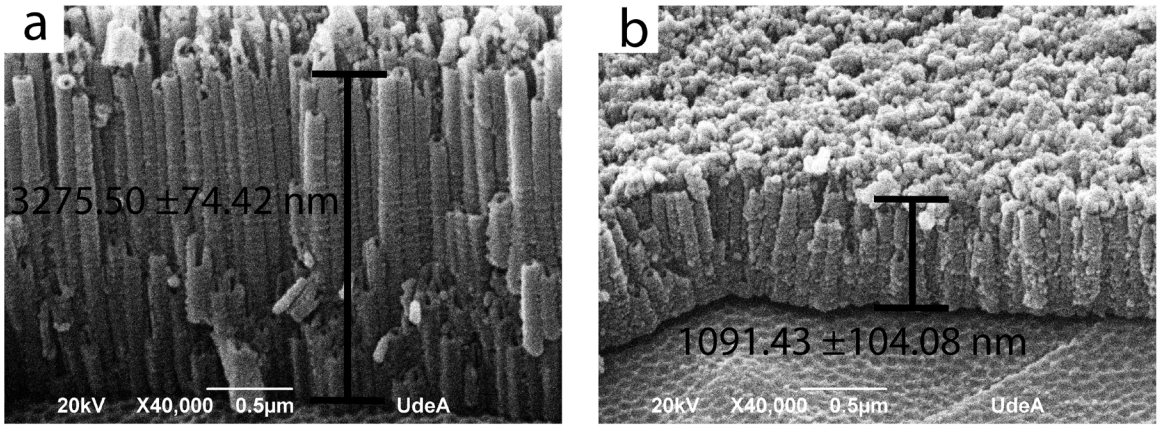

Figure 2. Thickness of nanotube TiO_2 coatings produced in (a) organic electrolytes, (b) aqueous electrolytes.

1.2.3 The anodic coating removal and re-anodization

With the objective of increasing the uniformity and self-organization several authors proposed the removal of the initial coating produced in the first anodization stage and then, the same sample is re-anodized under the same conditions. The removal of this coating can be carried out by ultrasonic waves [98], [99], adhesive tape [100] or using a chemical reagent [101], [102]; as a result a concave nano-texture can be formed on the titanium substrate and these act as nucleation sites for new nanotubes with a higher organization compared with the nanotubes produced in the first anodization stage.

1.3 Highly self-ordered TiO_2 nanotubes

The formation of highly self-ordered TiO_2 nanotubes using the anodization process generally is carried out using viscous organic electrolytes [78], [103]–[105]; this kind of electrolytes allow an equilibrated process with a lower dissolution rate due to low ion mobility, and those parameters had a strong influence in the uniformity and organization grade. Albu et al. [22] produced highly ordered TiO_2 nanotubes with

ethylene glycol and HF with a length of 250 μm; these authors found that the first stage of formation of these nanotubes included a highly ordered hexagonal close-packed structure, similar to the reported for anodized aluminum. Besides the above, the authors said that control of the fluoride content and the applied potential is necessary to obtain highly ordered TiO_2 nanotubes. Li et al. [17] produced highly ordered TiO_2 nanotubes with ethylene glycol and NH_4F using a two-step anodization method. They aged the electrolyte by 60 hours with a dummy titanium sheet, after that, the titanium sample was anodized for 24 hours, and then after, the nanotube coating was removed using an ultrasonic bath. A pattern appeared on the titanium sheet, and after anodizing the sample by a second time, highly ordered nanotubes were obtained. Wu et al. [82] produced highly ordered TiO_2 nanotubes with ethylene glycol and NH_4F with a length of 24 μm; the authors reported that the nanotubes as-anodized were made of the anatase phase. Sulka et al. [100] produced highly ordered TiO_2 NTs, using a three step anodization process: the titanium samples were electropolished until mirror condition, and the first step of anodization was carried out during three hours in ethylene glycol and NH_4F at 60 V and 20 ^{0}C. This coating was removed by ultrasonic agitation, and the titanium surface showed non-uniform concaves. The second step of anodization was carried out at the same conditions than the first step producing a better organization and pore arrangement in contrast with the produced in the first step. This coating was removed once more by ultrasonic agitation, and the titanium this time had uniform concaves; after the third anodization step, the nanotubes produced had a higher uniformity and organization compared with those produced in the first and second anodization steps.

1.4 The biologic activity of TiO_2 nanotubes

The TiO_2 nanotubes have been used in implantology since this material combines a geometry with a high surface area [24], [72], [80] together with the titanium dioxide biological properties which encourage cell adhesion (see **Figure 3**) [89], [106]–[108] and prevent bacterial adhesion [43], [109], [110]. The nanotube properties can be enhanced with heat treatment [43], [111], [112], which change the nanotubes amorphous structure of the as-anodized surface for a defined crystalline phase (either rutile or anatase,) or a mix between them. Another heat treatment consequence is that the nanotubes increase its mechanical stability [107] and this fact, influences cell adhesion and antibacterial properties [9], [113]. **Table 2** is a summary of the experimental work explored this part of the review, which compares type of electrolyte, internal diameter, cell or bacteria used, and main conclusion of the article. For the antibacterial properties it should be highlighted the intrinsic antibacterial properties of TiO_2 nanotubes without silver doping or antibiotic load.

Table 2. Review of biological behavior of TiO_2 nanotubes obtained with different electrolytes

Electrolyte	Fluoride Source	Internal diameter (nm)	Cells or bacteria used	Main conclusions	Ref
H_2O, Acetic Acid	HF	45	MG-63 osteoblast	The nanotubular coatings of TiO_2 after thermal treatment have a more hydrophilic character and better stability in biological fluids, resulting in a better biocompatibility.	[114]

H_2O	HF	70	MC3T3-E1 osteoblast cells	Treatment after anodizing with a NaOH solution makes it more bioactive, the growth of hydroxyapatite accelerated by a factor of 7 and adhered cells increased by 400% with respect to not anodized Ti.	[112]
H_2O	HF	70	MC3T3-E1	Adhesion and proliferation of osteoblasts were improved by the nanotubular morphology, the number of cells adhered increased in the nanotubular surfaces in ~300-400% with respect to the surface without anodizing.	[115]
H_2O, H_3PO_4	HF	100	MC3T3-E1	TiO_2 nanotubular coatings have excellent hydrophilicity, excellent cell response in *in vitro* assays, and also osseointegration in *in vivo* assays.	[116]
H_2O, H_2SO_4, citric acid	NaF	70	Osteoblastic precursor cell line (OPC1)	Nanotubes show a better adhesion and a spacing of osteoblasts and therefore exhibit better proliferation and differentiation than cells planted on Ti without anodizing.	[36]

Glycerol, H_2O	NH_4F	50,85	--------	Thermal treatment is necessary to provide nanotubes with bioactivity and chemical stability for longer periods.	[117]
Ethylenglycol	NH_4F	Nanopore: ~ 100 Nanotube: ~ 70	SaOS2	Titanium with a highly ordered nanoporous layer at the surface, shows lower biocompatibility and the filopodia of the cells attached to it are shorter, compared with other structures.	[39]
H_2O, Acetic Acid	HF	30,50,70,100	MC3T3-E1 mouse osteoblast	Effect of different methods of autoclave sterilization on cell adhesion on TiO_2 nanotube coatings with internal diameter of 70 and 100 nm and it was compared with 30 and 50 nm nanotube coatings. Nanotube size effect on bioactivity was observed only for low cell seeding density.	[37]
H_2O, H_3PO_4	HF	30	In vivo test, animal chose: adult pig	TiO_2 nanotubes improve the function of osteoblasts at an early stage of bone development; besides, the nanotubes structure did not suffer damage as a consequence of implantation process.	[38]

H_2O	HF	~ 80	In vivo test, animal chose: one year old rabbits	TiO_2 nanotubes show a considerable increase in tensile strength at the junction between the living bone and the implant compared to samples without anodizing.	[118]
Ethylenglycol, H_2O	NH_4F	150,260,360, 470,570	MC3T3-E1	All nanotubular surfaces promote a high proliferation rate and high levels of ALP (alkaline phosphatase) compared to titanium without anodizing, the highest ALP level was achieved with internal diameters of 150 nm and the highest proliferation was achieved for diameters of 470 nm.	[83]
H_2O, H_3PO_4	HF	15,20,30,50, 70,100	GFP-labeled MSCs	An internal diameter of 15 nm is optimal for cell adhesion, proliferation, and differentiation, whereas very large sizes such as 100 nm do not allow good cell adhesion and therefore proliferation and differentiation are affected.	[89] [90]
Glycerol, H_2O	NH_4F	40,60,80,100 ,110,120	Human osteosarcoma U2OS cells	Nanotubes with a diameter greater than 100 nm (i.e. 110 and 120 nm) increase proliferation, while the differentiation is increased	[107]

				in coatings with diameters around 80 nm.	
H_2O, Acetic Acid	HF	30,50,70,100	MC3T3-E1 mouse osteoblast	Coatings with a large internal diameter (> 100 nm), have great potential as a material for implants because they induce elongation of osteoblasts, have great capacity for bone formation, and increase levels of ALP with respect to lower diameter (<70nm).	[119]
H_2O, $(NH4)_2SO_4$	NH_4F	30,50,70,90	MG-63 cells (ATCC-1427)	Nanotubes with a diameter of 30 nm promote adhesion, proliferation and differentiation in contrast with the larger diameters.	[120]
H_2O, NaH_2PO_4	HF	15, 100	------	Small nanotube (15 nm) diameters have a higher number of fibronectin binding sites therefore greater cell adhesion than large (100 nm) diameters, in which fibronectin interacts only at the edges of the nanotubes.	[121]
Glycerol	NH_4HF_2	30,70,100	In vivo test, 10 months old minipigs	70 nm is the optimum size for implants of TiO_2 nanotubes because it favors Osseo conductivity and osseointegration.	[122]

H_2O, H_3PO_4	HF	15,30,50,70, 100	In vivo test, domestic pigs	The BIC (bone implant contact) is higher for nanotubes with an internal diameter greater than 50 nm as the BMP-2 (bone morphogenetic protein-2) analysis indicates. In addition, nanotubes with larger diameters would have more capacity to introduce medicinal products in their interior with respect to nanotubes with inferior diameters.	[123]
Glycol	NH_4F	30, 50, 60, 80, 100	*P. Gingivalis*	TiO_2 nanotube coatings with an internal diameter in the range of 60-80 nm inhibit the growth of this type of bacteria.	[113]
Glycerol, H_2O	NH_4F	75	*S. Aureus P. Aeruginosa*	Nanotubes treated thermally at high temperatures (> 550 ° C) have a higher corrosion resistance compared to coatings treated at lower temperatures. Besides, nanotubes treated at high temperatures increase the inhibitory activity of bacteria *S. Aureus* and *P. Aeruginosa.*	[43]

H_2O	HF	20, 80	*S. Aureus* *S. Epidermidis*	20nm diameter thermally treated nanotubes reduce the growth of bacteria compared to titanium without anodizing and TiO_2 coatings with 80nm diameter with and without heat treatment and 20nm diameter with no heat treatment.	[9]
H_2O	HF	20, 40, 60, 80	*S. Aureus* *S. Epidermidis*	80 nm nanotubes thermally treated had the higher antibacterial effect, besides, the crystallinity, nanotube size, surface chemistry and hydrophilicity had a direct effect on the adhesion of the analyzed bacteria.	[109]

From the data presented in **Table 2**, it is observed that although in all cases it is reported that nanotubular structures on Ti are beneficial for biological applications of this material, there are still uncertainties on the optimal characteristics of these structures for such applications. One aspect that remains under discussion is the effect of the internal diameter, there is not agreement if this value should be in the order of 100 nm [107], [119] or well below this value, i.e.15-30 nm [120] [121]. Regarding, the effect of self-ordering level of the nanotubes structure, there is just little information, but it appears that highly ordered structures are not beneficial for biological applications [39]; further investigation is required on this aspect, in which

structures with various levels of self-ordering will be compared so clear differences on biological tests allow to fully clarify this topic. Finally, published reports indicate that the formation of nanotubular structures on Ti are an efficient antibacterial method, which is improved when the surface is thermally processed after anodizing [9], [43], [109], [113]. Following some of these issues are further discussed.

1.4.1 Effect of diameter in the biological performance of TiO2 nanotubes

The relationship between the biological response and nanotube size is under discussion. In the in vitro tests, researchers are divided principally in two groups; the first group affirm that nanotubes with an internal diameter between 15 and 30 nm improves the biological response of a TiO_2 surface whilst the second group indicates that diameters higher than 100 nm increase this biological response. Park et al [90][89] found that sizes between 15 and 30 nm induced osteoblast cell proliferation and adhesion mainly through the integrin clustering and focal contact. Besides, nanotubes with diameters greater than 70 nm do not promote focal contact and thus apoptosis appears accompanied with a big decrease of cellular activity. Gongadze et al [121] found that osteoblast cells have a big attraction for the sharp convex edges of nanotubes, small nanotubes have a large amount of sharp convex edges per unit area compared with large nanotubes, and this condition promotes the absorption of fibronectin and vitronectin; those proteins facilitate the interaction between the osteoblast cells and the surface (See Fig.3). Similar results has been reported by other authors [120], [124], [125]. On the other hand, K. Brammer et al [119] found that nanotubes with diameters larger than 100 nm have a great potential as osseous implant because they induce elongation of osteoblasts and increase the

levels of ALP (alkaline phosphatase) with respect to smaller diameters (< 70nm). Zhang et al [83] produced nanotubes with internal diameters between 150 and 570 nm, the authors found that all anodized surfaces have a high proliferation rate and high ALP levels compared with un-anodized titanium; besides, nanotubes with internal diameters of 150 nm had the highest level of ALP, whereas diameters of 470 nm had the highest proliferation rate. Other authors [107], [108], [122] reported similar results. Wilmowsky et al [123] did in vivo tests for nanotubes with diameters between 15 and 100 nm and found that the osteocalcin expression was higher in nanotubes with 70 nm in diameter, the BMP-2 (bone morphogenetic protein-2) and BIC (bone implant contact) analyses show better results in diameters above 50 nm. Wang et al [126] experimented with nanotubes with a sizes between 15 and 100 nm, these authors suggest that 70 nm is the optimum size as these nanotubes promote osseous-integration and osseous-conductivity.

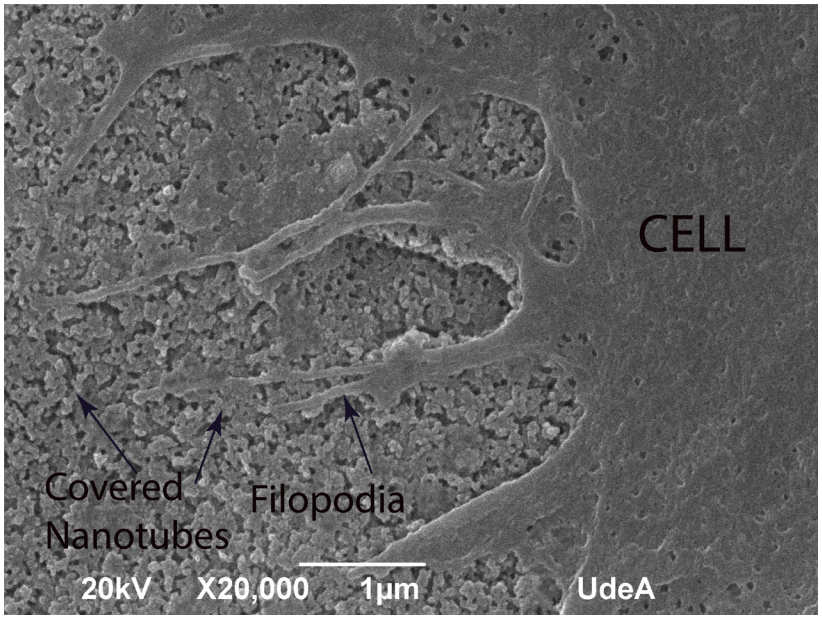

Figure 3. Osteoblast cell adhered to TiO_2 nanotube coating.

1.4.2 Effect of heat treatment on the biological activity of TiO2 nanotubes

Nanotubes produced through the anodized process have an amorphous structure [111], [127], [128].The amorphous structure can be converted in a defined crystalline structure with a heat treatment [129]–[131]. The polymorphs obtained after the heat treatment are dependent on the temperature employed, for temperatures equal or higher than 600˚C rutile and anatase phases are present in the coating, but with the rutile phase in higher proportion. On the other hand, for temperatures lower than 600°C the anatase phase is predominant [129], [131]. After the heat treatment the concentration of fluoride ion decrease in TiO_2 nanotubes surface, and the wettability increases for the presence of rutile and anatase phases which have a higher surface energy in contrast to the amorphous phase, these phenomena contribute to cell adhesion and proliferation [71], [75], [95], [96], [97]. Bai et al [134] produced nanotubes with ethylene glycol and NH_4F; the nanotubes produced were heat treated at 450, 600 and 750°C and the anatase phase was found at 450°C whilst at 600°C the rutile phase was observed with a partial nanotubes disintegration and at 750˚C, the nanotubes completely collapsed. The authors found that nanotubes heat treated at 600˚C had the highest cellular activity. Yu et al [132] produced nanotubes in a aqueous solution with HF, the nanotubes were heat treated at 450, 550 and 650˚C, at 450˚C the anatase phase was found, at 550°C both anatase and rutile phases were present and the nanotubes collapsed at 650°C. These authors found that nanotubes with anatase and rutile had a higher proliferation and mineralization in contrast with amorphous nanotubes and non-anodized surfaces.

1.4.3 Antibacterial properties of TiO2 nanotubes

Titanium is widely used in implantology, but close to 30 % of titanium implants are contaminated with bacteria and this contamination implies surgical removal of the implant and antibiotics treatment for eradicating the bacteria [135]. TiO_2 nanotubes on a titanium surface has been used for decreasing bacteria adhesion and proliferation, due to the characteristics of these coatings in contrast with the non-anodized titanium [9], [113], [136]. Narendrakumar et al [137] evaluated the adherence of *S. sanguinis* and *S. mutans* on three different size nanotubes (100, 50 and 15 nm). They concluded that the lower size nanotubes had the lowest adhesion of those bacteria strains. On the other hand, Ercan et al [109] evaluated the adherence of *S. epidermis* and *S. aureus* and the effect of heat treatment at 500°C, combined with various diameters of nanotubes (20, 40, 60 and 80 nm). The authors found that the 80 nm nanotubes with heat treatment had the better antibacterial effect of all analyzed surfaces and concluded that the antibacterial action can be controlled modifying these parameters in the nanotubes (heat treatment and diameter). Mazare et al [43] produced nanotubes with glycerol and NH_4F and then applied heat treatment at 350, 450, 550, 650 and 750°C. These authors found that the samples heat treated at higher temperatures had the lower adherence of *S. aureus* and *P. aeruginosa*; they correlate this behavior with the presence of a crystalline phase on the coatings, especially the rutile phase.

1.5 Contact angle and surface free energy

The titanium surface treatments have as an aim the enhancement of their superficial properties to modify the interaction with foreign agents, in this case, cells and

bacteria. One way to measure the surface interaction with external agents is through contact angle (CA) measurements, the probe liquid in those tests is generally water. Koch et al. [138] report four classifications based on the contact angle value. A superhydrophilic surface have a CA value less than 10° degrees, a surface with a CA value higher than 10° and lower than 90° is called hydrophilic, a hydrophobic surface has a CA value more than 90° and less than 150°, and, finally, if the surface has a CA higher than 150° is called super hydrophobic. The CA is closely related to the surface free energy (SFE), namely, a CA value higher is associated with a lower SFE and vice versa [139], [140]. Some authors reported changes in the TiO_2 nanotubes contact angle after heat treatments [42], [43], [107], [110], [111], [141], UV irradiations [9], [128], [141] and, as an effect of internal diameter [42], [109], [120]. Generally, those treatments decrease the CA; thus, increasing the SFE. It is worth to highlight that the nanotube coating as-anodized produces a decreasing in the CA compared with the titanium without anodizing [39], [142], [143]. The CA and SFE influence the biological behavior of TiO_2 nanotubes, as a consequence of the individual morphologic characteristics [43], [51], [109], [135]. Peng et al. [51] produced nanotubes with an internal diameter of 30 and 80 nm. The authors report that the 80 nm nanotubes have a lower CA in contrast to the 30 nm nanotubes; thus, this characteristic allows cells adhesion and prevent bacteria colonization.

1.6 Novel applications of TiO2 nanotubes as biomaterial

Nanotubes generally are used in the biomedical field for bone generation (osteoblast) [35], [39], [107], [144], fibroblast [145], [146] and Mesenchymal stem cell [125], [147]; but others authors found other applications in this field. Sorkin *et al*

[148] used nanotubes on titanium as neural prostheses, the authors compared nanotubes obtained in an aqueous solution with nanotubes obtained in an organic solution; both types of nanotubes were produced using HF and heat treated at a 530°C. The authors found that the nanotubes increased the wettability of titanium samples in contrast to un-anodized samples. Besides, the biological behavior of Murine neural stem cells in the anodized surfaces was better compared with the un-anodized surfaces. On the other hand, the nanotubes produced in organic systems had a biological behavior slightly better compared with the nanotubes produced in an aqueous system. These authors concluded that for this application, nanotubes produced in an organic system are better because they have better conductance, which improves neural stimulation by electric pulses. Shen et al [149] produced nanotubes with 30 nm diameter in phosphoric acid and HF and heat treated at 500˚C for 3 hours. The authors evaluated the nanotubes with and without ECM (extracellular matrix) and they found that the combination of nanotubes with anatase and rutile phases and ECM, improved adhesion and proliferation of HUASMC (human umbilical artery smooth muscle cell).

1.7 Conclusions

In this work we reviewed anodizing as a technique to produce nanotubes on the titanium surface, the formation mechanisms reported in the literature, the effect of the anodizing parameters on the nanotubes characteristics (length, internal diameter and uniformity) and how these process parameters can be carefully controlled to produce highly ordered TiO_2 nanotubes. Regarding mechanism of nanotubes formation, it is still under discussion and some models such as “plastic flow”, and

“oxygen bubble mold” has been proposed, but the most reported mechanism is the field assisted oxidation and dissolution. In the literature, four generations have been recognized for TiO_2 nanotubes formation by the anodizing technique. Each generation have a different sort of electrolyte, thus, the nanotubes produced in each generation have different characteristics. Anodizing parameters such as: anodizing time, pH, electrolyte reuse, anodic coating removal and re-anodization, and applied potential can be modified to control the nanotube characteristics; besides, under certain conditions, highly self-ordered TiO_2 nanotubes can be produced. Regarding biological applications, it is still disagreement on the effect of internal diameter on cells behavior. According to in vitro tests results, researchers are divided principally in two groups, the first group affirm that nanotubes with an internal diameter between 15 and 30 nm improve the biological response and on the other hand, the second group indicates that the diameters higher than 100 nm increase the biological response. One possible explanation of the contradiction in opinions, could be related with the different protocols used and the different origin of the cells tested (human, mouse). In-vivo tests results indicate that coatings with a diameter higher than 50 nm have the better behavior, but more studies are needed to clarify this point. Finally, it is clear the intrinsic antibacterial properties of TiO_2 nanotubes and it is also accepted that antibacterial properties can be enhanced by heat treatment, but the effect of the internal diameter remains unclear.

2.Chapter 2
Effect of the anodization parameters on TiO_2 nanotubes characteristics produced in aqueous electrolytes with CMC

Several parts of the text and figures have been taken from:

Effects of fluoride source on the characteristics of titanium dioxide nanotubes.
Robinson Aguirre Ocampo, Félix Echeverría Echeverría.
Applied Surface Science 445 (2018) 308–319.
https://doi.org/10.1016/j.apsusc.2018.03.139

Abstract

Nanotube structures were produced on the titanium surface by anodization using an aqueous electrolyte composed of carboxymethylcellulose (CMC) and NaF. The aim of using this kind of the electrolyte is to study the effect of the addition of CMC in the nanotube morphology and organization. To the best of our knowledge, for the first time a comprehensive study about the effect of the anodization parameters on the nanotubes characteristics, using aqueous electrolytes with CMC was reported. The regularity ratio (RR) based on the FFT images was used to measure the nanotube organization. The addition of CMC at the aqueous electrolyte does not affect the packability and increase the nanotube organization in contrast to the nanotubes produced in an aqueous electrolyte without CMC. The nanotubes length was

affected by the CMC concentration on the electrolyte, furthermore, the highest nanotube length measured in this work was about 5.85 μm. The internal diameter measured at potentials of 20, 15 and 10 V was about 100, 63 and 48 nm respectively, however, at lower potentials diameters lower than 30 nm were obtained, and the lowest value measured was about 9.5 nm.

2.1 Results and discussion

2.1.1 The current density vs time curves

Figure 4 (a) shows a typical curve for the anodization to produce TiO_2 nanotubes, the process starts with a suddenly current rise, after that, the current decrease quickly due to the barrier layer formation [25], [150], [151]. Afterwards, it occurs a change in the slope of the curve (S_I), that indicates the commencement of pore nucleation [152], [153]. The barrier layer continues growing until the current reach a minimum value (J_{min}), at this point, the oxygen ions movement through the barrier layer is restricted due to the oxide thickness reached and consequently the oxidation/dissolution equilibrium is displaced towards the dissolution side, thus, the pore formation increases (S_{II}); this process continues until the maximum density of pores is achieved (J_{max}). Next, the nanopores begin to reorganize and to compete between them to convert into nanotubes. The change in the slope of the curve indicates the beginning of a new stage (S_{III}) in the nanotube formation process, in which the nanotubes start to grow as the process advances. Apolinaro et al. [152] defined the nucleation time as: $t_n = t_{III} - t_I$, where t_{III} and t_I were the times to achieve S_{III} and S_I, respectively. According to Apolinaro et al., the nucleation time is directly related to the degree of ordering and uniformity of the nanotubes, thus, the higher

nucleation time the better nanotubes ordering. **Figure 4** (b) and (c) shows the current density vs time curves for aqueous electrolytes with and without CMC, respectively, keeping the other parameters unaltered (20 V, 0.5 wt.% CMC,0.5 wt.% NaF and 5 hours). Both curves had the typical form described in **Figure 4** (a), showing the nanotubes formation stages described before. On the other hand, some differences can be observed, especially in the time required at each stage. **Table 3** shows the times for all stages, the time required for each stage is higher for the nanotubes produced using CMC in contrast to the electrolyte without CMC. Besides the above, the nucleation time for the CMC electrolyte is around 8 times higher compared to the electrolyte without CMC.

Comparing the nanotubes produced with CMC (**Figure 4** (e) and (f) and without CMC (**Figure 4** (g) and (h)) it is clear that both the organization and circularity increased in the nanotubes produced with the electrolyte that contains CMC in contrast to the aqueous electrolyte without CMC. The main reason for the changes in the nucleation time is the increase in viscosity due to the CMC addition. In viscous electrolytes the ion movement is restricted, thus, nanotubes with a higher organization can be achieved [17], [22], [84]. Generally, the electrolytes used to obtain highly ordered nanotubes are viscous organic solvents (for example ethylene glycol, glycerol, and dimethyl sulfoxide). However, several authors reported some issues related to the packing and coating uniformity (for example cracks, no regular spaces between nanotubes, and coral-like structures) [79], [154]–[160].On the other hand, in aqueous electrolytes due to their lower viscosity (higher ion movement), the organization is

low (polygonal shape instead of circular shape and non-uniformity nanotubes size), but generally they had a higher packability [42], [70], [94], [114], [161].

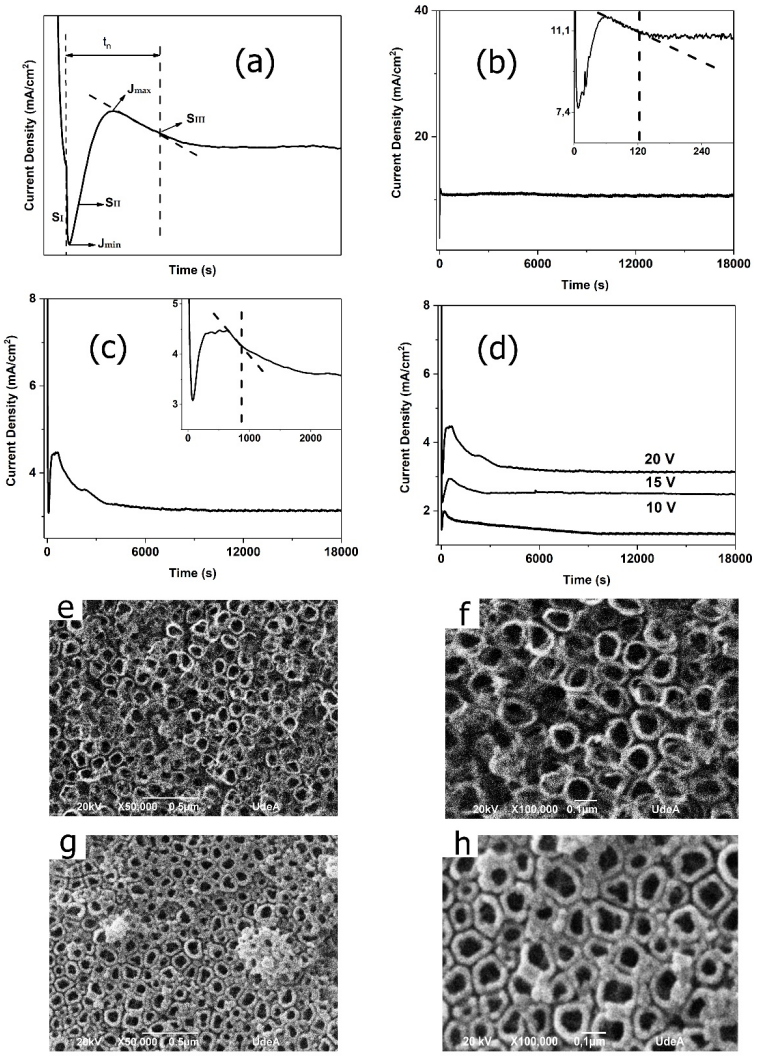

Figure 4. Current-time responses during the anodization of titanium (a) typical form (b) in an aqueous electrolyte without CMC (c) in an aqueous electrolyte with CMC (d) in an aqueous electrolyte with CMC for several voltages. SEM images of coatings obtained in (e)-(f) an electrolyte with CMC (g)-(h) an aqueous electrolyte without CMC.

Table 3. Times for different stages of the anodization

Electrolyte	t_I (s)	t_{II} (s)	t_{III} (s)	t_n (s)
Aqueous Without CMC	5.60	20.37	122.77	117.17
Aqueous With CMC	9.58	101.98	933.22	923.64

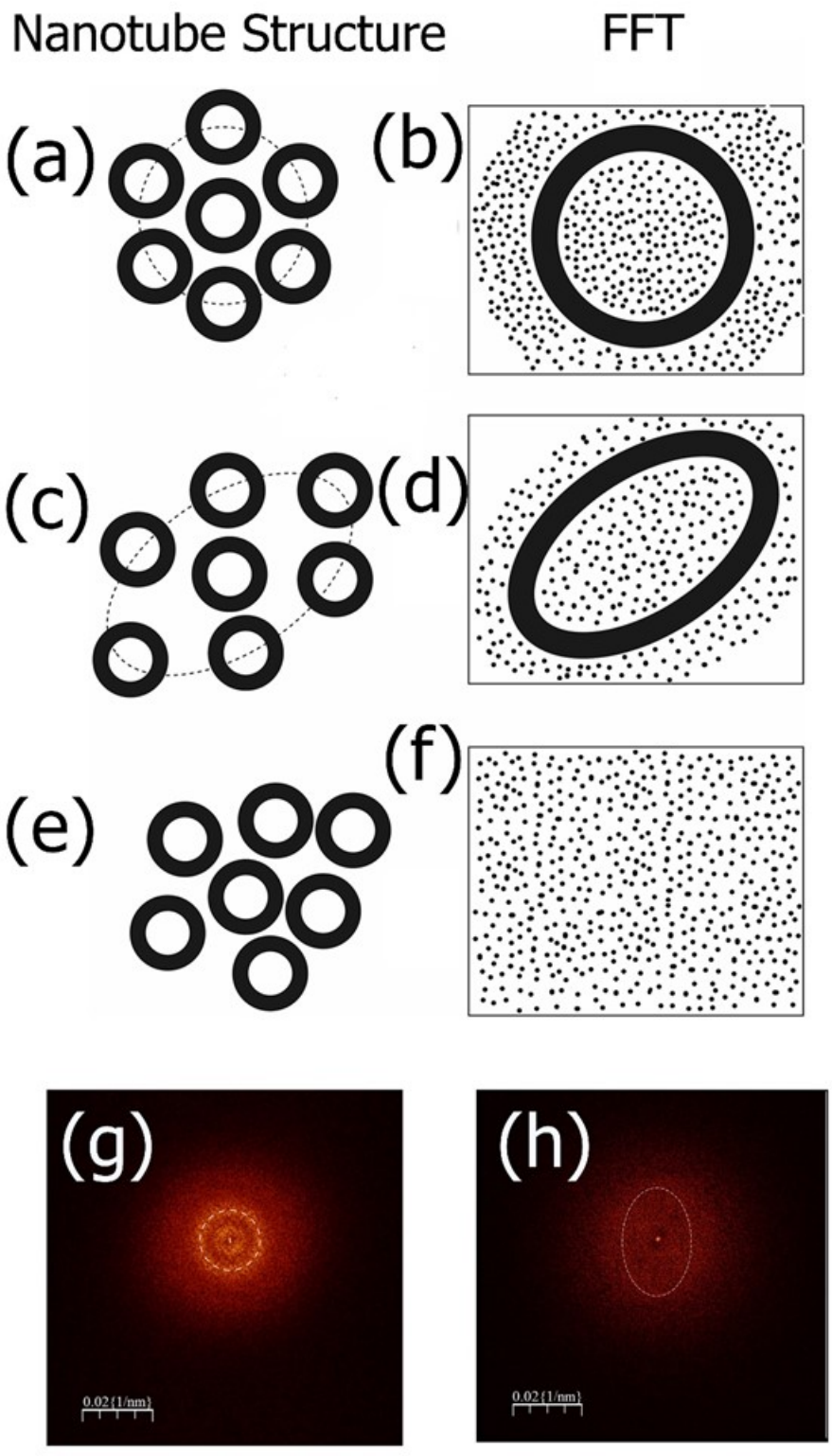

Figure 5. Illustration of different kind of nanotubes organization ((a), (c) and (e)) and their respective FFT images ((b), (d) and (f)); different kind of FFT images ((g) and (h)).

Using SEM images, it is possible to make a qualitative organization analysis. However, it is necessary to measure the nanotube ordering in a quantitative way, for that reason, the averaged regularity ratio (RR) [162]–[167] method based in the FFT measurements was used, whose equation is:

$$RR = \frac{I}{W_{1/2}} \frac{\sqrt{n}}{S^{3/2}} \quad \textbf{(8)}$$

Where I is the intensity of the radial average, $W_{1/2}$ the width of the radial average at the half of its height, n is the number of nanotubes analyzed and S is the area. According with Stępniowski [164] the interpore distance is the physical interpretation of the radial average and the peak width is related to the data dispersion. Besides the numerical analysis described before, the FFT shape can be also analyzed. Thus, for practical purposes, a nanotube structure with a desirable organization had an FFT image with a circular shape (**Figure 5** (a) and (b)). However, in nanotube structures with a lower organization, the FFT shape has other geometrical forms, for instance, in **Figure 5** (c) and (d) an ellipse is obtained, although, other polygonal shapes could be generated. **Figure 5** (e) and (f) shows a disorganized nanotube structure and their respective FFT image; in this case the FFT image does not have a defined shape, instead, a completely blurred image is produced. **Figure 5** (g) and (h) show two FFT images from nanotube structures showed in **Figure 4** (e) and (f) and **Figure 4** (g) and (h), respectively. In the first case, in **Figure 5** (g), a circular shape is clearly observed, as a consequence of the organized nanotube structure seen in the **Figure 4** (e) and (f). In the second case, **Figure 5** (h) shows a blurred FFT image with an ellipse shape, due to the disorganized nanotube structure (no

circular with a higher variability in the internal diameter) observed in the **Figure 4** (g) and (h).

2.1.2 Electrolyte Temperature Effect

The electrolyte temperature effect has been analyzed by several authors [20], [168]–[171] with the aim to improve the nanotubes characteristics. Kapusta-Kołodziej et al [168] produced nanotubes using an electrolyte composed by glycerol and NH_4F and water varying the temperature between 10 and 40 °C. The authors reported that the temperature had a high influence on characteristics such as oxide thickness, pore diameter and porosity. In our case, the main purpose was to improve the organization. Thus, we selected electrolyte temperatures below and above the room temperature (≈ 25 °C). **Figure 6** shows the SEM images of the anodic coatings produced at 5, 25 and 60 °C keeping the other parameters unaltered (20 V, 0.5 wt.% CMC, pH 4, and 0.5 wt.% NaF). For 5 °C nanotubular structures were formed, but with particles that cover the nanotubes, those particles are made of TiO_2 and titanium hydroxide (corroborated by EDX). Similarly, in order to clean the anodized surface, the anodization time was increased up to 16 hours using the same temperature; nevertheless, the particles still covering the nanotubes. However, at 60 °C only few nanotubes were produced, and they were disorganized and immersed in an oxide layer. On the other hand, at room temperature, the nanotubes had a surface free of particles or residues and a higher organization in contrast to the other temperatures. As the electrolyte temperature is changed also its viscosity varies, consequently affecting the nanotube morphology [168], [170]–[174]. At high temperatures (60 °C) the electrolyte viscosity decreases [175] producing a non-homogeneous dissolution

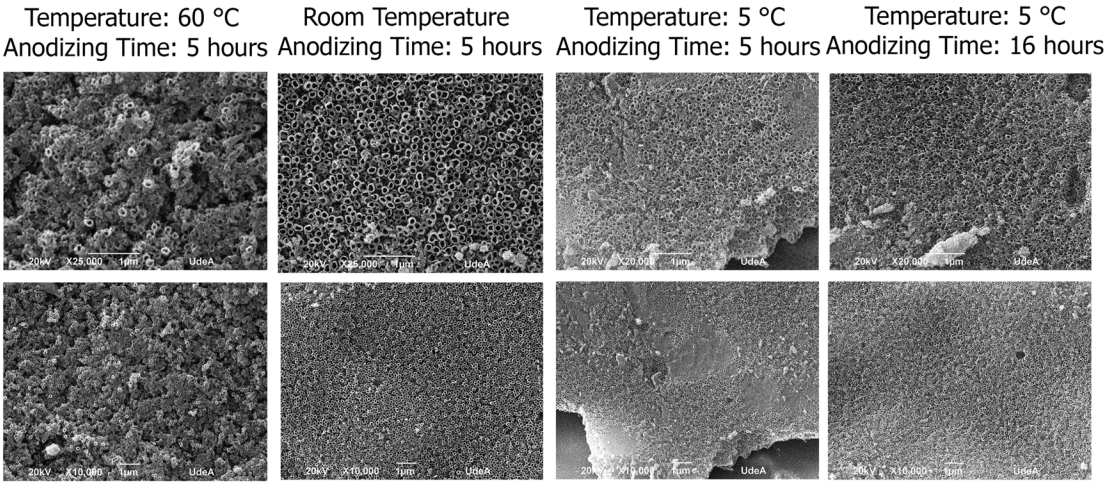

Figure 6. SEM images showing the temperature electrolyte effect on nanotubes morphology.

during anodization; thus, producing non-uniform anodic coatings with both nanotubes and compact oxide layers. At low temperatures (5 °C), the electrolyte viscosity rises [175], producing well defined nanotubular structures, but with oxide particles on the nanotubes tip due to an insufficient rate of dissolution. Hence, the optimal equilibrium between oxide dissolution and formation was achieved at room temperature. Ying-Chin Lim et al [172] produced nanotubes in aqueous solutions with NH_4F and H_2SO_4. They found covered nanotubes at 10 °C and partially formed nanotubes at 40 °C. The findings of Ying-Chin Lim et al. are in agreement with our results.

2.1.3 Aging Electrolyte Effect

The aging electrolyte process consists in anodize dummy samples before to anodize the sample of interest, this process has been used by several authors [17], [26], [155], [176]–[178] seeking to improve the organization of TiO_2 nanotubes**.** Although, the mechanism is not completely understood, some authors have proposed an

explanation. Regonini et al. [26] and Roy et al [13] indicate that the main reason why the aging process improves the organization of TiO_2 nanotubes is related to the increase in concentration of the TiF_6^{2-} ion, thus reducing the TiO_2 dissolution and increasing the rate of TiO_2 formation due to the conductivity arise. **Figure 7** show the aging electrolyte effect (50 hours) on the anodic surfaces for two pH values (1.5 and 4) keeping the other parameters unaltered (20 V, 1.5 wt.% CMC 0.5 wt.% NaF, and 20 hours). As observed in **Figure 7**, for a pH value of 4, without aging the nanotube structures obtained present individual walls, however, after the aging process, the nanotubes were similar to coral-like structures and from the cross-section view is not possible to easily identify individual nanotubes. One possible explanation for this phenomenon is related to the H^+ ion concentration. Due to the aging process, the H^+ ions in the electrolyte are gradually consumed. These ions, according to ***equation 9***, are needed to the occurrence of the titanium dioxide dissolution, which is in turn required to nanotubes formation. Thus, the lack of H^+ ions produces a not homogeneous dissolution which affects the nanotube morphology.

$$\boldsymbol{TiO_2 + 6F^- + 4H^+ \rightarrow TiF_6{}^{2-} + 2\,H_2O} \quad \textbf{(9)}$$

On the other hand, for a pH value of 1.5 with and without aging, nanotubes with individual walls were observed, with not important changes of the nanotubular coatings. This could be explained as in this case the electrolyte has an excess of H^+ ions, thus, the concentration remains high enough to support the nanotube formation, even after 50 hours of aging. From our results, we can conclude that the aging process have not a positive effect on the nanotubes organization in these

electrolytes. Generally, a positive effect of an aging process has been reported only in organic electrolytes [17], [155], [177], [179]; however, the result found in our work

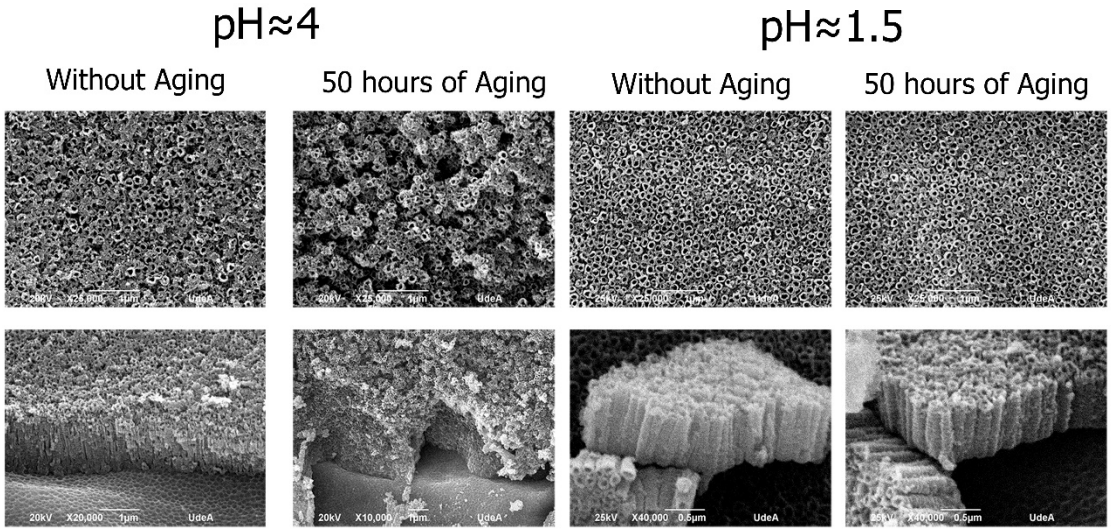

Figure 7. SEM images showing the electrolyte aging effect on the nanotubes organization.

is very interesting as the electrolyte at a pH value of 1.5 could be easily implemented in an industrial process of nanotube coatings production, because it is capable of growth similar coatings both in fresh and aged electrolytes (before and after of 50 hours of aging).

2.1.4 The anodization time effect

Figure 8 shows the SEM images of nanotube coatings obtained using different anodization times but without changing the rest of experimental variables (20 V, 0.5 wt.% CMC, pH 4, 25 °C, and 0.5 wt.% NaF). The aim of this experimental sets was to know the lowest anodization time that allows getting uniform and clean nanotube coatings (without residues from the anodization). For an anodization time of 3 hours, organized nanotubes were present in all analyzed surfaces, showing individual walls, which are characteristic of this kind of structure; however, some particles cover

the nanotube tip. Tang et al. [180]] reported the same phenomenon in nanotubes produced in an electrolyte composed of glycerol, NH_4F and a low amount of water. The authors showed that those particles were formed by the partial dissolution of a thin and compact titanium dioxide layer formed in the early stage of the nanotubes formation process. Those particles remain on the surface due to the lower etching rate in viscous electrolytes, also the authors propose two ways to clean the anodic surfaces. The first one is related to increase the anodization time to allow the chemical dissolution of those particles and the second one is associated to a posterior chemical etching process assisted by ultrasound in a diluted aqueous solution of HF.

In our case, the CMC increased the electrolyte viscosity and hence decreased the etching rate; thus, oxide aggregates appear in nanotubes produced at 3 hours due to the short anodization time. According to our results, an anodization time of 5 hours produced the better result (based on the RR). When analyzing the effect of a longer anodization time (20 hours) on the nanotube characteristics, it was observed the occurrence of significant changes in the morphology, decreasing the nanotube structure ordering in contrast with the results from the nanotube coating got at 5 hours (see **Figure 8**). Regonini et al. [181] reported similar results using an electrolyte composed of glycerol, NaF, and water at 20 V for 20 hours. According to the literature, a certain time it is necessary to allow the nanotubes to organize themselves and increase their uniformity and organization degree [25], [26], [161].However, an extreme long anodization time promotes the corrosion at the tip, affecting the nanotube morphology [6], [24], [26]. The anodizing time effect on the

nanotube length has been reported by several authors [91], [154], [161], [182], [183] and confirmed here in **Figure 8**.

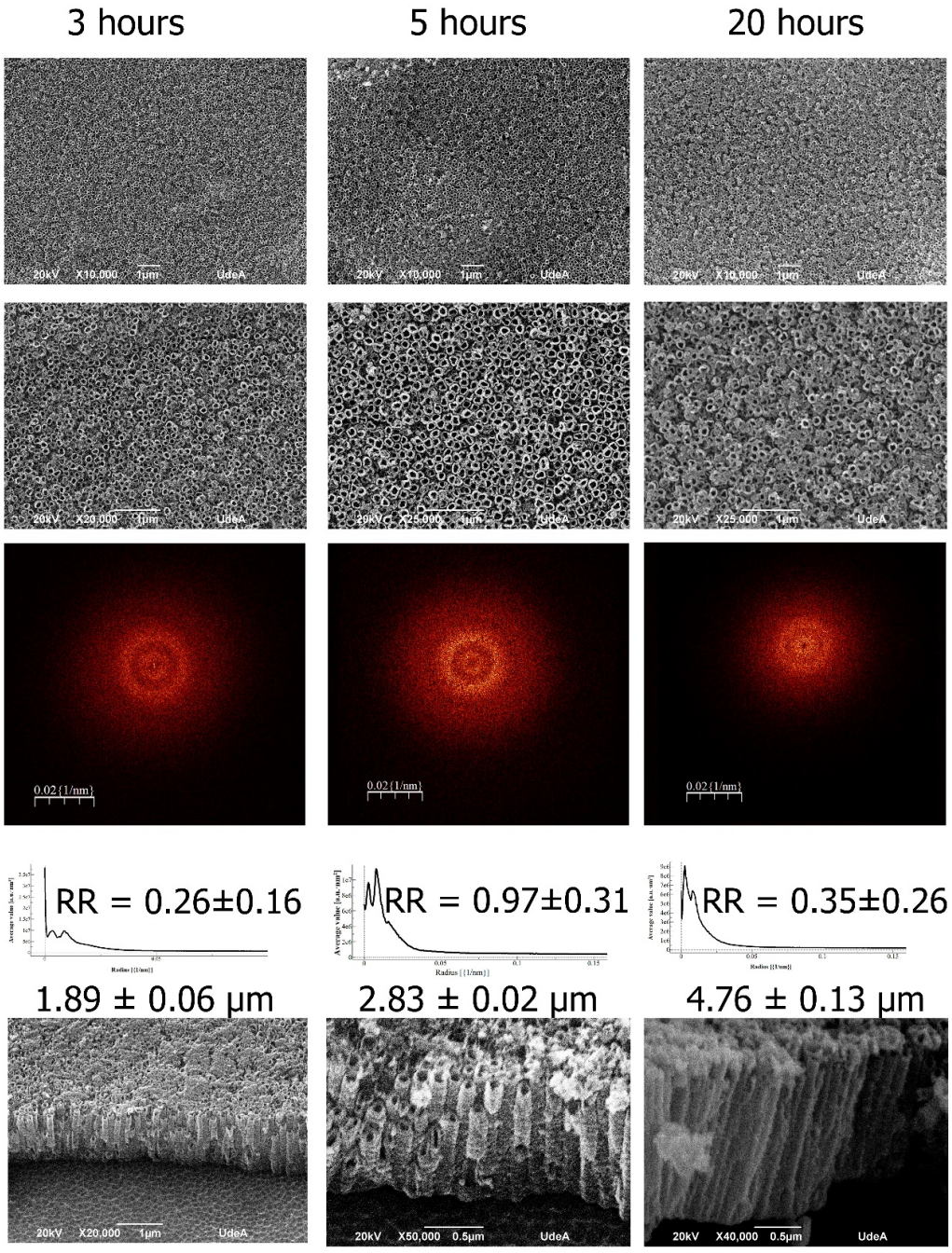

Figure 8. SEM images showing the anodization time effect on nanotubes organization and length.

2.1.5 Fluoride Concentration Effect

Generally, the electrolyte used to produce TiO_2 nanotubes through the anodization contains between 0.20 and 1 wt. % of fluoride sources (HF, or fluoride salts) [13], [26], [183]. Concentrations below of 0.20 wt. % propitiate barrier layer formation instead of TiO_2 nanostructures. On the other hand, using concentrations upper than 1 wt. % is not viable to produce TiO_2 nanotubes due to the higher dissolution rate that affects the barrier layer formation [12], [26]. However, a certain amount of fluoride is necessary to produce nanotubes, although, it is worth to highlight that the fluoride excess affects the nanotube morphology and adhesion to the substrate [184]–[186]. Thus, it is necessary to identify the lower concentration that allows the nanotube formation without affecting their properties. **Figure 9** shows the nanostructures produced using two concentrations of NaF (0.25 and 0.50 wt.%) keeping the other anodization parameters unaltered (20 V, 0.5 wt.% CMC ,5 hours, pH 4 and room temperature). From that figure, it is clear formation of nanotubes in both cases, but with some differences; for 0.25 wt.% a dense layer covers the nanotubes, this layer is clearly observed in the SEM images at 5,000X and 10,000X. From eq.1, 6 moles of F^- are necessary to dissolve the TiO_2, thus, if exist a lack of fluoride ions, the chemical dissolution rate is not enough to dissolve this top layer that covers the nanotubes. Previous works have reported this kind of layer [13], [187]–[189] on the nanotube surface. Roy et al. [13] defined this coating as an initiation layer remnants that cover the nanotubes top whereas the nanotubes continues growing beneath; under auspicious conditions of dissolution, this layer is removed in the final stages of nanotube formation process [187]. In contrast, the

nanotubes produced using 0.50 wt.% does not have this dense layer; thus, this concentration leads to form clean nanostructures, namely, without oxide layers or particles covering the nanotubes. Furthermore, the nanotubes produced using 0.50 wt.% had a higher organization in contrast to the produced using 0.25 wt.%. From the literature, the most popular concentrations of fluoride source are 0.50 wt.% [70], [109], [190]–[192] and 0.25 wt.% [17], [18], [23], [78], [84], [193], [194], however, in some cases higher values have been used too [94], [160], [184].

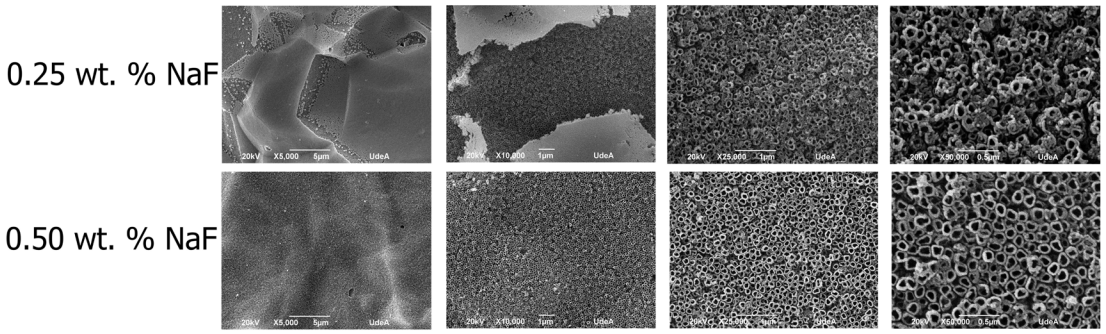

Figure 9. SEM images showing the fluoride concentration effect on nanotubes morphology.

2.1.6 pH and electrolyte composition effect

Figure 10, **Figure 11** and **Figure 12** shows the effect of the electrolyte pH and CMC concentration on nanotubes organization for 20, 15 and 10 V, respectively. In these experiments, the values for anodizing time, fluoride concentration and temperature were the better values reported above (5 hours, 0.5 wt.% and room temperature respectively). In **Figure 10** the results obtained for the nanotubular coatings formed at 20 V of anodizing voltage are presented. From **Figure 10** at pH 5 and 0.5 wt.% of CMC, only few nanotubes are visible surrounded by an oxide layer; thus, the RR is equal to zero. A possible reason is related to the lack of H^+ ions that affects the oxide

dissolution rate (**equation 9**). Sreekantan et al. [91] produced nanotubes using an aqueous electrolyte composed by Na_2SO_4 and NH_4F at 20V. They explained the reduced rate of nanotube growth at higher pH values based on

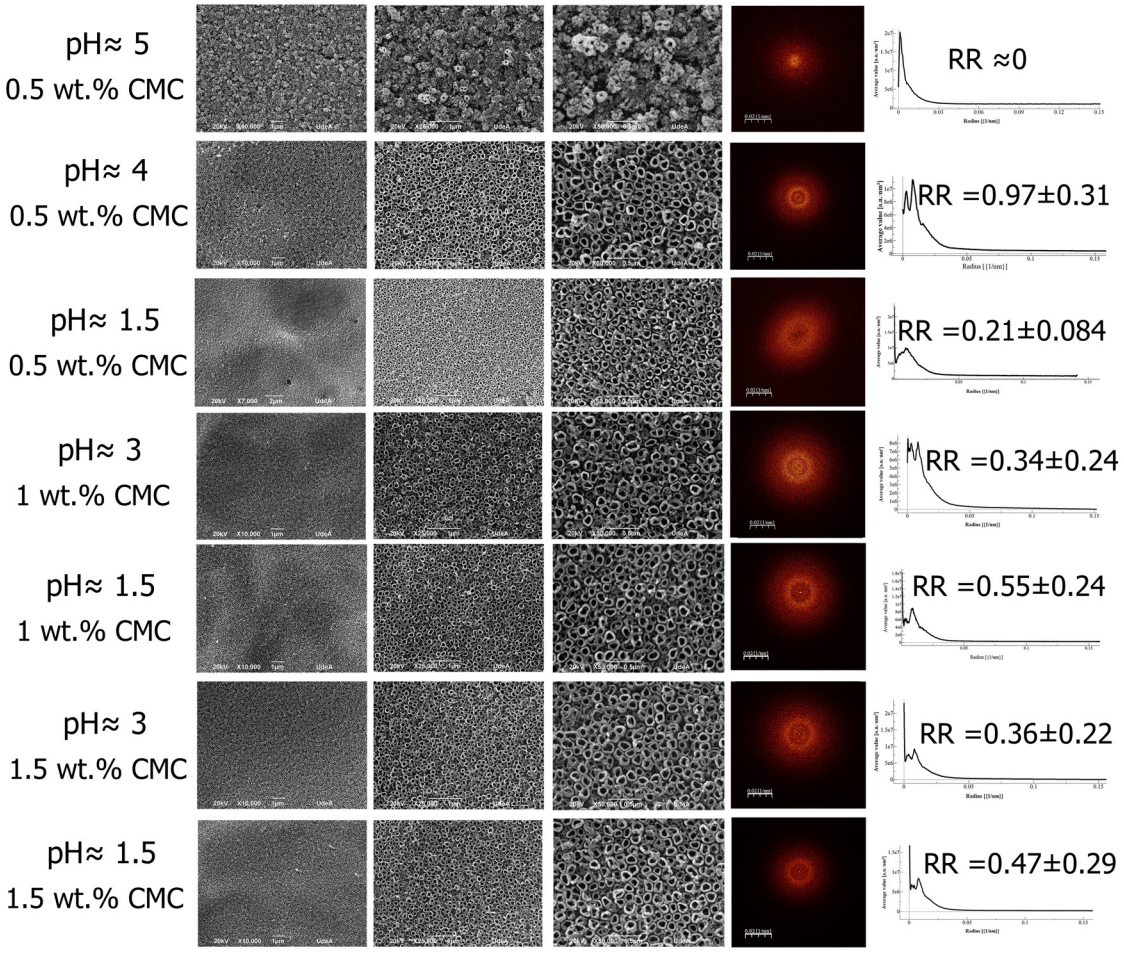

Figure 10. Effect of the electrolyte pH and CMC concentration on nanotubes organization using a potential of 20 V.

the deficiency of H^+ ions and therefore they recommended to increase the anodizing time to produce well defined and ordered nanotubes at those pH values.

From **Figure 10**, at pH 4 and 0.5 wt.% of CMC a highly organized nanotube structure can be observed with an RR of about 0.97; this value is the highest of all RR values

obtained in this research work. On the other hand, using the same CMC concentration but with a pH value of 1.5, the organization decreased, resulting in a RR of about 0.21. Furthermore, the FFT shape is oval instead of circular. A possible reason for this result is related to the excess of H^+ ion, that increases the dissolution rate producing disorganized nanotube structures [70], [75]. The remaining conditions showed the formation of nanotubes structures, but with a lower organization compared to the condition at pH 4 and 0.5 wt.% of CMC. It is important to mention that all tested conditions at 20 V had a high packability (see SEM images at 10,000X). In addition, the use of CMC does not affect this coating feature, prevailing the characteristic good packability of the coatings produced in aqueous electrolytes. Similarly, excluding the nanotube structure produced at pH 1.5 and 0.5 wt.% of CMC, the FFT images with an RR different to zero, has a high circularity (>0.90).

When using 15 V as anodizing potential (**Figure 11**), at high pH values (4 and 5) and using 0.5 wt.% of CMC, although nanotube structures were produced, most of them are fully covered and disorganized. In contrast, at pH of 1.5 and 0.5 wt.% of CMC an organized nanotube structure was observed with an RR of about 0.56; this value is the highest for anodization at 15 V. The condition at pH 1.5 and 1 wt.% of CMC, had an RR close to the highest value at this potential. Thus, to produce organized nanotubes at 15 V, low pH values and high CMC concentrations are required, in contrast to the results obtained at 20 V. Likewise, the coatings produced at 15 V has a high packability (see SEM images at 10,000X), furthermore, the FFT images show a high circularity (excluding those with RR=0).

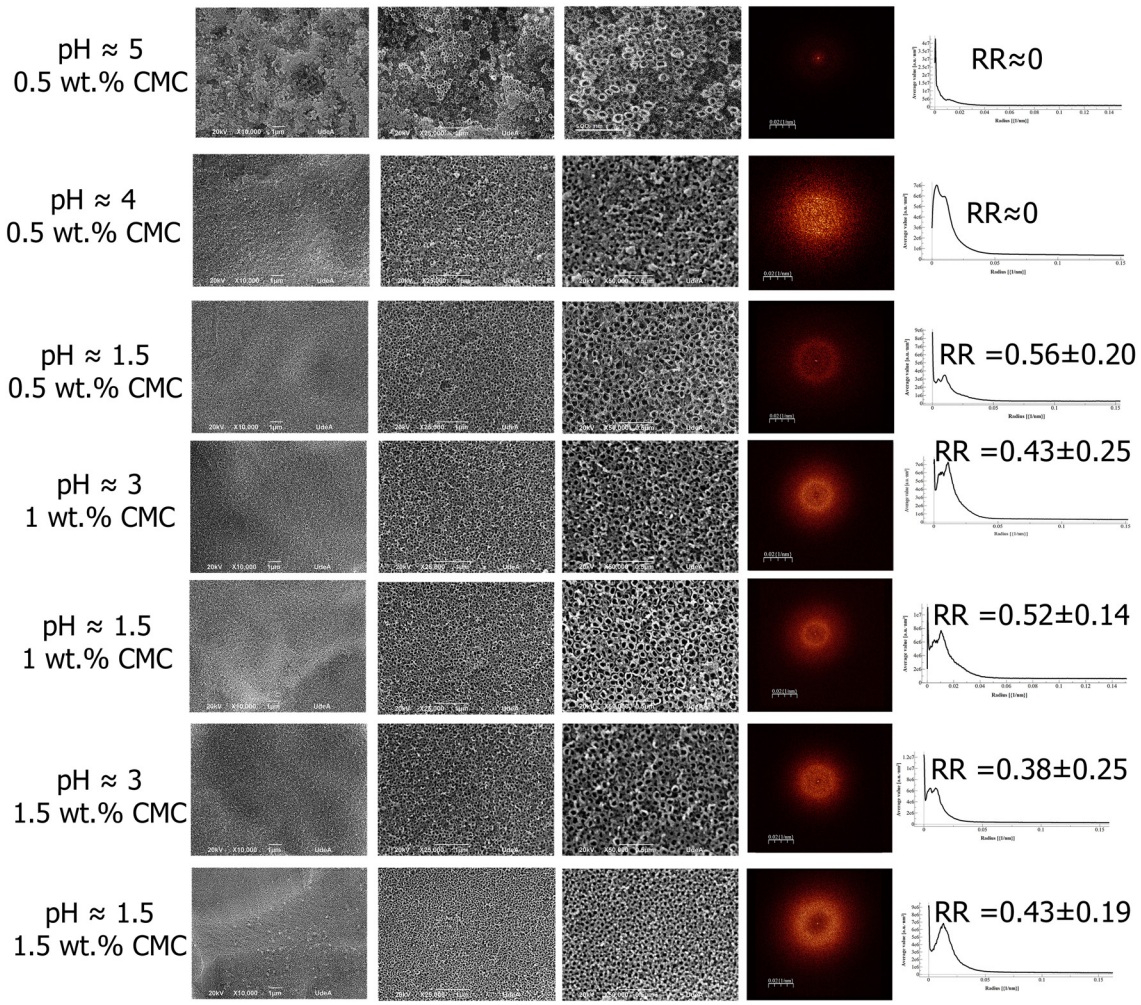

Figure 11. Effect of the electrolyte pH and CMC concentration on nanotubes organization using a potential of 15 V.

Finally, the coatings obtained at 10 V of anodization potential are shown in **Figure 12**. These results reveal how when using 0.5 wt.% of CMC the nanotubes produced were disorganized or not formed at all, disregarding the pH value employed. Similarly occurs for anodization at pH 3 and 1.5 wt.% of CMC. However, at pH 1.5 and 1.5 wt.% of CMC the highest value of RR was obtained, although at pH 1.5 and 1 wt.% of CMC a high value was also obtained. Thus, from our results, to form organized nanotube at 10 V, low pH values and high CMC concentrations are needed, similar

to what was observed for the nanotubes obtained at 15 V. As in the samples treated at higher potentials, for 10 V, the SEM images at low magnification show a high packability of these coatings; additionally, the FFT images show a high circularity (excluding those with RR=0).

The RR calculations to measure the organization of nanostructures has been widely used in alumina arrays [162], [164]–[166], [195]–[199]. Nevertheless, from the best of our knowledge, in TiO_2 nanotubes only exist few reports which calculate the RR [200]–[202] and other works only report the FFT images as an indirect measure of organization [203].

Table 4 shows the measurements of internal diameter, circularity and interpore distance for the nanotube structures showed in **Figure 10**, **Figure 11** and **Figure 12**, (excluding those with RR=0). The interpore distance measurements were calculated using the procedure reported by Stępniowski et al [167]. From **Table 4**, it is clear the direct relationship between voltage and internal diameter, furthermore, there is also a correlation between voltage and interpore distance. The values of internal diameter and interpore distance are similar for each set of samples prepared at a given value of voltage; it is for 20 V, the average values for internal diameter and interpore distance are 100.54 and 119.71 nm, for 15 V, 63.43 and 92.84 nm, and for 10 V, 47.5 and 69.37 nm. Circularity has been used as an indicative of organization in previous works [163]–[166], [197]. From our results, it is observed that the use of electrolytes that contains CMC promotes the formation of nanotubes with higher circularity values (>0.80) in contrast to the nanotubes produced in aqueous

electrolyte without CMC. In addition, these results indicated that higher values of circularity are related with higher values of RR.

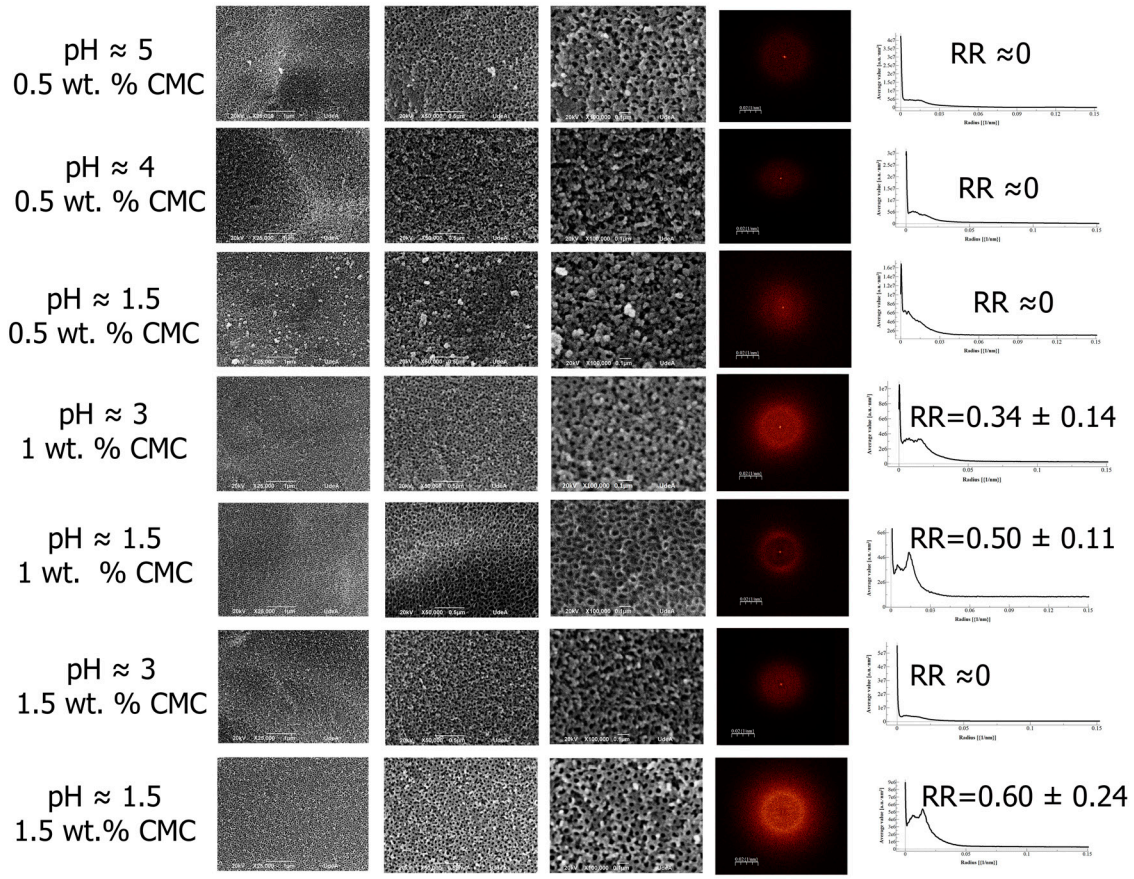

Figure 12. Effect of the electrolyte pH and CMC concentration on nanotubes organization using a potential of 10 V.

Figure 13 shows the cross-section SEM images of nanotubes obtained in electrolytes with different contents of CMC keeping the other anodization parameters unaltered (20 V, 0.5 wt.% NaF, 20 hours, and pH 4). From this figure, the nanotubes length increased with the rise of CMC content from 0.5 wt. % to 1 wt.%; however, when the CMC content was raised from 1 to 1.5 wt.%, that parameter dramatically

decreased. An explanation of this phenomenon can be based on the electrolyte viscosity; an increase in the viscosity affects the diffusion rate producing a slow motion of ions (especially fluoride ion) which allows to get higher thickness [79], [181]. However, if the viscosity continues raising, at some point, the opposite effect

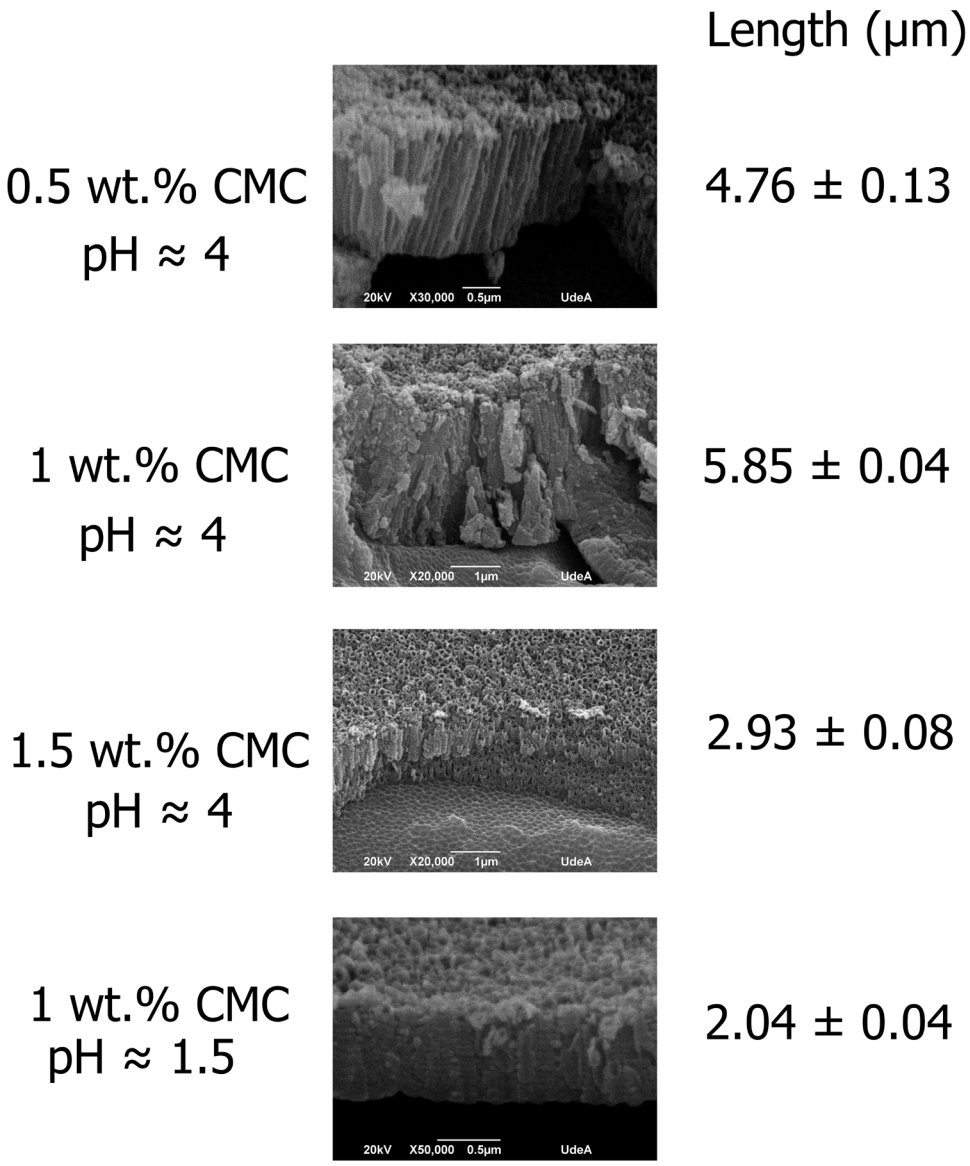

Figure 13. CMC content and pH value effect on nanotubes length.

is presented, namely, short nanotubes are produced in highly viscous electrolytes [136], [190].In an electrolyte with high viscosity, besides the dissolution control, the

oxide formation is also affected due to the ions low movement (principally O^{2-}), thus shorter nanotubes are achieved. Dumitriu et al [190] compared two kind of electrolytes (ethylene glycol (EG) and polyethylene glycol (PEG)) under the same anodization parameters and found that the length of nanotubes produced in PEG was very short (330.4 nm) in contrast to those produced in EG (2.40 μm). Additionally, to the best of our knowledge, the nanotubes obtained at 1wt.% CMC had the higher length (about 5.85 μm) reported in an aqueous electrolyte at 20 V and pH 4 [11], [204]. The pH effect on the nanotube length has been reported by several authors [69], [91], [92], [151], [204], [205]. From **Figure 13**, decreasing the pH value from 4 to 1.5 the length decreased from 5.85 to 2 μm. Beranek et al [151] produced nanotubes structures in an aqueous electrolyte composed by H_2SO_4 and HF. These authors reported that nanotubes formed during 20 hours at 20 V had a length of about 550 nm. From those results and the values obtained in the present study, it can be concluded that the use of CMC inhibits the TiO_2 high dissolution produced in aqueous acidic electrolytes. Furthermore, the nanotube lengths obtained in this experimental work are close to the previously reported [171], [181] at similar anodizing conditions in glycerol.

From **Figure 10**, **Figure 11** and **Figure 12**, it can be concluded that for the formation of organized nanotubes, lower pH values and higher CMC concentrations are needed when the applied potential decreasing. Previous reports in anodic alumina layer [162]–[164] show a direct relationship between the voltage and the regularity ratio. According to the present results, the maximum RR value (about 0.97), calculated at 20 V was higher in contrast to the highest values obtained at 15 and

10 V (about 0.56 and 0.60, correspondingly). However, when analyzing the maximum RR values at 15 and 10 V, the same tendency was not observed. Additionally, the results obtained here indicate that the use of CMC in the aqueous electrolyte does not affect the packability (see **Figure 9**) and increases the nanotube organization compared with the nanotubes produced in an aqueous electrolyte without CMC (RR about 0.16) (see Figs. 1 and 2).

Table 4. Internal Diameter, circularity and interpore distance of anodic coatings.

Experimental Condition	Internal Diameter (nm)	Circularity	Interpore Distance (nm)	Potential (V)
pH 4 and 0.5 wt.% CMC	99.08 ± 15.13	0.90 ± 0.05	123.11 ± 5.46	
pH 1.5 and 0.5 wt.% CMC	88.60 ± 12.82	0.82 ± 0.08	109.77 ± 3.66	
pH 3 and 1 wt.% CMC	104.26 ± 15.21	0.86 ± 0.06	118.38 ± 6.27	20
pH 1.5 and 1 wt.% CMC	111.93 ± 17.13	0.87 ± 0.06	121.33 ± 3.75	
pH 3 and 1.5 wt.% CMC	98.47 ± 17.18	0.88 ± 0.04	123.10 ± 2.46	
pH 1.5 and 1.5 wt.% CMC	100.95 ± 12.47	0.88 ± 0.05	122.59 ± 5.90	

pH 1.5 and 0.5 wt.% CMC	63.62 ± 7.46	0.88 ± 0.05	97.11 ± 1.88	15
pH 3 and 1 wt.% CMC	62.85 ± 11.84	0.89 ± 0.04	90.36 ± 0.93	
pH 1.5 and 1 wt.% CMC	73.30 ± 11.69	0.88 ± 0.06	94.97 ± 2.25	
pH 3 and 1.5 wt.% CMC	66.29 ± 10.03	0.88 ± 0.04	104.23 ± 4.19	
pH 1.5 and 1.5 wt.% CMC	51.08 ± 7.32	0.92 ± 0.04	77.56 ± 2.55	
pH 3 and 1 wt.% CMC	41.69 ± 5.49	0.85 ± 0.06	68.32 ± 2.96	10
pH 1.5 and 1 wt.% CMC	55.92 ± 5.43	0.91 ± 0.02	70.63 ± 2.25	
pH 1.5 and 1.5 wt.% CMC	44.89 ± 6.79	0.90± 0.04	69.16 ± 2.01	
Without CMC	83.04 ± 26.02	0.68 ± 0.05	99.32 ± 15.46	20

2.1.7 Other potentials evaluated

According to the literature the more common nanotube diameters reported are higher than 30 nm [159]; furthermore, reports about nanotubes with lower diameters are scarce [20], [161], [206]–[210]. One of the advantages of obtaining nanotubes

with lower diameters is the increase of the surface area [210], which is a promising property in applications like solar cells and biomedical devices, among others.

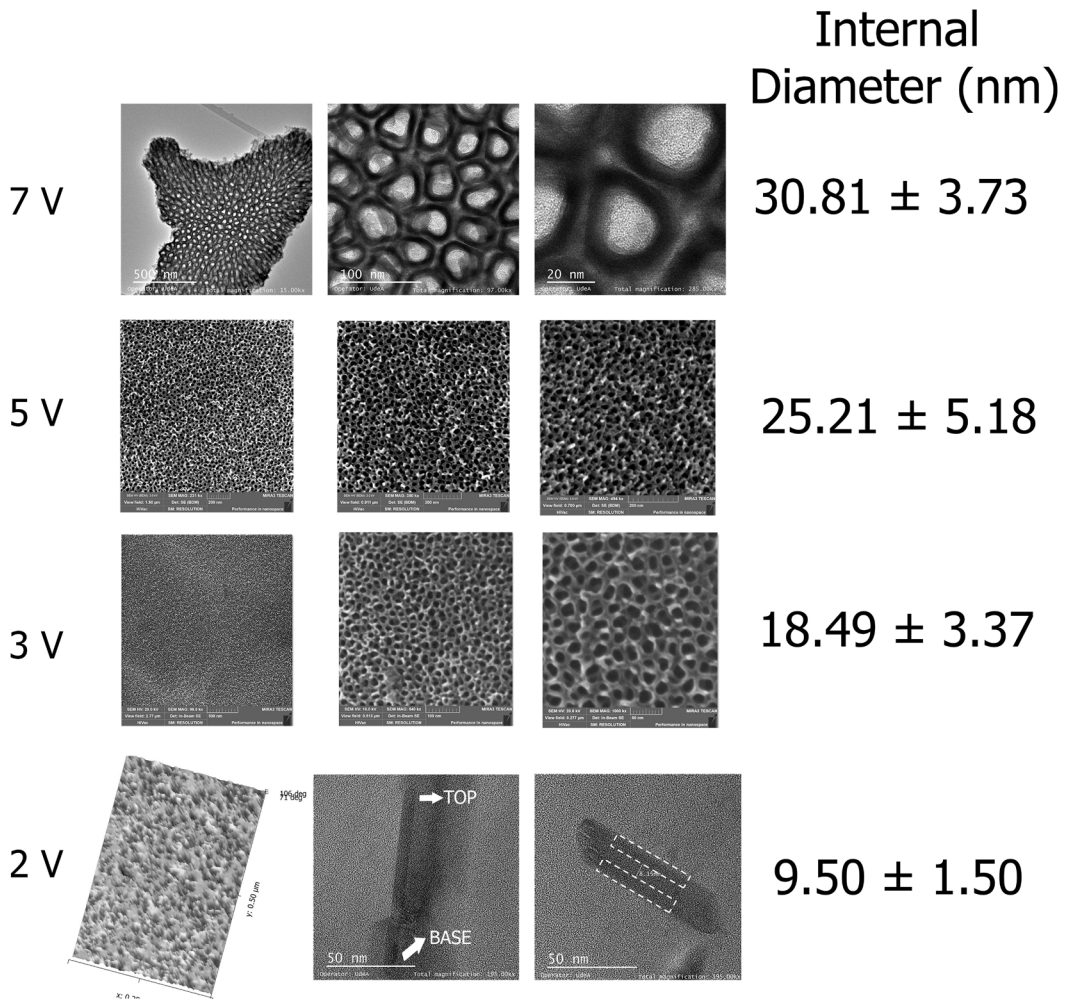

Figure 14.TEM, FESEM and AFM images of nanotubes produced at 7, 5, 3 and 2 V.

Based on the better condition to produce nanotubes at 10 V, it is pH 1.5 and 1.5 wt.% of CMC experimental essays were made at 7, 5, and 3 V. For 2 V the condition to produce nanotubes was pH 4 and 1 wt.% of CMC; for potentials lower than 2 V was not possible to produce nanotubes. The anodizing time for the assays at 7, 5 and 3 V was 20 hours and for 2 V was 24 hours. **Figure 14** show TEM, FESEM and AFM images of nanotubes produced at those potentials. From the low magnification

images is clearly seen the high packability of those small nanotubes. In this figure, it can be observed that the nanotubes obtained at 7 V (TEM images) present individual walls and an internal diameter of about 31 nm. In the same figure, the FESEM images also reveal the formation of nanotubes structures when anodizing at 5 and 3 V, with smaller internal diameters as expected, around 25 and 19 nm, correspondingly. For analysis of the nanotubes formed at 2 V, both AFM and TEM were employed. From the AFM image it is clear the nanotubular structure of the surface. Furthermore, from the TEM image at the middle in the bottom row, it is possible to observe that those nanotubes are quite short, just about 103 nm, despite the long anodization process (24 h). In addition, the TEM image at the right in the bottom row, shows the nanotubes walls, which are about 7.6 nm thick (indicated by dashed lines). To the best of our knowledge, these nanotubes, with an internal diameter of 9.5 nm, have the smallest diameter reported in the literature.

2.2 Conclusions

We have analyzed the role of CMC as additive in aqueous electrolytes to produce organized TiO_2 nanotubes. The use of CMC in the aqueous electrolyte did not affect the packability and increase the nanotube organization in contrast to the nanotubes produced in an aqueous electrolyte without CMC. Furthermore, this kind of electrolyte promoted the formation of nanotubes with higher circularity values (>0.80) in contrast to the nanotubes produced in aqueous electrolyte without CMC. Organized nanotubes formed at 15 and 10 V needed lower pH values in contrast to the nanotubes produced at 20 V. Nanotube length is affected by the pH value, anodization time and CMC content on the electrolyte. The highest nanotube length

measured in this work was about 5.85 μm. Nanotubes with an internal diameter lower than 30 nm were obtained, furthermore, nanotubes with an internal diameter about 9.5 nm were successfully produced.

3.Chapter 3
Effect of surface characteristics on the antibacterial properties of TiO_2 nanotubes produced in aqueous electrolytes with CMC

Several parts of the text and figures have been taken from:

Effect of surface characteristics on the antibacterial properties of TiO_2 nanotubes produced in aqueous electrolytes with CMC.
Robinson Aguirre Ocampo, Mónica Echeverry-Rendón, I. DeAlba-Montero, Sara Robledo, Facundo Ruiz, Félix Echeverría Echeverría.
Journal of Biomedical Materials Research Part A. (2020) 1– 18.
https://doi.org/10.1002/jbm.a.37010

Abstract

Nanotubular structures were produced on a c.p. Titanium surface by anodization in an aqueous electrolyte that contained carboxymethylcellulose (CMC) and NaF. The internal diameters obtained at voltages of 20, 10, and 2 V were about 100, 48, and 9.5 nm, respectively. Those diameters were measured using Scanning Electron Microscopy (SEM), Transmission Electron Microscopy (TEM) and Atomic Force Microscopy (AFM). Several heat treatments at 200, 350 and 600 °C were made to produce nanotubes with different TiO_2 polymorphs (anatase, rutile), at 200 °C no phase change was observed, at 350 °C the nanotubes change from amorphous phase to anatase, and at 600 °C the rutile phase was predominant. It is worth to highlight that the nanotubes produced at 2 V and heat treated at 600 °C were

composed entirely by rutile and the nanotubular structure was maintained. These phases were corroborated by X-Ray Diffraction (XRD) and Micro-Raman microscopy. Titanium suboxides were found in all evaluated nanotube coatings using Selected Area Electron Diffraction (SAED) and High Resolution Transmission Electron Microscopy (HRTEM). d-spacing maps produced with Geometric Phase Analysis (GPA) showed that the titanium suboxides were uniformly distributed in the nanotubes. All tested surfaces were superhydrophilic (high surface free energy), and the superhydrophilic behavior was maintained after at least 30 days, regardless of the heat treatment. The nanotubes with UV treatment and heat treatment at 350, and 600 °C had a bacteriostatic comportment against *S. aureus* and *P. aeruginosa*. The nanotubular coatings obtained at 20 V and heat treated at 350 °C produced the lower bacteria adhesion against both strains evaluated.

3.1 Results and discussion

3.1.1 Morphologic characterization

In our previous work [3], we studied the production of nanotubular coatings using aqueous electrolytes with CMC varying anodization variables as voltage, electrolyte temperature, electrolyte aging, anodizing time, electrolyte fluoride concentration, electrolyte CMC concentration, and electrolyte pH. From our results, we selected three kinds of conditions that produce nanotubes with different internal diameters and better morphologic characteristics (nanotube organization and clean nanotube surface) (**Figure 15**). **Table 5** shows the experimental conditions for each nanotubular coating and the internal diameter and barrier layer thickness measurements. It is worth to highlight that the other anodization parameters remain

unaltered (electrolyte temperature: room, fluoride concentration: 0.5 wt% of NaF). From **Table 5**, it is clear that the barrier layer thickness and coating thickness depend directly on the applied voltage; this relationship has been proposed in previous experimental works [153], [199], [211], [212]. From our findings, for lower voltages (i.e. 2 V), the same behavior was observed.

Table 5. Morphologic characteristics of as-anodized anodic coatings

Voltage (V)	Experimental conditions	Internal diameter (nm)	Barrier layer thickness (nm)	Coating thickness (μm)
20	Anodizing time: 5 hours, pH 4 and 0.5 wt% of CMC	99.08 ± 15.13 [3]	40.83 ± 0.62	2.83±0.02 [3]
10	Anodizing time: 5 hours, pH 1.5 and 1.5 wt% CMC	44.89 ± 6.79 [3]	31.52 ± 1.21	0.63± 0.02
2	Anodizing time: 24 hours, pH 4 and 1 wt% of CMC	9.50 ± 1.50 [3]	4.60 ± 0.38	0.10 ± 0.01

To evaluate the heat treatment effect on the properties of the nanotubular coatings; we selected several temperatures (200, 350, and 600 °C). According to the literature review and previous work, the treatment was chosen to transform the amorphous phase into anatase or rutile, or a combination of them. However, the heat treatment at 200 °C does not produce a phase change. From the literature review, the heat treatment, especially at high temperature (>500°C) modify the crystalline structure and stability of TiO_2 nanotubes [42], [50], [94], [114], [128], [129], [131], [213]. Besides, in some cases the heat treatment produces a complete collapse of the nanotubular structure [42], [131], [214]–[217] For the best of our knowledge, the majority of scientific works only reports nanotubular coatings heat treated with internal diameters higher than 80 nm; however, the effect of heat treatment in nanotubes with lower diameters (< 40 nm) have not been extensively studied. The main reason for the nanotube collapse (partially or totally) is the phase transformation from anatase to rutile [129], [134], [213], [215], [216]; however, the transformation from the amorphous phase to the anatase phase does not produce significative changes on the nanotubes [43], [214], [218], [219].

In our previous work [42], we proposed a heat treatment to produce crystalline nanotubes with a combination of rutile and anatase phases. As a consequence of the heat treatment at 600 °C, the nanotubes with the lowest internal diameter collapsed, thus, a lower temperature (560 °C) was necessary to maintain the nanotubular structure.

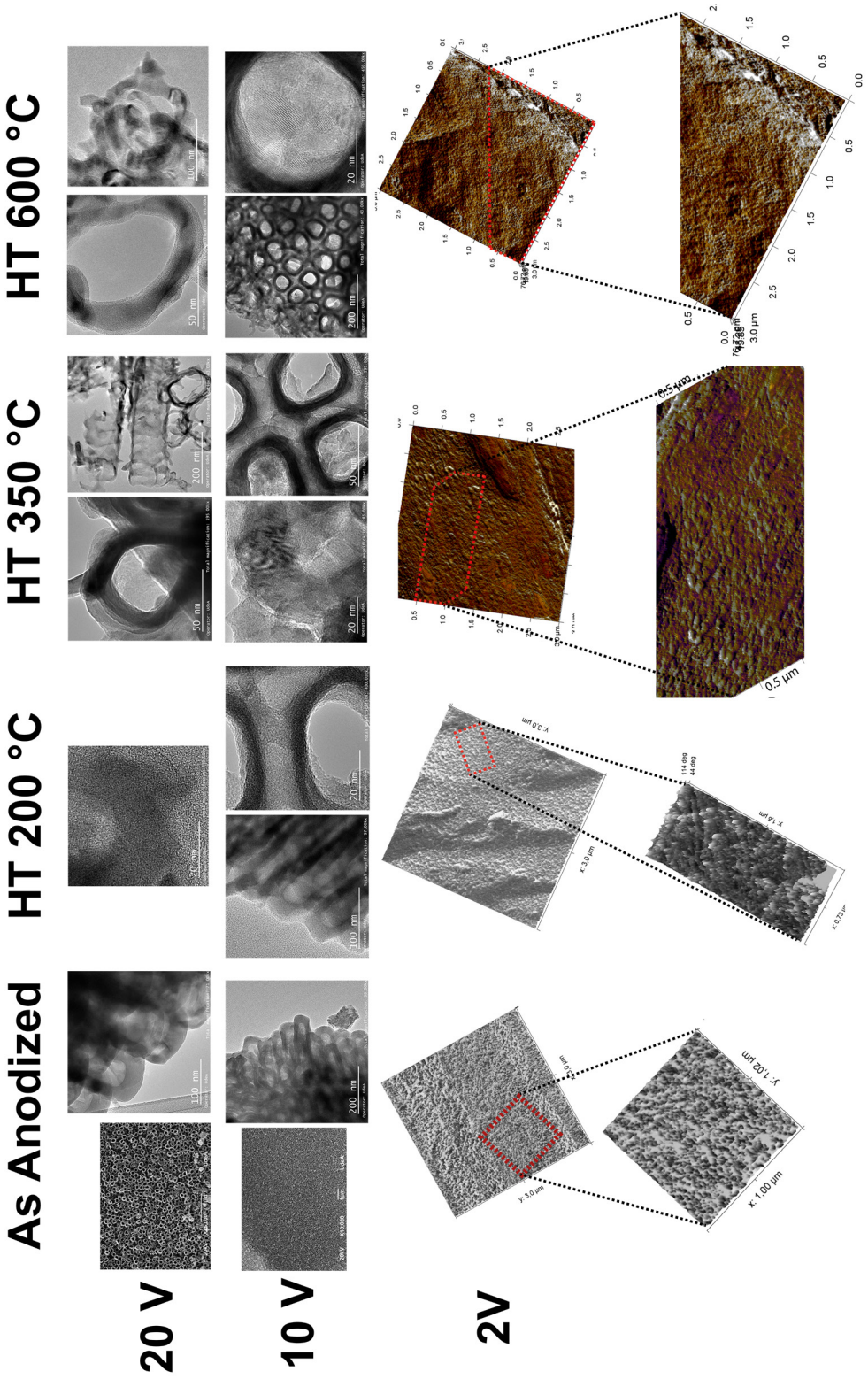

Figure 15.TEM, SEM and AFM images of nanotubes produced at 20, 10, and 2V.

Figure 15 shows the anodic coatings obtained in this experimental work. It is worth to highlight that the nanotubular structure was maintained at 600 °C, including the lowest internal diameters (about 45 nm and 9.5 nm). A possible explanation is related to the temperature ramp used in each heat treatment. From **Figure 16**, the ramp used in our previous work needed about 2 hours to increase the temperature from 25 °C to 600 °C. However, in the present work, the temperature ramp slowly increases and maintain the temperature during some time; besides, the highest temperature (600 °C) was kept only for two hours, in contrast to the four hours from our previous work.

Figure 17 shows the heat treatment effect on the nanotube length; as a consequence of the heat treatment, the nanotube length decrease; in our case, the length after heat treatment in both cases is similar (about 2.3 and 2.5 μm for 350 °C and 600 °C respectively). Previous studies indicated a decrease in length after heat treatment [42], [128], [213], [214], [218]. Chin-Lin et al. [214] produced nanotubes using an aqueous electrolyte composed by H_3PO_4 and NH_4F. They reported a decrease of 21 % in nanotube length after heat treatment at 600 °C for two hours. Fang et al. [128] produced nanotubes using an aqueous electrolyte composed by glycol, NH_4F, and water. They found a decrease of 36 % in nanotube length after heat treatment at 600 °C for two hours. However, in our experimental work, the nanotubular coatings only decrease by 12 % after heat treatment at 600 °C. Regarding the 350 °C heat treatment effect on nanotube lengths, our results were similar to those reported in previous works [43], [128], [214].

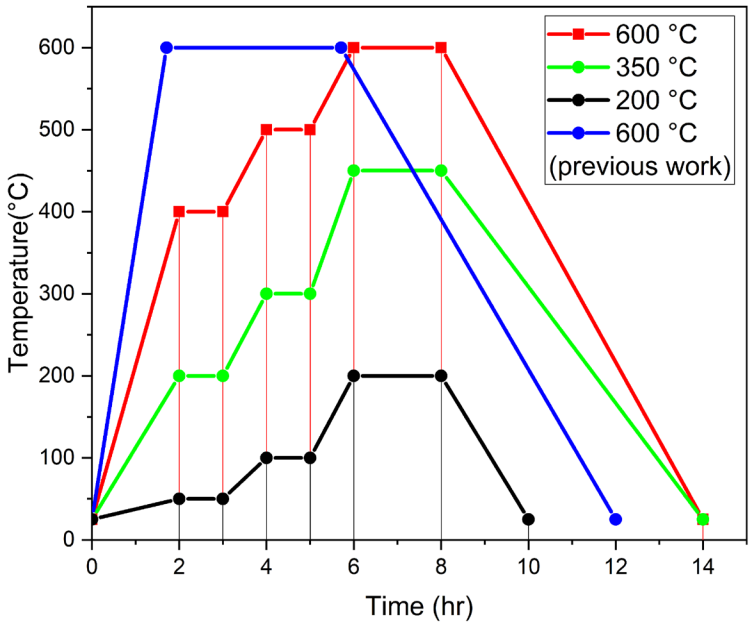

Figure 16. Temperature ramps for each heat treatment.

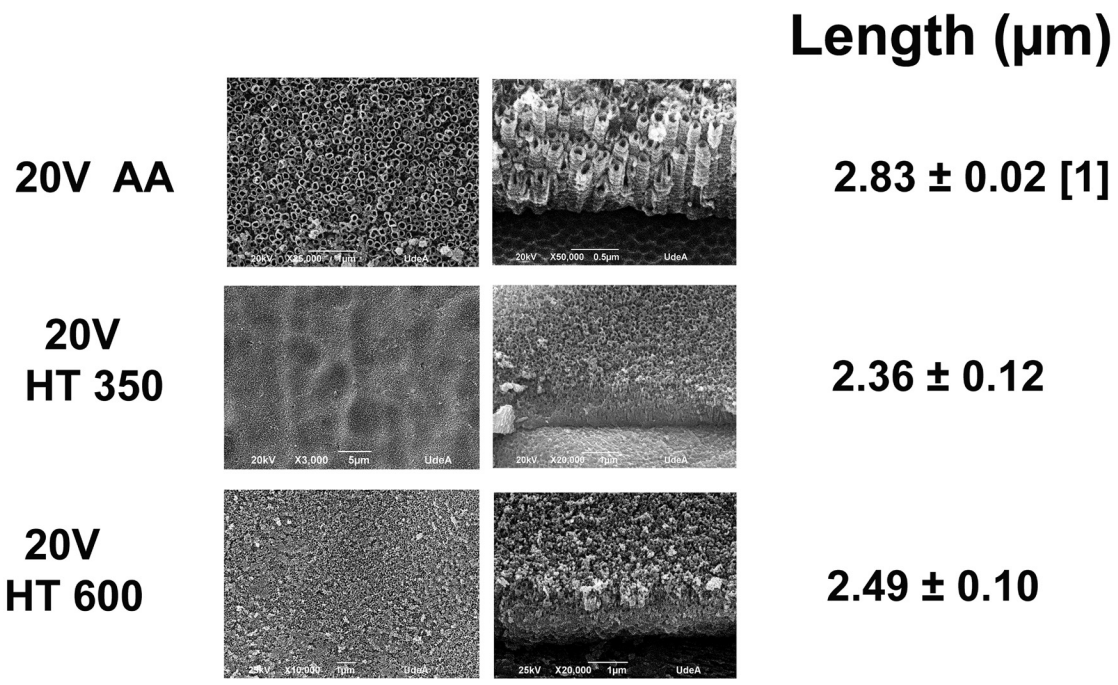

Figure 17.Heat treatment effect on nanotube length, AA (As anodized) and HT (Heat Treated).

3.1.2 Raman Characterization

Figure 18 shows the Raman spectra of all nanotube coatings with (350 and 600°C) and without heat treatment. From **Figure 18** (a), the Raman spectra for the layers without heat treatment have the characteristic form with broad peaks about 150,450 and 600 cm^{-1} reported in previous experimental works for the amorphous phase of TiO_2 [94][42][220]. Furthermore, after the heat treatment at 200 °C, the Raman spectra was equal to the coatings without heat treatment; thus, it can be concluded that it does not occur a phase change. **Figure 18** (b) and (c) show the Raman spectra for the anodic coatings after heat treatment at 350 and 600 °C respectively. From **Figure 18** (b), the predominant phase in all nanotubular layers after heat treatment at 350 °C was anatase. From **Figure 18** (c), after heat treatment at 600 °C, anatase and rutile phases were present on the nanotubes produced at 20V and 10V; however, the nanotubes produced at 2 V only was composed by rutile phase. Previous works have reported stabilization of the rutile phase in TiO_2 nanotubes with small diameters (< 30 nm) after heat treatment [206], [221], [222]. Bauer et al. [221] produced TiO_2 nanotubes in both aqueous and organic electrolytes with internal diameters lower than 30 nm and about 100 nm. The authors found that the nanotubes with an internal diameter lower than 30 nm were transformed to rutile and the nanotubes with internal diameter about 100 nm were turned into anatase after the same heat treatment at 450 °C, regardless the kind of electrolyte used. However, previous works reported that the rutile formation in TiO_2 nanotubes is highly influenced by the titanium substrate [130], [206], [221], [222], including the stabilization of the rutile phase in TiO_2 nanotubes with small diameters (< 30 nm)

[130], [206], [221]. Yang et al.[130] produced TiO_2 nanotubes using an electrolyte composed by glycerin and 0.5 wt% NH_4F at 20 V. The authors found that the nanotubes connected to the titanium surface started the transformation to the rutile phase at 550 °C. On the other hand, the authors reported that the nanotubes in a free form, namely, detached from the titanium surface, were composed entirely by anatase, inclusive after a heat treatment at 700 °C. The relationship in weight between the rutile and anatase **(**W_R/W_A) was calculated for the Raman spectra of anodic coatings heat treated at 600 °C, using the **equation 10** described by Hardcastle et al [220] and Zhang et al [223]; where I_{445} and I_{396} are the intensities at 445 and 396 cm^{-1} respectively. From **Table 6**, the rutile phase proportion increases with the decrease of voltage, namely, nanotubes with lower diameters and lengths had higher percentages of rutile phase after heat treatment at 600 °C. The last behavior has been reported by Liu et al.[206] and is closely related with the stabilization phenomenon of the rutile phase in TiO_2 nanotubes with small diameters discussed above. The authors found that the rutile phase appeared in small nanotubes compared to the bigger nanotubes, which were composed entirely by anatase, after the same heat treatment at 450 °C.

$$\frac{W_R}{W_A} = 3.64\left(\frac{I_{445}}{I_{396}}\right) \quad \textbf{(10)}$$

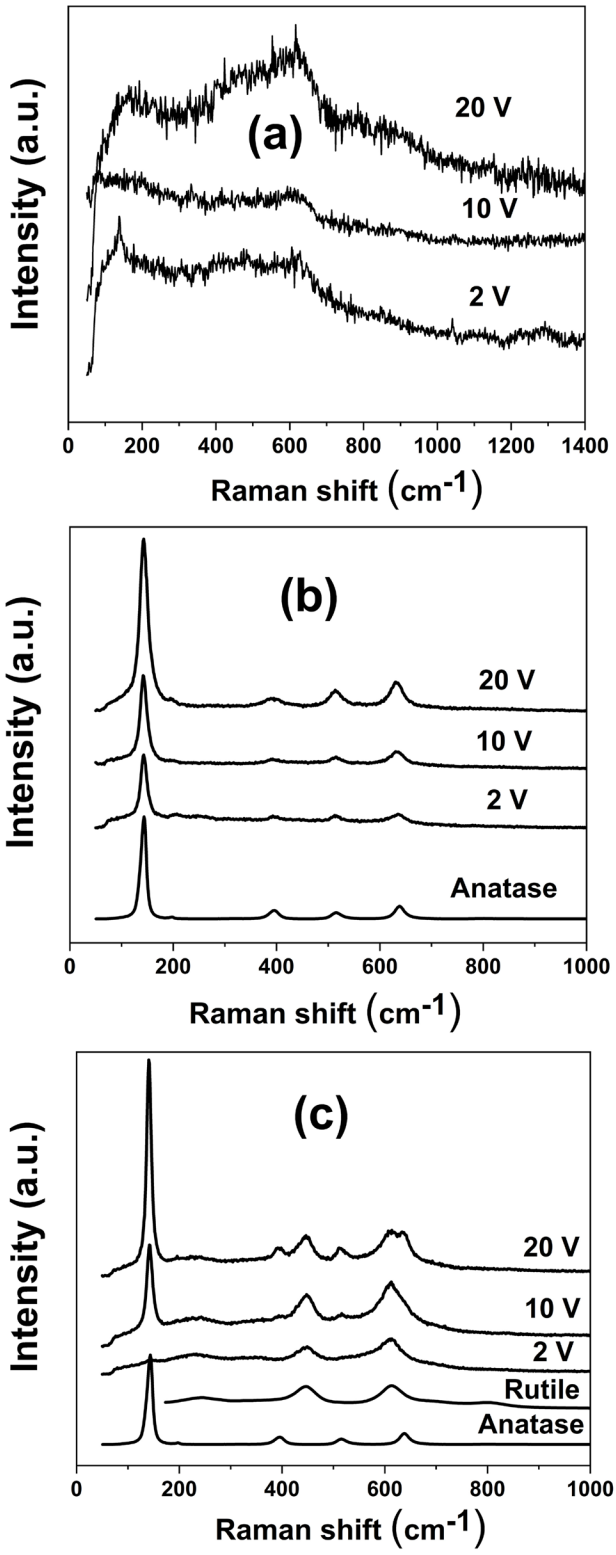

Figure 18. Raman spectra of nanotube coatings obtained without heat treatment (a) heat treated at 350 °C (b) and heat treated at 600 °C (c).

Table 6. The relationship in weight between the rutile and anatase **(**W_R/W_A) and mass fraction of rutile (f_r) for the coatings after heat treatment at 600 °C.

Voltage (V)	W_R/W_A	f_R
20	3.85	0.57
10	4.16	0.60
2	6.42	1

3.1.3 XRD Characterization

Figure 19 shows the XRD spectra of nanotube coatings as-anodized and after heat treatment at 350 and 600°C. The XRD spectra for the anodic coatings without heat treatment and heat treated at 200 °C (**Figure 19** (a)) only show peaks associated to the Titanium substrate; furthermore, those peaks are present in all XRD spectra analyzed, and from now it is not necessary to mention them. From **Figure 19** (a), at lower 2θ values (From 5 to 15°), intensity value starts in a higher value and decreasing with the increase of 2θ, with a bump about 13°; the last behavior has been reported in previous works [39], [224], [225]. Valeeva et al.[224] produced nanotubes using an electrolyte composed by ethylene glycol, NH_4F, and water. They found the same comportment in the XRD spectra at small 2θ values, and they concluded that the absence of peaks and the shape of the spectra were related to the amorphous phase. From **Figure 19** (b) after heat treatment at 350 °C, only peaks related to the anatase phase were observed for the anodic coatings obtained at 20 and 10 V. However, the XRD spectra for the nanotubes produced at 2 V after heat treatment at 350 °C do not show peaks associated with the anatase phase. **Figure 19** (c) shows characteristic peaks associated to anatase and rutile phases for anodic

coatings obtained at 20 V and 10 V after heat treatment at 600 °C; however, the nanotubes produced at 2 V after the same heat treatment were composed only by rutile phase. Spurr and Myers proposed the **equation 11** to calculate the mass fraction of rutile; where I_A and I_R are the intensities of peaks (110) and (011) of anatase and rutile respectively.

From **Table 6**, the mass fraction of rutile increases with the decrease of applied voltage; corroborating the previous results found by Raman spectroscopy. The XRD spectra confirm the previous finding from Raman spectra, showing only anatase phase after the heat treatment at 350 °C for the anodic coatings obtained at 20 and 10 V; however, the XRD spectra did not show peaks related to the anatase phase. The differences between the Raman and the XRD spectra are associated with the technique sensitivities. Previous works have been reported that the Raman technique has a higher sensitivity to the TiO_2 crystalline phases compared to XRD [226]–[228]. Wei Lu et al. [228] reported anatase trace amount detection in TiO_2 thin films using Raman characterization; on the other hand, the XRD method did not detect any anatase. Furthermore, the anodic coatings obtained at 20 and 10 V, and heat treated at 600 °C had a composition of anatase and rutile phases, and the rutile proportion increased with the decrease of voltage. The anodic coatings produced at 2V and heat treated at 600 °C were composed only by rutile phase; generally, the complete transformation to rutile phase destroys the nanotubular structure [129], [213], [215], [216]; however, for the best of our knowledge, this is the first report of nanotubes with an internal diameter about 10 nm composed entirely by rutile, which maintained the nanotubular structure (see **Figure 15**).

$$f_R = \frac{1.26 I_R}{I_A + 1.26 I_R} \quad (11)$$

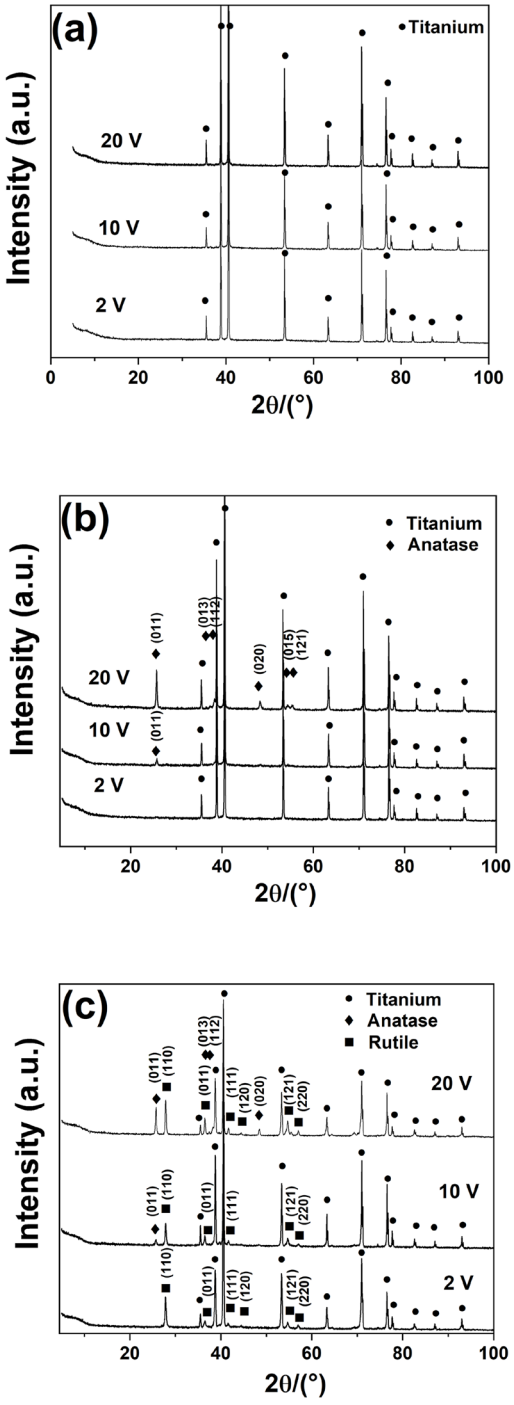

Figure 19. XRD spectra of nanotube coatings without heat treatment (a) and after heat treatment at 350 °C (b) and 600 °C (c).

3.1.4 TEM Characterization

According to the results of previous sections, the nanotubular coatings have an amorphous structure in the as-anodized condition; however, as a result of the anodization process, non-stoichiometric oxides can be formed [94], [229]–[232]. The non-stoichiometric oxides are called titanium suboxides or Magnely phases which have the empirical formula Ti_nO_{2n-1}. The Magnely phases have remarkable properties as high electrical conductivity, high corrosion resistance, and optical properties, among others [233]–[235]. Recently, Jemec Kokalj et al. [236] evaluated the environmental hazard of titanium suboxides on six organisms and two human cell lines. They found that Magnely phases can be classified as non-hazardous material. Although, the mechanism of suboxide formation on the TiO_2 nanotubes is under discussion some authors propose different explanations based on OH^- incorporation [26], and O^{2-} concentration gradients [231], [237]. Regonini et al. [26] propose an explanation to this phenomenon based on the OH^- incorporation. According to Regonini, electrolytes with compounds with bonds C=O or C-OH inject into the barrier layer OH^- ions instead O^{2-} ions producing a non-stoichiometric oxide due to the oxygen deficiency. Chen et al. [231] and Wang et al. [237] proposed a mechanism based on the O^{2-} concentration gradient. According to these authors, O^{2-} ions travel inside the barrier layer to react with Ti^{4+} ions travelling in the opposite way; depending on the coating zone more or less O^{2-} will be available to react, i. e. the deeper region in the titanium dioxide layer has the higher oxygen lack. To identify the possible crystalline phases, present on the nanotubes with and without heat treatment, we measured d-spacings from the SAED and HRTEM images and

correlated those with crystallographic databases (see materials and methods section). From **Figure 20**, d-spacing analysis was divided into two zones, in the first zone (overlapped zone), d-spacing values under 0.3509 nm are related to both titanium suboxides and TiO_2 polymorphs (anatase and rutile); thus, the phase identification in this zone was difficult. However, d-spacing values above 0.3509 nm are related only to titanium suboxides; thus, in this zone, the phase identification is easier.

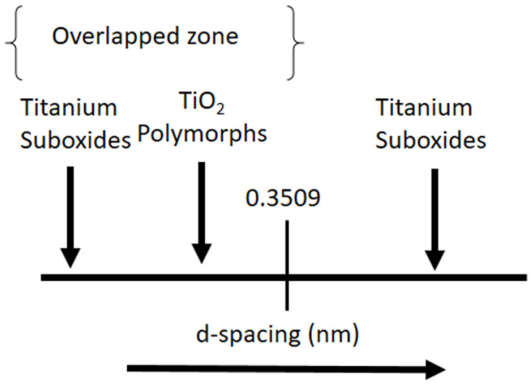

Figure 20. d-spacing distribution.

3.2.4.1 SAED Analysis

According to previous sections (XRD and Raman characterization), the TiO_2 nanotubes as-anodized have an amorphous structure. However, from **Figure 21**, SAED images in all evaluated conditions without heat treatment (as-anodized) and heat treated at 200 °C show reflections associated to titanium suboxides, anatase and rutile phases; nevertheless, the results of XRD and Raman characterization did not reveal the presence of those phases. This behavior has been reported in previous works [94], [224], [232], and a possible explanation could be related to the existence of nanocrystalline phases. Petukhov et al. [232] produced nanotubes

using an electrolyte composed by glycerol, NH_4F, and water. The authors found reflections on the SAED images associated with TiO_2 (both anatase and rutile) TiO, and Ti_2O_3; although, the XRD spectra show that the nanotubes were completely amorphous. The findings of Petukhov et al. are in agreement with our results. SAED

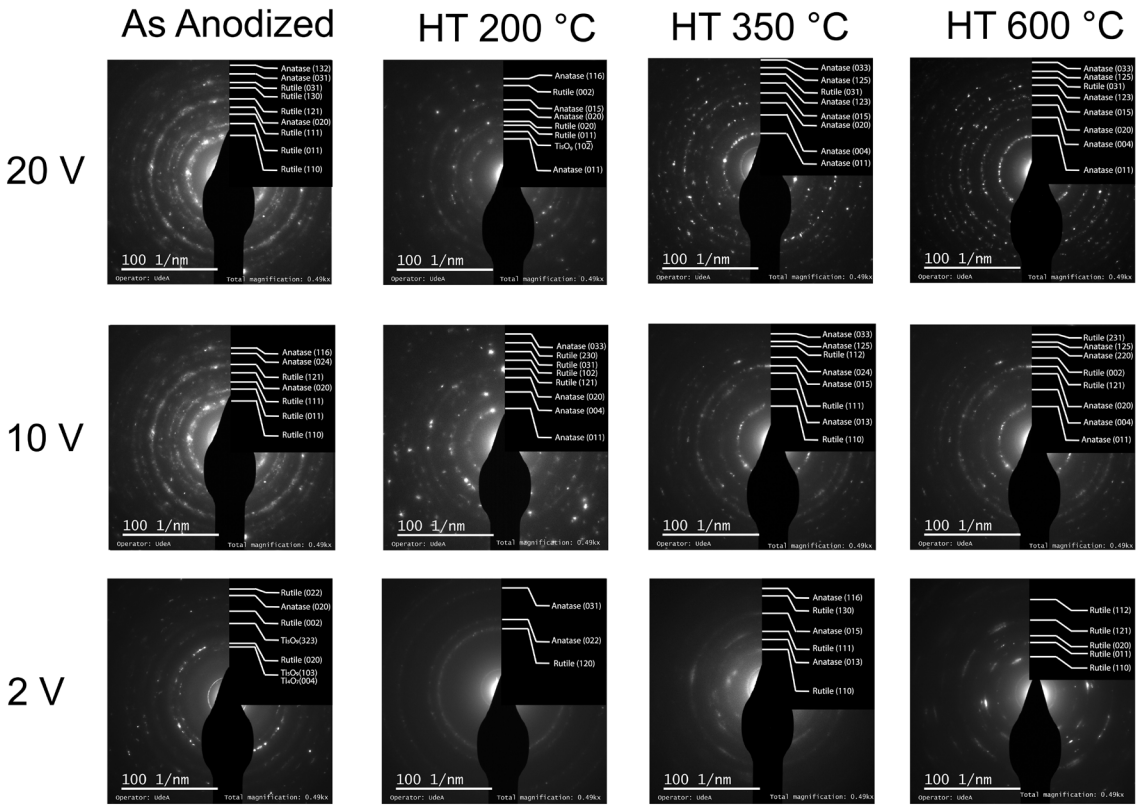

Figure 21.SAED images of the as-anodized and heat-treated anodic coatings.

images for the nanotubes heat treated at 350 °C shows mainly reflections associated to anatase phase, in accord with the previous Raman results; however, some reflections associated to rutile phase were found in all evaluated anodic coatings heat treated at 350 °C. Some authors [128]–[131], [215] have reported several temperatures in the range between 400 – 600°C in which the anatase phase starts the transformation to rutile phase. However, according to our findings, at 350 °C

already exists reflections associated with the rutile phase; the differences between rutile nucleation temperatures could also be explained based on nanocrystalline phases. Using SAED is possible to reveal weak reflections that do not have enough intensity to show up in the XRD spectra. The results for the nanotubes heat treated at 600 °C agree to previous findings which show a mix between anatase and rutile phases for anodic coatings obtained at 20 and 10 V and only the rutile phase for 2 V.

3.2.4.2 HRTEM Analysis

Figure 22 shows the HRTEM images of nanotube coatings as-anodized and after heat treatment at 350 and 600°C; and **Table 7** shows the d-spacing values measured using the FFT images (inset on the HRTEM images). d-spacing values associated with titanium suboxides were found in all evaluated nanotube coatings; even, for those anodic coatings in which SAED characterization did not reveal the presence of those phases. In the scientific literature some crystallization mechanism has been proposed [128]–[131], [215], [217]; at temperatures about 600 ° C, all the mechanism proposed show that the rutile phase formation zone is the nanotube base, and rutile does not form at the nanotube tip. From **Table 7**, d-spacing values were correlated to the characteristic peaks found in XRD spectra allowing the identification of rutile phase on different nanotube positions (Top and bottom). From our results, d-spacing values related to rutile were found at nanotube top for the anodic coatings obtained at 20 and 10 V after heat treatment at 600 °C; our findings are not in agreement to the literature mechanism proposed. It is worth to highlight that the differences on the findings could be explained based on the techniques used

to measure the reflections associated to rutile phase, due to the majority of those works used XRD in contrast with the HRTEM analysis used in this experimental work. Furthermore, the anodic coatings obtained at 10 V and heat treated at 350 °C (base and top) shows reflections associated with the rutile phase, corroborating the findings of the SAED analysis in the previous section.

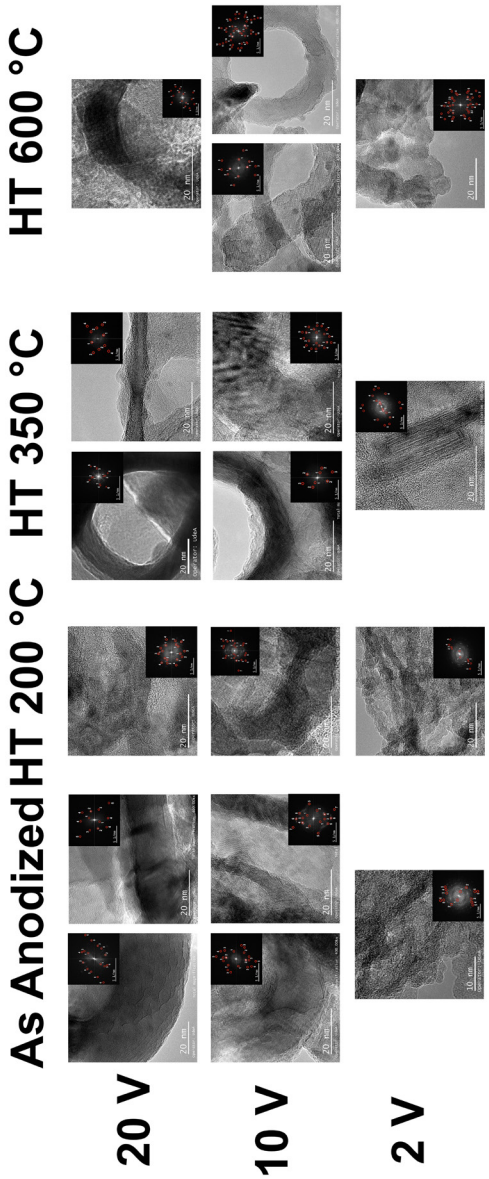

Figure 22.HRTEM and FFT images of the as-anodized and heat-treated anodic coatings.

Table 7.d-spacing measurements for the coatings produced.

View	Measured interplanar distance (nm)	Reported interplanar distance (nm)	Possible crystalline phases	Condition
Top	0.6492 (1)	0.6465	Ti_8O_{15} (0 0 4)	20 V-HT600
	0.3723 (2)	0.3782	Ti_7O_{13} (1 0 1)	
		0.3709	Ti_8O_{15} (1 0 1)	
		0.3771	Ti_4O_7 (1 0 2)	
	0.2537 (3)	0.2476	Rutile (0 1 1)	
	0.2017 (4)	0.2042	Rutile (1 2 0)	
	0.1826 (5)	0.1890	Anatase (0 2 0)	
	0.1739 (6)	0.1754	Anatase (0 2 2)	
		0.1726	Ti_4O_7 (2 0 $\bar{6}$)	
		0.1736	Ti_5O_9 (3 0 $\bar{3}$)	
		0.1750	Ti_6O_{11} (1 $\bar{4}$ $\bar{5}$)	
		0.1734	Ti_7O_{13} (3 $\bar{2}$ 5)	
		0.1753	Ti_8O_{15} (1 $\bar{4}$ $\bar{7}$)	
		0.1732	Ti_9O_{17} (1 $\bar{4}$ $\bar{7}$)	
Top	0.9178 (1)	0.9544	Ti_6O_{11} (0 0 2)	20 V-HT350
	0.7314 (2)	0.7874	Ti_5O_9 (0 0 1)	
		0.7316	Ti_9O_{17} (0 0 4)	
	0.6136 (3)	0.6170	Ti_4O_7 (0 0 2)	
		0.6465	Ti_8O_{15} (0 0 4)	
	0.5256 (4)	0.5263	Ti_4O_7 (1 0 0)	
		0.5204	Ti_5O_9 (1 0 $\bar{1}$)	
		0.5173	Ti_6O_{11} (1 0 5)	
		0.5249	Ti_7O_{13} (1 0 5)	
		0.5147	Ti_8O_{15} (1 0 5)	
		0.5231	Ti_9O_{17} (1 0 7)	
	0.4927 (5)	0.4950	Ti_6O_{11} (1 0 3)	
		0.4808	Ti_7O_{13} (1 0 7)	
		0.5001	Ti_9O_{17} (1 0 5)	
	0.3725 (6)	0.3782	Ti_7O_{13} (1 0 1)	
		0.3709	Ti_8O_{15} (1 0 1)	
		0.3771	Ti_4O_7 (1 0 2)	
Side	0.3812 (1)	0.3782	Ti_7O_{13} (1 0 1)	20 V-HT350
		0.3888	Ti_6O_{11} (1 0 1)	
		0.3771	Ti_4O_7 (1 0 2)	
	0.2623 (2)	0.2629	Ti_4O_7 (2 0 0)	
		0.2606	Ti_5O_9 (2 0 $\bar{1}$)	
		0.2623	Ti_6O_{11} (2 0 8)	
		0.2625	Ti_7O_{13} (2 0 1)	
		0.2620	Ti_8O_{15} (2 0 1)	

		0.2619	Ti_9O_{17} (0 2 1)	
	0.1750 (3)	0.1754	Anatase (0 2 2)	
		0.1726	Ti_4O_7 (2 0 $\bar{6}$)	
		0.1736	Ti_5O_9 (3 0 $\bar{3}$)	
		0.1750	Ti_6O_{11} (1 $\bar{4}$ $\bar{5}$)	
		0.1734	Ti_7O_{13} (3 $\bar{2}$ 5)	
		0.1753	Ti_8O_{15} (1 $\bar{4}$ $\bar{7}$)	
		0.1732	Ti_9O_{17} (1 $\bar{4}$ $\bar{7}$)	
	0.1547 (4)	0.1540	Ti_4O_7 (0 0 8)	
		0.1570	Ti_5O_9 (0 0 5)	
		0.1540	Ti_6O_{11} (3 0 7)	
		0.1568	Ti_7O_{13} (3 0 4)	
		0.1542	Ti_8O_{15} (1 2 2)	
		0.1546	Ti_9O_{17} (3 0 2)	
Top	0.3825 (1)	0.3782	Ti_7O_{13} (1 0 1)	20 V-HT200
		0.3888	Ti_6O_{11} (1 0 1)	
		0.3771	Ti_4O_7 (1 0 2)	
	0.2967(2)	0.3080	Ti_4O_7 (0 0 4)	
		0.2945	Ti_5O_9 (0 2 $\bar{2}$)	
		0.2968	Ti_6O_{11} (1 0 $\bar{1}$)	
		0.3008	Ti_7O_{13} (1 0 $\bar{1}$)	
		0.2999	Ti_8O_{15} (1 0 1)	
		0.2945	Ti_9O_{17} (0 2 4)	
	0.2602 (3)	0.2629	Ti_4O_7 (2 0 0)	
		0.2606	Ti_5O_9 (2 0 $\bar{1}$)	
		0.2623	Ti_6O_{11} (2 0 8)	
		0.2625	Ti_7O_{13} (2 0 1)	
		0.2620	Ti_8O_{15} (2 0 1)	
		0.2619	Ti_9O_{17} (0 2 1)	
	0.2377 (4)	0.2476	Rutile (0 1 1)	
Bottom	0.5656 (1)	0.5617	Ti_7O_{13} (0 0 4)	20 V-AA
	0.3968 (2)	0.3925	Ti_5O_9 (0 0 2)	
		0.3888	Ti_6O_{11} (1 0 1)	
		0.3890	Ti_7O_{13} (1 0 9)	
	0.3762 (3)	0.3782	Ti_7O_{13} (1 0 1)	
		0.3709	Ti_8O_{15} (1 0 1)	
		0.3771	Ti_4O_7 (1 0 2)	
	0.3332 (4)	0.3347	Ti_4O_7 (0 2 0)	
		0.3348	Ti_5O_9 (0 2 $\bar{1}$)	
		0.3364	Ti_6O_{11} (1 $\bar{2}$ $\bar{1}$)	
		0.3357	Ti_7O_{13} (1 $\bar{2}$ $\bar{1}$)	
		0.3347	Ti_8O_{15} (1 $\bar{2}$ $\bar{1}$)	
		0.3343	Ti_9O_{17} (1 $\bar{2}$ $\bar{1}$)	
	0.2527 (5)	0.2476	Rutile (0 1 1)	

	0.1840 (6)	0.1890	Anatase (0 2 0)	
Side	0.6306 (1)	0.6465	Ti_8O_{15} (0 0 4)	20 V-AA
	0.3672 (2)	0.3655	Ti_8O_{15} (1 0 1)	
		0.3654	Ti_9O_{17} (1 0 1)	
	0.3027 (3)	0.3080	Ti_4O_7 (0 0 4)	
		0.2945	Ti_5O_9 (0 2 $\bar{2}$)	
		0.2968	Ti_6O_{11} (1 0 $\bar{1}$)	
		0.3008	Ti_7O_{13} (1 0 $\bar{1}$)	
		0.2999	Ti_8O_{15} (1 0 1)	
		0.2945	Ti_9O_{17} (0 2 4)	
	0.2439 (4)	0.2476	Rutile (0 1 1)	
	0.1535 (5)	0.1540	Ti_4O_7 (0 0 8)	
		0.1570	Ti_5O_9 (0 0 5)	
		0.1540	Ti_6O_{11} (3 0 7)	
		0.1568	Ti_7O_{13} (3 0 4)	
		0.1542	Ti_8O_{15} (1 2 2)	
		0.1546	Ti_9O_{17} (3 0 2)	
Top	1.0943 (1)	0.9544	Ti_6O_{11} (0 0 2)	10 V-HT600
	0.7463 (2)	0.7874	Ti_5O_9 (0 0 1)	
		0.7316	Ti_9O_{17} (0 0 4)	
	0.6050 (3)	0.6170	Ti_4O_7 (0 0 2)	
		0.6465	Ti_8O_{15} (0 0 4)	
	0.3884 (4)	0.3888	Ti_6O_{11} (1 0 1)	
		0.3890	Ti_7O_{13} (1 0 9)	
	0.3686 (5)	0.3655	Ti_8O_{15} (1 0 1)	
		0.3654	Ti_9O_{17} (1 0 1)	
	0.2430 (6)	0.2476	Rutile (0 1 1)	
	0.2221 (7)	0.2283	Rutile (0 2 0)	
	0.2104 (8)	0.2177	Rutile (1 1 1)	
	0.2042 (9)	0.2042	Rutile (1 2 0)	
	0.1733 (10)	0.1754	Anatase (0 2 2)	
		0.1726	Ti_4O_7 (2 0 $\bar{6}$)	
		0.1736	Ti_5O_9 (3 0 $\bar{3}$)	
		0.1750	Ti_6O_{11} (1 $\bar{4}$ $\bar{5}$)	
		0.1734	Ti_7O_{13} (3 $\bar{2}$ 5)	
		0.1753	Ti_8O_{15} (1 $\bar{4}$ $\bar{7}$)	
		0.1732	Ti_9O_{17} (1 $\bar{4}$ $\bar{7}$)	
	0.1536 (11)	0.1540	Ti_4O_7 (0 0 8)	
		0.1570	Ti_5O_9 (0 0 5)	
		0.1540	Ti_6O_{11} (3 0 7)	
		0.1568	Ti_7O_{13} (3 0 4)	
		0.1542	Ti_8O_{15} (1 2 2)	
		0.1546	Ti_9O_{17} (3 0 2)	

	0.1309 (12)	0.1335	Anatase (2 2 0)	
Bottom	0.3691 (1)	0.3655	Ti_8O_{15} (1 0 1)	10 V-HT600
		0.3654	Ti_9O_{17} (1 0 1)	
	0.2544(2)	0.2476	Rutile (0 1 1)	
	0.1767 (3)	0.1754	Anatase (0 2 2)	
		0.1726	Ti_4O_7 (2 0 $\bar{6}$)	
		0.1736	Ti_5O_9 (3 0 $\bar{3}$)	
		0.1750	Ti_6O_{11} (1 $\bar{4}$ $\bar{5}$)	
		0.1734	Ti_7O_{13} (3 $\bar{2}$ 5)	
		0.1753	Ti_8O_{15} (1 $\bar{4}$ $\bar{7}$)	
		0.1732	Ti_9O_{17} (1 $\bar{4}$ $\bar{7}$)	
Bottom	0.6733 (1)	0.6170	Ti_4O_7 (0 0 2)	10 V-HT350
		0.6465	Ti_8O_{15} (0 0 4)	
	0.3844 (2)	0.3888	Ti_6O_{11} (1 0 1)	
		0.3890	Ti_7O_{13} (1 0 9)	
	0.2871 (3)	0.2817	Ti_4O_7 (1 0 $\bar{4}$)	
		0.2833	Ti_6O_{11} (0 2 2)	
		0.2808	Ti_7O_{13} (0 0 8)	
		0.2808	Ti_8O_{15} (1 $\bar{2}$ $\bar{7}$)	
		0.2897	Ti_9O_{17} (1 $\bar{2}$ 3)	
	0.2518 (4)	0.2476	Rutile (0 1 1)	
	0.2138 (5)	0.2177	Rutile (1 1 1)	
Top	0.6329 (1)	0.6170	Ti_4O_7 (0 0 2)	10 V-HT350
		0.6465	Ti_8O_{15} (0 0 4)	
	0.3705 (2)	0.3782	Ti_7O_{13} (1 0 1)	
		0.3709	Ti_8O_{15} (1 0 1)	
		0.3771	Ti_4O_7 (1 0 2)	
	0.2462 (3)	0.2476	Rutile (0 1 1)	
	0.8464 (1)	0.7874	Ti_5O_9 (0 0 1)	
		0.9544	Ti_6O_{11} (0 0 2)	
		0.7316	Ti_9O_{17} (0 0 4)	
	0.5324 (2)	0.5263	Ti_4O_7 (1 0 0)	
		0.5204	Ti_5O_9 (1 0 $\bar{1}$)	
		0.5173	Ti_6O_{11} (1 0 5)	
		0.5249	Ti_7O_{13} (1 0 5)	
		0.5147	Ti_8O_{15} (1 0 5)	
		0.5231	Ti_9O_{17} (1 0 7)	
	0.3625 (3)	0.3655	Ti_8O_{15} (1 0 1)	
		0.3654	Ti_9O_{17} (1 0 1)	

Bottom	0.2621 (4)	0.2629	Ti_4O_7 (2 0 0)	10 V-HT200
		0.2606	Ti_5O_9 (2 0 $\bar{1}$)	
		0.2623	Ti_6O_{11} (2 0 8)	
		0.2625	Ti_7O_{13} (2 0 1)	
		0.2620	Ti_8O_{15} (2 0 1)	
		0.2619	Ti_9O_{17} (0 2 1)	
	0.2321 (5)	0.2283	Rutile (0 2 0)	
	0.1778 (6)	0.1754	Anatase (0 2 2)	
		0.1726	Ti_4O_7 (2 0 $\bar{6}$)	
		0.1736	Ti_5O_9 (3 0 $\bar{3}$)	
		0.1750	Ti_6O_{11} (1 $\bar{4}$ $\bar{5}$)	
		0.1734	Ti_7O_{13} (3 $\bar{2}$ 5)	
		0.1753	Ti_8O_{15} (1 $\bar{4}$ $\bar{7}$)	
		0.1732	Ti_9O_{17} (1 $\bar{4}$ $\bar{7}$)	
	0.1310 (7)	0.1335	Anatase (2 2 0)	
Side	0.5411 (1)	0.5263	Ti_4O_7 (1 0 0)	10 V-AA
		0.5204	Ti_5O_9 (1 0 $\bar{1}$)	
		0.5173	Ti_6O_{11} (1 0 5)	
		0.5249	Ti_7O_{13} (1 0 5)	
		0.5147	Ti_8O_{15} (1 0 5)	
		0.5231	Ti_9O_{17} (1 0 7)	
	0.4697 (2)	0.4722	Ti_5O_9 (1 0 0)	
		0.4705	Ti_7O_{13} (1 0 3)	
	0.3623 (3)	0.3655	Ti_8O_{15} (1 0 1)	
		0.3654	Ti_9O_{17} (1 0 1)	
	0.3382 (4)	0.3347	Ti_4O_7 (0 2 0)	
		0.3348	Ti_5O_9 (0 2 $\bar{1}$)	
		0.3364	Ti_6O_{11} (1 $\bar{2}$ $\bar{1}$)	
		0.3357	Ti_7O_{13} (1 $\bar{2}$ $\bar{1}$)	
		0.3347	Ti_8O_{15} (1 $\bar{2}$ $\bar{1}$)	
		0.3343	Ti_9O_{17} (1 $\bar{2}$ $\bar{1}$)	
	0.2664 (5)	0.2629	Ti_4O_7 (2 0 0)	
		0.2606	Ti_5O_9 (2 0 $\bar{1}$)	
		0.2623	Ti_6O_{11} (2 0 8)	
		0.2625	Ti_7O_{13} (2 0 1)	
		0.2620	Ti_8O_{15} (2 0 1)	
		0.2619	Ti_9O_{17} (0 2 1)	
	0.2271 (6)	0.2283	Rutile (0 2 0)	
	0.1748 (7)	0.1754	Anatase (0 2 2)	
		0.1726	Ti_4O_7 (2 0 $\bar{6}$)	
		0.1736	Ti_5O_9 (3 0 $\bar{3}$)	
		0.1750	Ti_6O_{11} (1 $\bar{4}$ $\bar{5}$)	
		0.1734	Ti_7O_{13} (3 $\bar{2}$ 5)	
		0.1753	Ti_8O_{15} (1 $\bar{4}$ $\bar{7}$)	
		0.1732		

			Ti_9O_{17} (1 $\bar{4}$ $\bar{7}$)	
Bottom	0.4820 (1)	0.4950	Ti_6O_{11} (1 0 3)	10 V-AA
		0.4808	Ti_7O_{13} (1 0 7)	
		0.5001	Ti_9O_{17} (1 0 5)	
	0.3712 (2)	0.3782	Ti_7O_{13} (1 0 1)	
		0.3709	Ti_8O_{15} (1 0 1)	
		0.3771	Ti_4O_7 (1 0 2)	
	0.2851 (3)	0.2817	Ti_4O_7 (1 0 $\bar{4}$)	
		0.2833	Ti_6O_{11} (0 2 2)	
		0.2808	Ti_7O_{13} (0 0 8)	
		0.2808	Ti_8O_{15} (1 $\bar{2}$ $\bar{7}$)	
		0.2897	Ti_9O_{17} (1 $\bar{2}$ 3)	
	0.2140 (4)	0.2177	Rutile (1 1 1)	
	0.1842 (5)	0.1890	Anatase (0 2 0)	
Side	0.5040 (1)	0.5263	Ti_4O_7 (1 0 0)	2 V-HT600
		0.5204	Ti_5O_9 (1 0 $\bar{1}$)	
		0.5173	Ti_6O_{11} (1 0 5)	
		0.5249	Ti_7O_{13} (1 0 5)	
		0.5147	Ti_8O_{15} (1 0 5)	
		0.5231	Ti_9O_{17} (1 0 7)	
	0.3812 (2)	0.3782	Ti_7O_{13} (1 0 1)	
		0.3888	Ti_6O_{11} (1 0 1)	
		0.3771	Ti_4O_7 (1 0 2)	
	0.3547 (3)	0.3509	Anatase (0 1 1)	
	0.3129 (4)	0.3228	Rutile (1 1 0)	
	0.2710 (5)	0.2798	Ti_4O_7 (0 2 2)	
		0.2725	Ti_5O_9 (0 2 1)	
		0.2750	Ti_7O_{13} (0 2 2)	
	0.2390 (6)	0.2476	Rutile (0 1 1)	
	0.1835(7)	0.1890	Anatase (0 2 0)	
Side	1.0564 (1)	0.9544	Ti_6O_{11} (0 0 2)	2 V-HT350
	0.6356 (2)	0.6170	Ti_4O_7 (0 0 2)	
		0.6465	Ti_8O_{15} (0 0 4)	
	0.3799 (3)	0.3782	Ti_7O_{13} (1 0 1)	
		0.3771	Ti_4O_7 (1 0 2)	
	0.2091 (4)	0.2042	Rutile (1 2 0)	
	0.1515 (5)	0.1540	Ti_4O_7 (0 0 8)	
		0.1570	Ti_5O_9 (0 0 5)	
		0.1540	Ti_6O_{11} (3 0 7)	
		0.1568	Ti_7O_{13} (3 0 4)	
		0.1542	Ti_8O_{15} (1 2 2)	
		0.1546	Ti_9O_{17} (3 0 2)	

	0.8760 (1)	0.9544	Ti_6O_{11} (0 0 2)	
	0.2671 (2)	0.2629	Ti_4O_7 (2 0 0)	
		0.2606	Ti_5O_9 (2 0 $\bar{1}$)	
		0.2623	Ti_6O_{11} (2 0 8)	
		0.2625	Ti_7O_{13} (2 0 1)	
		0.2620	Ti_8O_{15} (2 0 1)	
		0.2619	Ti_9O_{17} (0 2 1)	
	0.2302 (3)	0.2283	Rutile (0 2 0)	
Side	01818 (4)	0.1890	Anatase (0 2 0)	2 V-HT200
	0.1552 (5)	0.1540	Ti_4O_7 (0 0 8)	
		0.1570	Ti_5O_9 (0 0 5)	
		0.1540	Ti_6O_{11} (3 0 7)	
		0.1568	Ti_7O_{13} (3 0 4)	
		0.1542	Ti_8O_{15} (1 2 2)	
		0.1546	Ti_9O_{17} (3 0 2)	
	0.6498 (1)	0.6170	Ti_4O_7 (0 0 2)	
		0.6465	Ti_8O_{15} (0 0 4)	
	0.2645 (2)	0.2629	Ti_4O_7 (2 0 0)	
		0.2606	Ti_5O_9 (2 0 $\bar{1}$)	
		0.2623	Ti_6O_{11} (2 0 8)	
		0.2625	Ti_7O_{13} (2 0 1)	
		0.2620	Ti_8O_{15} (2 0 1)	2 V-AA
		0.2619	Ti_9O_{17} (0 2 1)	
	0.2322 (3)	0.2283	Rutile (0 2 0)	
Side	0.2048 (4)	0.2042	Rutile (1 2 0)	
	0.1805 (5)	0.1890	Anatase (0 2 0)	
	0.1522 (6)	0.1540	Ti_4O_7 (0 0 8)	
		0.1570	Ti_5O_9 (0 0 5)	
		0.1540	Ti_6O_{11} (3 0 7)	
		0.1568	Ti_7O_{13} (3 0 4)	
		0.1542	Ti_8O_{15} (1 2 2)	
		0.1546	Ti_9O_{17} (3 0 2)	

3.2.4.3 d-spacing maps

Previous experimental works [94], [229]–[232], [237] reveal the presence of titanium suboxides; however, from the literature reviewed so far, there is not enough evidence about suboxides have a preferred nucleation zone on the nanotube (i.e., base, top or walls). Thus, Geometric Phase Analysis (GPA) [56], [238], [239] was used to generate d-spacing maps using the tool "gpagui" in the CrysTBox software.

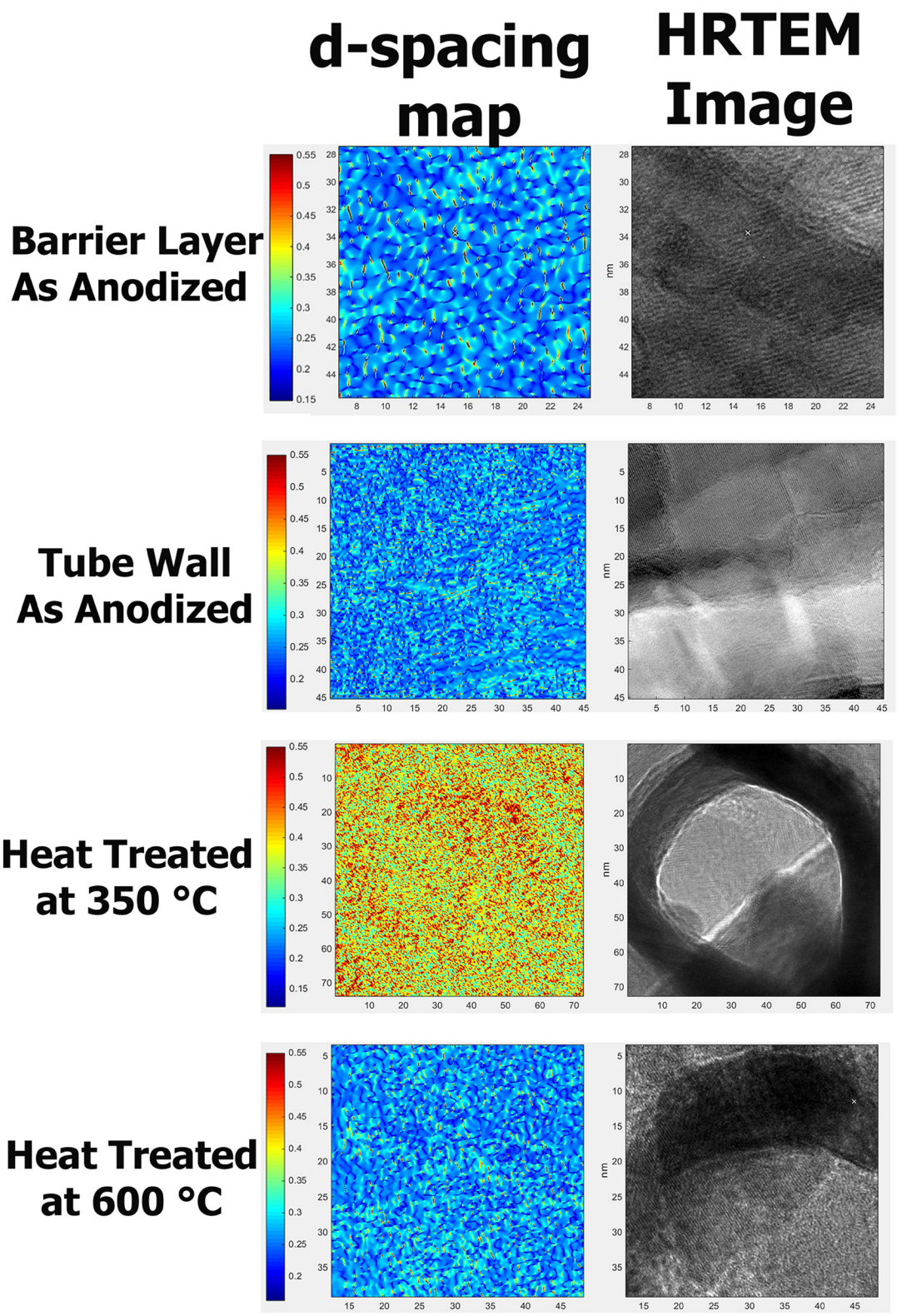

Figure 23.Geometric phase analysis of the as-anodized and heat-treated anodic coatings obtained at 20 V.

The d-spacing maps show the distribution of d-spacing values of an HRTEM image. **Figure 23** shows HRTEM images of anodic coatings obtained at 20 V with and without heat treatment and their d-spacing map. According to previous sections, d-spacing values upper 0.3509 nm are related to titanium suboxides; thus, from **Figure 23**, it is clear that the titanium suboxides are uniformly distributed in all evaluated conditions. Wang et al. [231] proposed a mechanism for TiO_2 nanotube formation in which the formed oxide is mainly TiO_2, however, the oxide located at the interior is composed by titanium suboxides formed due to the lack of O^{2-}. Our results are in agreement and corroborate the findings obtained for these authors.

Table 8. Contact angle at three different times and surface free energy measurements.

Sample	Contact angle (°) t=0 days	Contact angle (°) t=30 days	Contact angle (°) t=60 days	Surface free energy (mJ/m^2) t=60 days
20 V-AA	≈0	11.32	18.44	69.32
20 V-UV	≈0	≈0	≈0	72.80
20 V-TT 200	≈0	≈0	10.62	71.59
20 V-TT 350	≈0	≈0	≈0	72.80
20 V-TT 600	≈0	≈0	≈0	72.80
10 V-AA	≈0	8.76	9.92	71.73
10 V-UV	≈0	≈0	≈0	72.80
10 V-TT 200	≈0	10.63	12.34	71.18
10 V-TT 350	≈0	≈0	≈0	72.80
10 V-TT 600	≈0	≈0	≈0	72.80
2 V-AA	≈0	23.89	27.60	69.59
2 V-UV	≈0	≈0	≈0	72.80
2 V-TT200	≈0	≈0	12.16	71.22
2 V-TT350	≈0	≈0	≈0	72.80
2 V-TT600	≈0	≈0	≈0	72.80

3.1.5 Contact angle, surface free energy, and roughness measurements.

Table 8 shows the contact angle measurements at three different times (0, 30, and 60 days) and the surface free energy (SFE) calculations at 60 days. From **Table 8**, all anodic coatings at t=0 days (as produced) had a superhydrophilic comportment (≈0 °) regardless, the samples were heat treated, UV treated, or only anodized. After 30 days, the samples heat and UV treated continued with a superhydrophilic behavior; however, although the as-anodized samples (20 and 10 V) had a superhydrophilic comportment, the anodic coating obtained at 2 V as-anodized change to a hydrophilic behavior. After 60 days, the samples heat treated at 350 and 600 °C and UV treated continued with a superhydrophilic behavior. Anodic coatings with a superhydrophilic comportment have the higher SFE values; our results are in agreement to previous works [1], [42], [240]. From the literature review, the nanotubular coatings as-anodized are generally hydrophilic [42], [51], [96], [107], [143], [241]–[243]; however, the hydrophobic [42], [141], [244], [245] and superhydrophilic [109], [147], [246] behavior also have been reported. From **Table 8**, all anodic coatings as-anodized were superhydrophilic, regardless of the internal diameter and roughness differences (**Table 9**). Previous works have reported differences in the contact angle values related to the inner diameter [96], [147], [241], [245] and roughness [51], [87], [242], [247]; however, our results are not in agreement with those previous investigations. Possible explanations for the contact angle values of the as-anodized surfaces could be related to aggregations on the nanotube tip (nanograss) [248] and the anodizing time [249], [250]. Yang et al. [248]

produced nanotubes using an electrolyte composed by ethylene glycol, NH_4F, and water. They found that the clean nanotubes, namely, those without aggregations on

Table 9. Roughness and surface potential measurements of the anodic coatings.

Sample	Ra (μm)	Rsm (μm)	Rz (μm)	Rq (μm)	Surface potential (mV)
20 V-AA	0.55 ± 0.06	85.47 ± 28.41	3.53 ± 0.51	0.69 ± 0.08	359.96 ± 14.99
20 V-UV	0.55 ± 0.06	85.47 ± 28.41	3.53 ± 0.51	0.69 ± 0.08	-24.08 ± 3.74
20 V-TT 200	0.79 ± 0.09	74.81 ± 10.20	4.48 ± 0.42	0.98 ± 0.09	426.86 ± 6.68
20 V-TT 350	0.86 ± 0.19	116.15 ± 27.07	4.66 ± 0.79	1.05 ± 0.21	421.37 ± 4.24
20 V-TT 600	0.55 ± 0.06	85.47 ± 28.41	3.53 ± 0.51	0.69 ± 0.08	420.45 ± 10.08
10 V-AA	0.19 ± 0.03	42.36 ± 6.38	1.47 ± 0.17	0.24 ± 0.03	407.17 ± 5.34
10 V-UV	0.19 ± 0.03	42.36 ± 6.38	1.47 ± 0.17	0.24 ± 0.03	116.99 ± 2.73
10 V-TT 200	0.83 ± 0.08	68.02 ± 17.45	5.10 ± 0.55	1.05 ± 0.10	379.98 ± 10.65
10 V-TT 350	0.35 ± 0.02	41.12 ± 6.67	2.32 ± 0.17	0.43 ± 0.02	314.93 ± 12.78
10 V-TT 600	1.01 ± 0.14	97.62 ± 17.35	5.85 ± 0.74	1.25 ± 0.16	258.81 ± 5.24
2 V-AA	0.32 ± 0.03	52.85 ± 7.00	2.31 ± 0.21	0.40 ± 0.03	341.97 ± 5.27
2 V-UV	0.32 ± 0.03	52.85 ± 7.00	2.31 ± 0.21	0.40 ± 0.03	82.14 ± 3.40
2 V-TT200	0.70 ± 0.10	62.85 ± 28.80	4.32 ± 0.56	0.87 ± 0.12	253.06 ± 9.44
2 V-TT350	0.62 ± 0.09	55.72 ± 3.08	4.03 ± 0.67	0.78 ± 0.12	158.91 ± 6.44
2 V-TT600	0.64 ± 0.06	69.26 ± 16.45	3.74 ± 0.33	0.79 ± 0.08	423.45 ± 4.91

the nanotube tip or “nanograss” had a superhydrophilic behavior (≈0 °) in contrast to the nanograss covered nanotubes which have a hydrophilic behavior (40 °). The results found by Yang et al. are in agreement with our findings; from our previous work [3] and Figs. 1 and 3, the anodic coatings as-anodized were nanograss free; thus, this could be a reason for the superhydrophilic comportment of the as-anodized coatings. Luo et al. [249], [250] produced nanotubes using an electrolyte composed

by ethylene glycol, HF, and water. They found that increasing the anodizing time the contact angle decreased, and anodic coatings obtained between 6 and 8 hours had superhydrophilic behavior. The findings of Luo et al. are in agreement with our results; from **Table 5**, the anodizing time for the anodic coatings is greater than or equal to 5 hours, thus, this could be another cause for the superhydrophilic comportment of the as-anodized coatings. From the literature review, the nanotubes heat and UV treated had a superhydrophilic comportment [43], [109], [141], [142], [218]; furthermore, it is worth to highlight that superhydrophilic behavior of this kind of samples was kept for two months after they were produced. According to our results, the superhydrophilic behavior and time that this comportment continues depend both on the nanotubes and their crystallographic phases [143], [218], [240].

3.1.6 Antibacterial Properties

Figure 24 shows the results of the antimicrobial activity test of the anodized surfaces using *S. aureus* and *P. aeruginosa* strains. From **Figure 24**, not inhibition halo is present around the samples; however, some kinds of samples present *S. aureus* growing up on their surface (marked with an asterisk); on the other hand, *P. aeruginosa* did not grow up in any of the evaluated anodic coatings. According to Pankey et al. [251], a bacteriostatic material could be defined as a material that prevents bacteria growth. From our results, the coatings on which does not grow up bacteria could be described as bacteriostatic. The bacteriostatic behavior could be explained based on the anodic coating characteristics (wettability, surface free energy, crystallographic phase, among others) [34], [252] and the bacteria strain

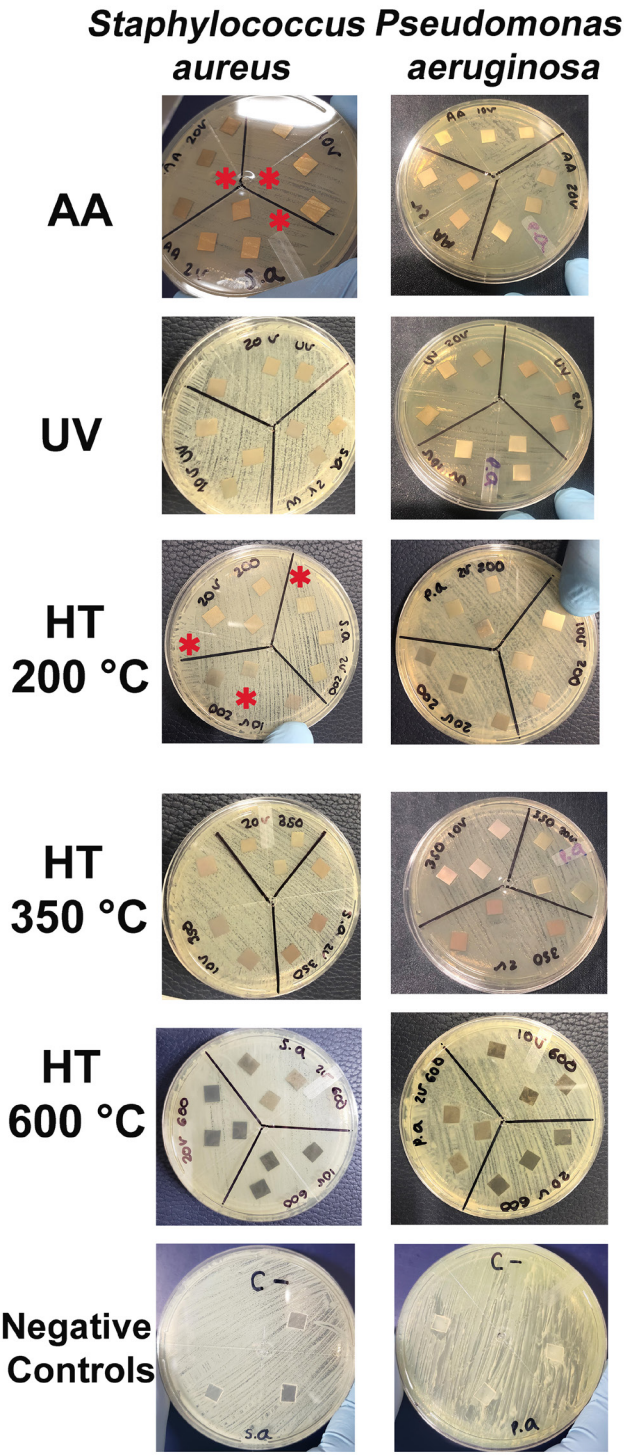

Figure 24. Photographs of the antimicrobial activity test *(S. aureus* and *P. aeruginosa)* of the anodized surfaces.

features. From the literature review, bacteria strain features as hydrophilicity or hydrophobicity have been reported in previous works [48], [109], [253]–[258].

S. aureus strain has been reported as hydrophilic [109], [255]–[257]; on the other hand, *P. aeruginosa* has been reported as very hydrophobic [253], [256], [257]. Orapiriyakul et al.[34] reports that the bacteria adhesion and proliferation depends on the material surface characteristic and bacteria features, namely, hydrophobic bacteria prefer a hydrophobic surface and vice versa. Likewise, Birkenhauer et al. [259] reported that material characteristics influence bacteria adherence, morphology, development, and growth. From **Table 8**, all anodic coatings as anodized were superhydrophilic; thus, this explains the reason why *S. aureus* grew up on all as-anodized surfaces no matter the internal diameter and, *P. aeruginosa* did not grow up in any of all as-anodized coatings despite the inner diameter. Previous works [34], [260]–[268] have reported that UV light on TiO_2 nanotubes reduce the bacteria colonization and inhibit biofilm formation; nevertheless, the majority of reports indicate that this effect remains only when the light source is on. On the other hand, some authors reports [263]–[266] a post-irradiation antibacterial effect on the TiO_2 nanotubes. According to our results, all UV treated were superhydrophilic; however, S. *aureus* and *P. aeruginosa* both did not grow up in any of the UV treated samples; the most probable explanation is related to the UV post-irradiation effect on the TiO_2 nanotubes. From **Table 9**, the surface potential of the samples UV-treated is lower than the as-anodized samples; according to Gallardo-Moreno et al. [264] and Zhang et al. [263], the UV irradiation produces an excess of surface charge due to the slow recombination of electron-holes pair. The antibacterial effect is due to the excess of electrons that can generate reactive oxide species (ROS) such as: hydroxyl radical, hydrogen peroxide and superoxide radical, which induce bacteria inactivation [261], [266], [269]–[274].

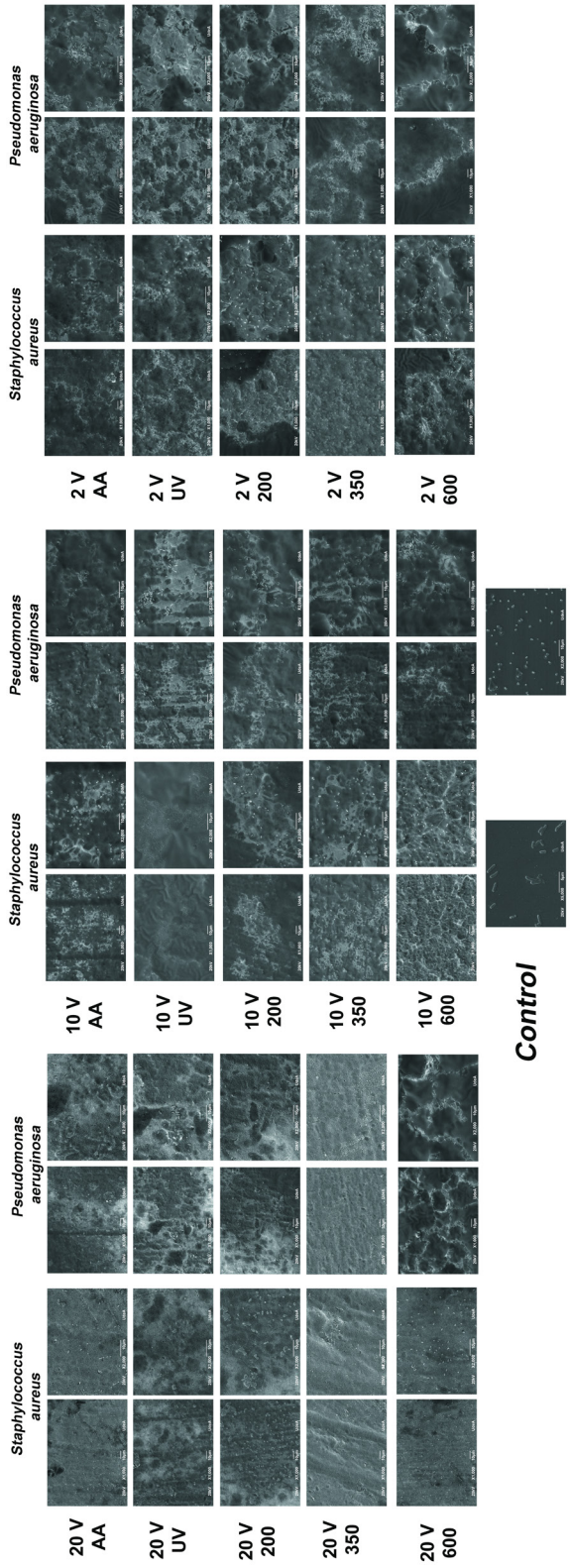

Figure 25. Representative SEM images of bacterial adhesion (*S. aureus* and *P. aeruginosa) on anodized surfaces.*

Likewise, Birkenhauer et al. [259] reported that materials with a tendency to negative surface potentials values had an antibacterial activity on *P. aeruginosa* and MRSA. Our results are in agreement with these authors, the values of surface potential in UV treated samples were lower (more negative) in contrast to the as-anodized samples; those results are in agreement with the previous works of Daviosdóttir et al. [275] and Motola et al. [267] . The samples heat treated at 200 °C have the same antibacterial behavior that the as-anodized samples; thus, this heat treatment does not have an additional effect on the antibacterial performance. S. *aureus* and *P. aeruginosa* both did not grow up in any of samples heat treated at 350 and 600 °C, despite they have different inner diameters and the superhydrophilic behavior of the anodic coatings after the heat treatment. From the literature, nanotubes composed by anatase and rutile phases have higher antibacterial properties in contrast to the amorphous phase [43], [50], [109]. In addition, in the literature there is no definite reason for the antibacterial properties of heat-treated nanotubes. The explanation could be based on the intrinsic properties of crystalline nanotubes; Lipovsky et al. [276] reported that anatase and rutile phases could generate ROS without any exposure to illumination. **Figure 25** shows SEM images of bacterial adhesion test of the anodized surfaces using *S. aureus* and *P. aeruginosa* strains. From **Figure 25**, *S. aureus* and *P. aeruginosa* strains adhered to all analyzed coatings; however, the number of bacteria adhered on the nanotubes produced at 20 V and heat treated at 350 °C is lower in contrast to the other kind of the anodic coatings; thus, both inner diameter (about 100 nm) and crystalline phase (anatase) have an effect on bacteria adhesion of both strains. Ercan et al. [109] produced TiO_2 nanotubes with diameters between 20 and 80 nm with and without heat treatment at 550 °C. The authors found

that the nanotubes with 80 nm diameter composed entirely by anatase phase had the higher antibacterial properties against both *S.epidermis* and *S. aureus* strains. Our results are in agreement to the authors. According to N. Gusnaniar et al.[255], bacteria strain could adhere to surfaces inclusive under unfavorable conditions. For instance, Bhadra et al. [277] report that *P. aeruginosa* is capable of adhering to many kinds of surfaces; however, under unfavorable adherence conditions occurs a membrane deformation which could affect their viability. According to our results (see **Table 9**), it is not a direct relationship between bacteria adhesion and roughness. Previous reports have shown that bacteria prefer rough surfaces [34], [278], [279]; on the other hand, recent studies report that nano-smooth surfaces promotes bacteria attachment [280]–[282]; thus, an unified opinion about the roughness effect on bacteria adhesion is not encountered on the scientific literature available.

3.2 Conclusions

We have analyzed the effect of heat and UV treatment on the characteristics of TiO_2 nanotubes and their antibacterial properties. Nanotubes heat treated at 600 °C using a ramp with stabilization steps keep the nanotubular structure, inclusive for the lowest inner diameters; furthermore, the nanotube length reduction after the heat treatment was lower compared with the scientific literature data. HRTEM and SAED revealed d-spacing values related to titanium suboxides; also, after the heat treatment at 350 and 600 °C. d-spacing values related to the rutile phase were detected in nanotubes different zones. The nanotubes UV treated, and heat treated at 200, 350, and 600 °C were superhydrophilic inclusive two months after

preparation. The nanotubes UV treated, and heat treated at 350, and 600 °C had a bacteriostatic behavior against *S. aureus* and *P. aeruginosa*. Anodic coatings obtained at 20 V at heat treated at 350 °C had the lower bacteria adhesion against both strains evaluated.

4.Chapter 4
Effect of TiO2 nanotubes size, heat treatment, and UV irradiation on osteoblast adhesion, proliferation and mineralization

Several parts of the text and figures have been taken from:

Effect of TiO_2 nanotubes size, heat treatment, and UV irradiation on osteoblast adhesion, proliferation and mineralization.
Robinson Aguirre Ocampo, Mónica Echeverry-Rendón, Sara Robledo, Félix Echeverría Echeverría.
In preparation

Abstract

The effect of the nanotube characteristics on the osteoblast cell adhesion and proliferation as well the cell mineralization was studied. All the anodic coatings were biocompatible; however, surface characteristics as surface topography, wettability, charge, and phase composition could affect the osteoblast adhesion, proliferation and mineralization. The nanotubular coatings with higher roughness and UV irradiated improved early cell adhesion; however, the nanotubes with a diameter about 10 nm and composed entirely by rutile or anatase phases affect negatively the early cell adhesion. The number of filopodia rise with the reduction in the internal diameter of the anodic coating, the mineralization had the same behavior, namely: decrease of the internal diameter induces a superior rate of matrix mineralization.

4.1 Results and discussion

4.1.1 Cell proliferation

Alamar Blue assay was used to obtain fluorescence emission measurements every day for a total of 4 days. **Figure 26** shows a graph of percentage of mitochondrial activity respect to the control for osteoblasts that were seeded on the nanotubular anodic coatings. In all kind of coatings, the graph has the typical form that shows the progressive cellular growth with time. All nanotubular coatings were non-cytotoxic irrespective of the applied voltage or post-anodization treatment that was used. From the statistical analysis between all different kind of coatings, it can be concluded there is no significant differences.

4.1.2 Cell morphology

From the literature review, three kind of cell morphology adhered to the surfaces has been identified: round, branched, and spindle (see **Figure 27**) [122], [191], [283]–[286]. The round shape is characteristic of the early stages of cellular adhesion [283] and also indicates a poor attachment to the surface [1], [2], [283]. On the other hand, branched or spindle shape of the adhered cells indicates adherence and affinity between cells and substrate [286], [287].

Obata et al [287] studied the correlation between the cell shape and percentage of living cells. The authors found a direct correlation between the branched and spindle shapes and the percentage of living cells. Fu et al. [284] reports that the spreading shape regulate cell differentiation and apoptosis. In fact, they report that cells with a

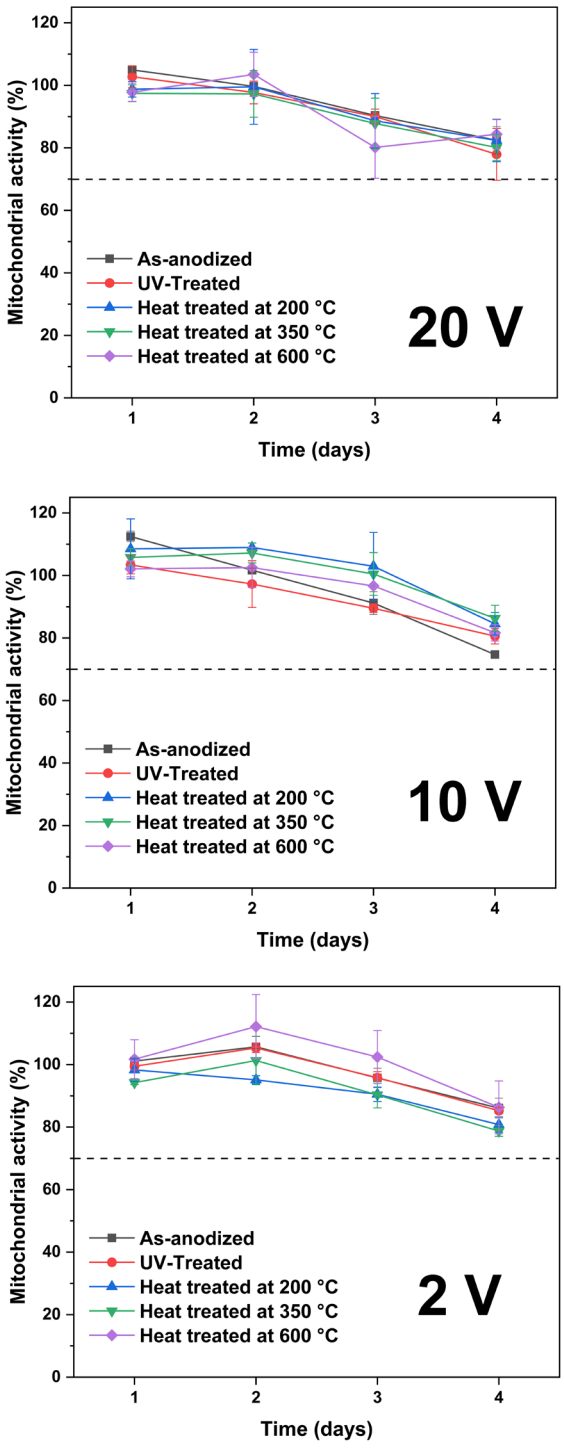

Figure 26. Osteoblast proliferation in nanotubular coatings.

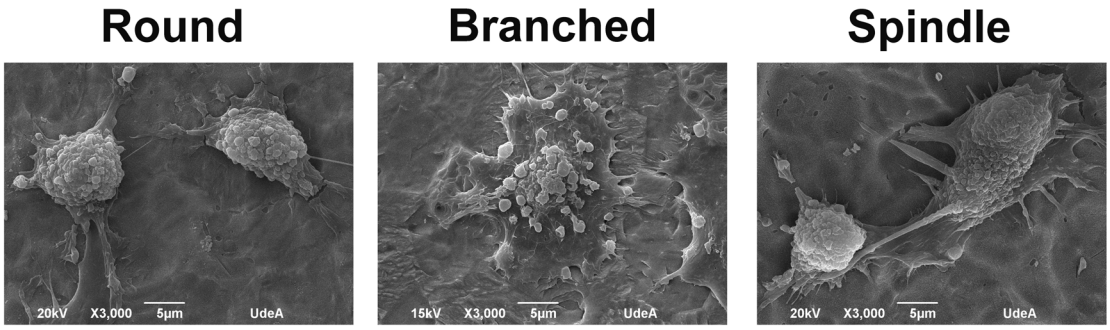

Figure 27 . Types of adhered osteoblast cells.

round shape had a higher level of apoptosis; on the other hand, the branched shape osteoblast cell grew in the same way to the original cell linage.

Figure 28 and **Figure 29** show the SEM images of osteoblast cells that grew up on the anodic nanotubular coatings after 1 and 24 hours of being seeded respectively. From the literature review, the physicochemical properties that had a higher influence on the osteoblast cell adhesion and proliferation on biomaterials are: the surface topography, wettability, charge, and phase composition [41], [121], [288]–[290]. Previous experimental works have been reported the influence of the surface wettability on the osteoblast cell adhesion [1], [35], [36], [41], [111], [114], [288], [289], [291], [292].The majority of authors report a better cell adhesion on superhydrophilic surfaces in contrast to hydrophobic surfaces [1], [291], [292]. Das et al. [36] produced nanotubes using an electrolyte composed by an aqueous solution of citric acid, sulfuric acid, and NaF. They found that the osteoblast cells seeded on hydrophobic anodic nanotubular surfaces produced a poor cell attachment.

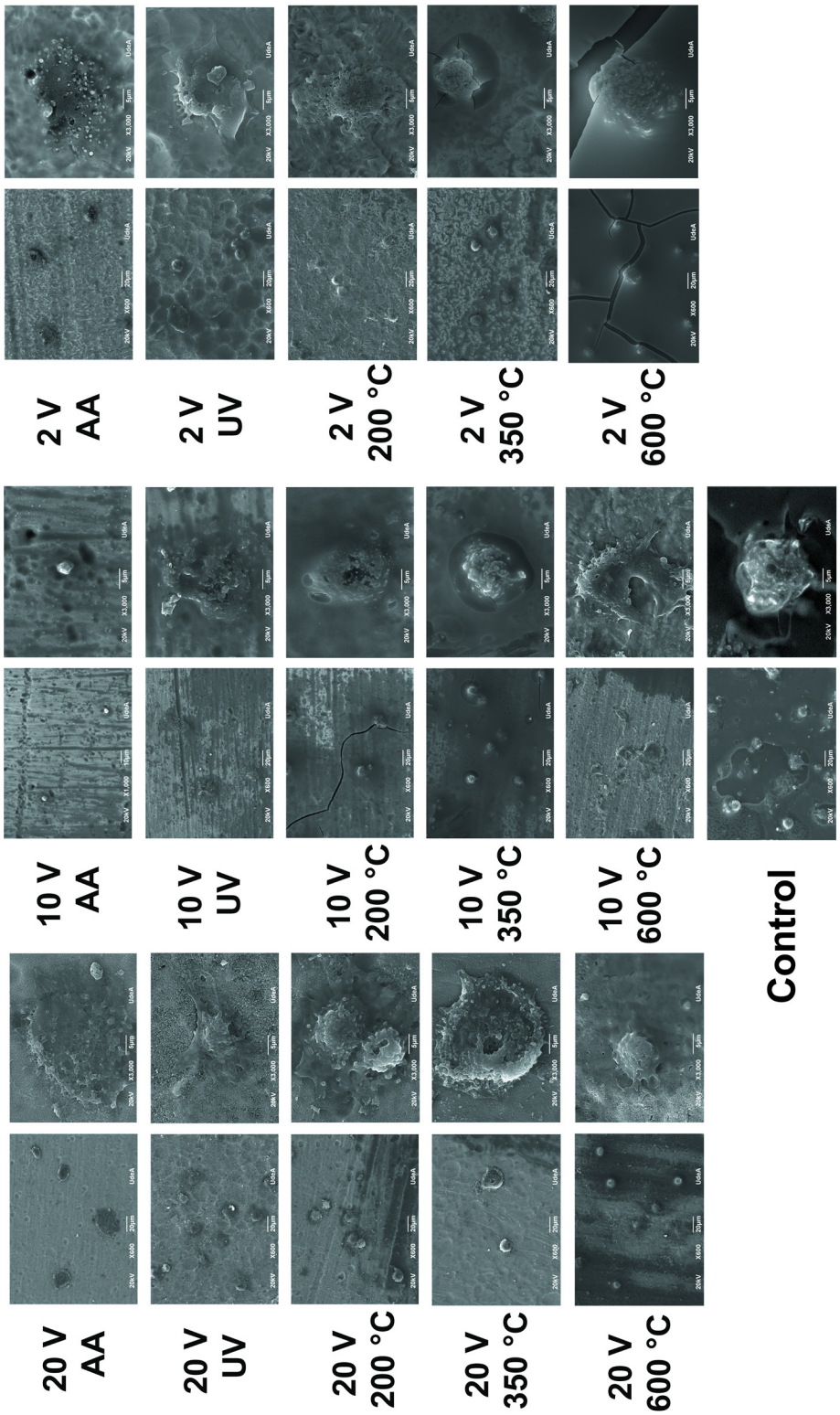

Figure 28. SEM images showing osteoblast growing on surfaces after one hour of being seeded.

Figure 28 shows the results of the early cell adhesion test (1 hour) in all kind of the anodic coatings; it is worth to highlight that for this short time, some kind of samples show spread (branched) cells, in contrast to the control that show round cells. From **Figure 28**, some different cell morphologies could be observed (round and branched); although, from the results of **Table 8**, all anodic coatings as-anodized were superhydrophilic. Thus, other characteristics also could influence the early cell adhesion. From the literature review, surface charge is a key factor in the cell adhesion process [41], [121], [286], [290], [293].In fact, one of key step on the early osteoblast cell adhesion involves the absorption of positively charged proteins (vitronectins, laminins, and fibronectins), these proteins act like bridges between the cell and the surface ;thus, surfaces with a negative surface charge could contributes positively to the osteoblast cell adhesion [39], [121], [290], [294]. From **Figure 28**, some differences were observed between the cell seeded on the 10 V and 2 V as-anodized samples in contrast to the 10 V and 2 V UV irradiated samples; in the as-anodized samples the cell have a round shape in contrast to the branched shape observed on the UV irradiated samples. From **Table 9**, the value of surface potential for the UV irradiated samples is lower in contrast to the as-anodized sample value, this could be an explanation for the differences in the cell morphology in this kind of samples. Previous works [263], [295]–[297] have reported an enhancement on the biocompability of TiO_2 nanotubular coatings irradiated with UV light. The authors reports an increasing in the osteoblast cell colonization and viability [297] combined with a rise in the adhesion, proliferation and differentiation [296]. Wu et al. [297] evaluated the UV irradiation effect on the bioactivity of TiO_2 nanotube coatings. The authors found that the irradiated samples absorbed the proteins related to the cell

adhesion process faster in contrast to the non-irradiated samples; besides, the irradiated samples show a higher percentage of surface colonization and early cell adhesion in contrast to the non- irradiated samples. It is worth to highlight that the only difference between the as-anodized and the UV irradiated samples at the same voltage was the irradiation process. Roughness is another important characteristic that affect the cell adhesion, some authors reports that increasing roughness could improves cell adhesion; however, after a maximum value ,the opposite effect is observed [41], [111], [283].

From **Table 9** and **Figure 28**, the direct relationship between roughness and the improving of early cell adhesion is evident, due to the cell seeded on the anodizing coatings with the higher roughness values have a branched shape. However, in the case of smaller nanotubes (2 V), it seems that the complete transformation to rutile or anatase phases is not beneficial to the early cell adhesion. In real conditions, in the surface implants occurs a “race for the surface” between the cells and the bacteria strains; thus, if cells quickly covered the implant surface this will be less susceptible to bacteria colonization [298], [299].

From the literature review, the cell attachment process involve the formation of filopodia and lamellipodia [39], [42], [124], [145], [300], [301]. The filopodia are composed of microtubules and actin filaments, with a morphology similar to “fingers” that help the cell to sense the surface searching desirable adhesive sites on the biomaterial surface. Once the filopodia detects the location, lamellipodia is formed conducting the cells to colonize that location. From the literature review, it can be concluded that a higher number of filopodia indicates a favorable compatibility

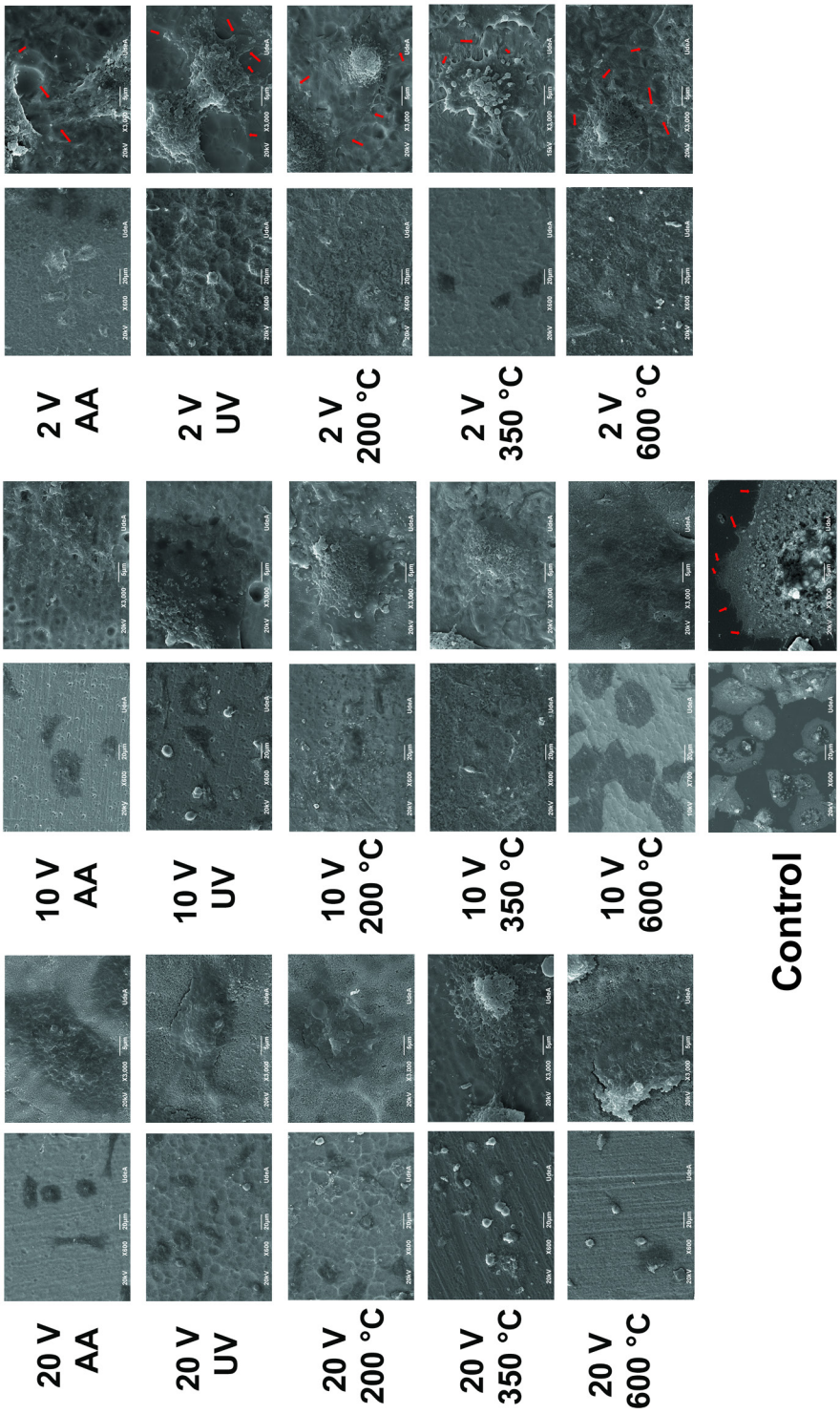

Figure 29. SEM images showing osteoblast growing on surfaces after 24 hours of being seeded.

between the cells and the biomaterial surface; as the filopodia acts like site of cell anchorage and attachment [39], [145], [301]. From **Figure 29**, after 24 hours of being seeded, the cells adhered to all kind of anodic coatings and they had a branched morphology. However, some specific differences were observed in the adhered cells morphology; the number of filopodia increases with the decrease of the nanotube internal diameter.

Nevertheless, the cells adhered to the anodic coating produced at 20 V and heat treated at 350 °C has a higher number of filopodia, similar to value presented in the lowest diameter nanotubes. Thus, from our results, it seems that the internal diameter and the nanotube phase has a higher influence on the number of filopodia, thus, in the cell anchorage.

4.1.3 Cell mineralization

According to the literature review, the mineralization is the last stage of the osteoblast differentiation (proliferation, matrix maturation, and mineralization) in which those cells are enriched with osteocalcin producing mineral compounds which are composed mainly for calcium phosphates [292], [302], [303]. Mineralization is a key stage in the process of production of new bone; an unequilibrated mineralization process could cause diseases as osteomalacia [304]. **Figure 30** and **Figure 31** show the optical images of osteoblast cells that grew up on the anodic nanotubular coatings after 7 and 14 days of being seeded respectively. Staining with alizarin red confirmed osteoblast cells proliferation and differentiation characteristic for this cell phenotype in all kind of the anodic coatings; extracellular mineralized nodules were observed similar to the reported in previous experimental works; sites of calcium

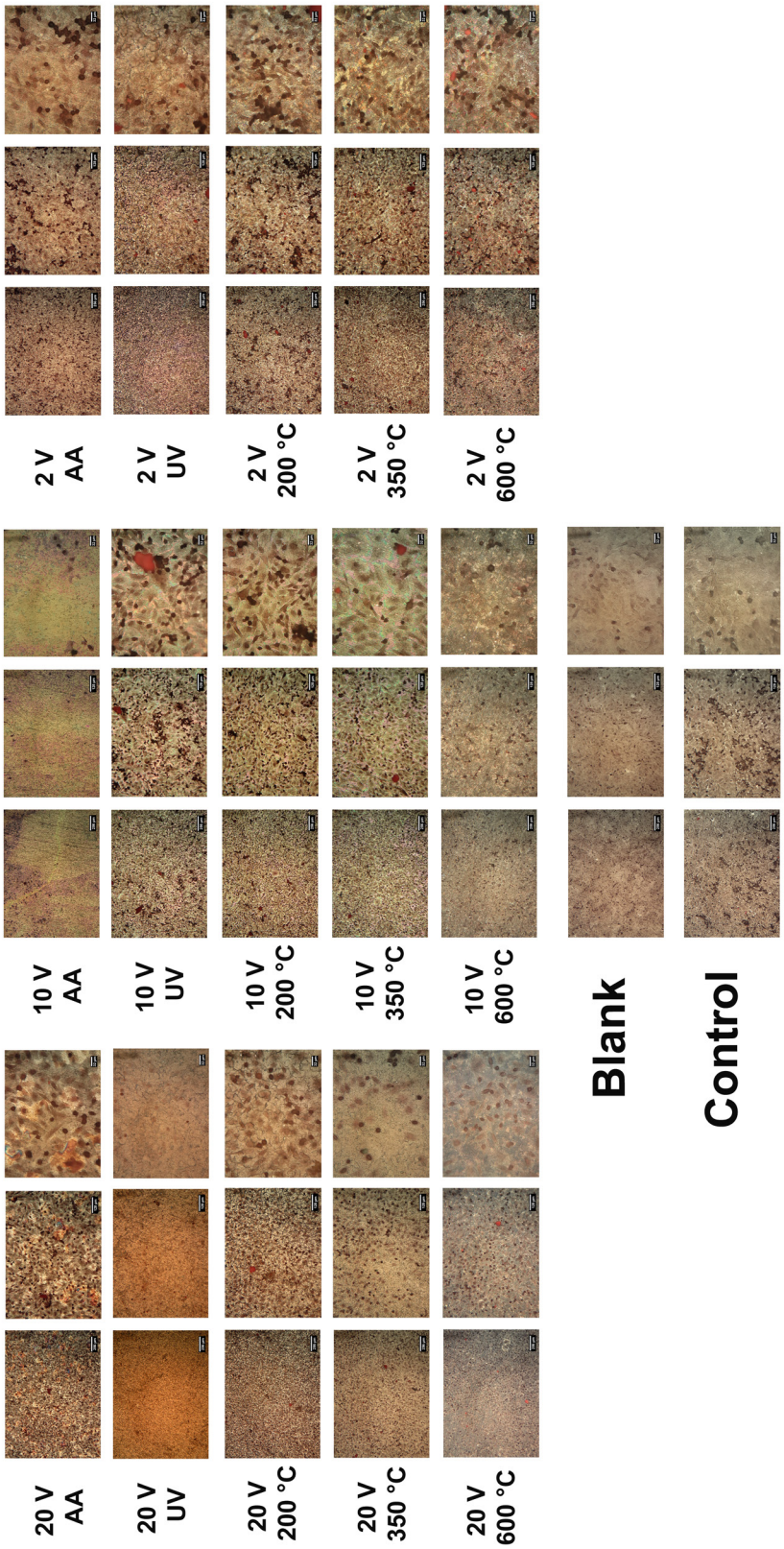

Figure 30. Differentiation and mineralization activity of osteoblasts on anodized surfaces after seven days.

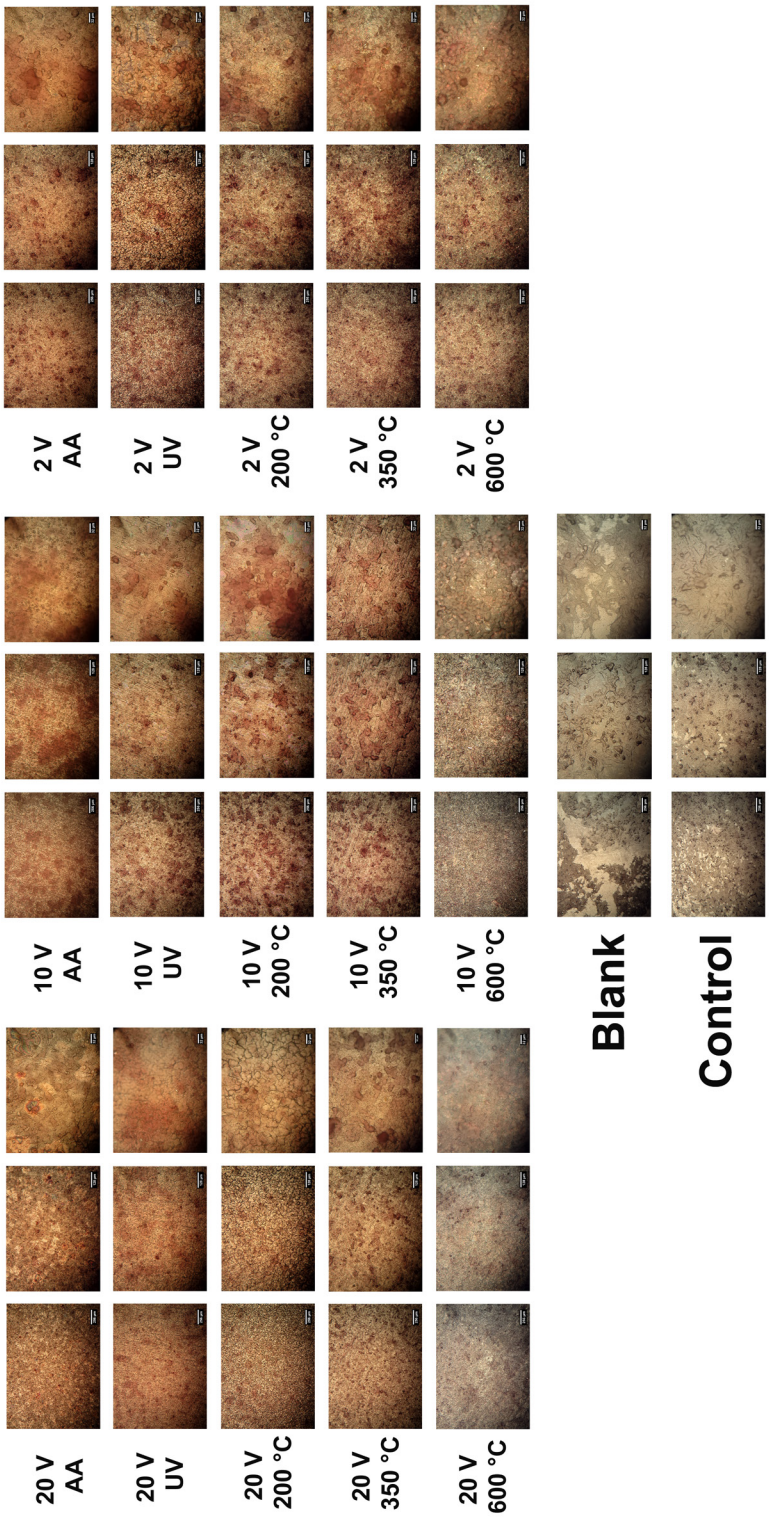

Figure 31. Differentiation and mineralization activity of osteoblasts on anodized surfaces after 14 days.

deposition were identified as red zones [292], [303]. From **Figure 30**, a higher number of mineralized nodules were observed after 7 days in the nanotubular coatings produced at voltages of 10 V and 2 V in contrast to the 20 V. From **Figure 31,** after 14 days the nodules are spread around all the anodic surfaces; however, a higher number of nodules or zones of calcium deposition were found in the nanotubular coatings produced at voltages of 10 V and 2 V in contrast to the 20 V. Nonetheless, the anodic coating produced at 20 V and heat treated at 350 °C had a number of nodules similar to the values found in anodic coatings with lower internal diameters. On the other hand, a lower number of nodules were found on the anodic coatings heat treated at 600 °C. Thus, from our results, it seems that the internal diameter and phase composition affect the mineralization process.

4.2 Conclusions

Implant failure or success depend principally of their surface characteristics which could propitiate the osteoblast cell adhesion and proliferation until achieve the mineralization and thus the formation of new bone. From this experimental work, all kind of anodic coatings were biocompatible, demonstrating that nanotubular coatings did not affect the cells viability and survival. However, some differences were found that directly depends of the surface physicochemical characteristics. The roughness improved the early cell adhesion and the decrease of the internal diameter increase the number of filopodia and the number of mineralization zones. Those results could help to design biomaterials based on TiO_2 nanotubes that encourage and helps to produce new peri-implant bone around the implant.

Discussion

In order to prevent the implant surface colonization by bacteria strains, various treatments have been used, some related to antibiotics release, or in other cases consisting in the liberation of silver ions from the implant [34], [305]. Antibiotics have been widely used to reduce of bacterial infections in patients recently implanted; however, the uncontrolled use of this kind of substances has allowed the development of new antibiotic-resistant bacteria strains [46]. On the other hand, the liberation of silver ions has been useful against both gram-positive and gram-negative bacteria strains proliferation; however, some authors have reported cell toxicity associated with the silver use [34], [305], [306].Thus, it is necessary to adopt new approaches for preventing implants bacterial infection without increase the bacteria resistance or loss biocompatibility [49], [247]. Among those new approaches are the implant surface modification with nanotopography or using nanostructured coatings [33], [34], [52], [247]. Previous works have reported that nanotubular structures have antibacterial properties against various bacterial strains such as *Staphylococcus epidermidis* [51], [307] ,*Streptococcus mutans* [266], *Porphyromonas gingivalis* [113], [266] *Staphylococcus aureus* [43], [308], *Pseudomonas aeruginosa* [43], [308] and *Escherichia coli* [309]. However, the effect of some nanotubular characteristics (diameter, crystalline phase and UV irradiation) on the antibacterial properties has not been reported yet. For instance, the effect of small internal diameters with and without different heat treatments and with and without UV irradiation on the bacteria strains comportment.

In real environments, it occurs a competition for colonization of the implant surface between the bacteria strains and the osteoblastic cells; therefore, if cells quickly cover the implant surface this will be less vulnerable to bacteria colonization. Both processes of adhesion (bacteria and cells), are mediated at the beginning by proteins adsorption on the implant surface [44]. Previous authors report the reduction on the bacteria adhesion in superhydrophobic surfaces due to prevention of proteins adsorption [44], [310]. In addition, some authors report a decrease of osteoblastic cells adhesion and proliferation in superhydrophobic surfaces and those authors related this behavior with the reduced capacity of adsorbing proteins [310], [311]. On the other hand, in previous works [42], [121], [294], [307] it has been reported that TiO_2 nanotubes coatings increase the osteoblastic cell adhesion and proliferation, due to higher rates of protein adsorption which is related to the hydrophilic comportment of this kind of coatings. From the results of the present experimental work, we showed the antibacterial properties of superhydrophilic TiO_2 nanotubes coatings; additionally, those nanostructures showed a higher bioactivity in terms of osteoblast adhesion, proliferation and mineralization.

General Conclusions

As a result of this experimental work, CMC and NaF aqueous electrolytes allows to obtain homogeneous nanotubes with different diameters (from ≈ 10 nm to ≈ 100 nm); furthermore, for the best of knowledge, the nanotubes with an internal diameter about 10 nm were the lowest found reported in the scientific literature. The last was achieved through the systematically study of the anodization parameters as: pH, electrolyte composition, electrolyte aging, voltage, current, electrolyte temperature and anodizing time. The addition of CMC changes the viscosity and helps to produce organized nanotubes; however, the carefully control of anodizing parameters is necessary to obtain organized nanotubes using aqueous electrolytes that contains CMC. As a consequence of higher dissolution of the aqueous electrolytes, the nanotube produced in aqueous electrolytes have a reduced length. However, the aqueous electrolytes with CMC allows to obtain thinner nanotubes, in our case, 5.85 μm.

Nanotubes with the higher organization levels were heat treated at 200, 350 and 600 °C and irradiated with UV light, after that, all kind of anodic coating were characterized using Raman spectroscopy, XRD, SEM, TEM, (GPA), HRTEM, SAED, AFM and contact angle. Nanotubes heat treated at 600 °C using a ramp with stabilization steps kept the nanotubular structure, even for the lowest inner diameters; furthermore, the nanotube length reduction after the heat treatment was lower compared with the scientific literature data. HRTEM and SAED revealed d-spacing values related to titanium suboxides; also, after heat treatment at 350 and 600 °C. d-spacing values related to the rutile phase were detected in different zones

of the nanotubes. The nanotubes UV treated, and heat treated at 200, 350, and 600 °C were superhydrophilic inclusive two months after preparation.

All kind of anodic coatings were submitted to antibacterial, cell adhesion, proliferation and mineralization essays. The data from the biological essays were correlated with the information from the characterization essays. The nanotubes UV treated, and heat treated at 350, and 600 °C had a bacteriostatic behavior against *S. aureus* and *P. aeruginosa*. Anodic coatings obtained at 20 V and heat treated at 350 °C had the lower bacteria adhesion against both strains evaluated. All kind of anodic coatings were biocompatible, demonstrating that nanotubular coatings did not affect the cells viability and survival. However, some differences were found that directly depends on the surface physicochemical characteristics. The roughness improved the early cell adhesion and the decrease of the internal diameter led to increase the number of filopodia and the number of mineralization zones.

Finally, correlating the antibacterial essays with the osteoblast cell adhesion, proliferation and mineralization results, all kind of conditions produced at 10 V and 2 V had good results in the antibacterial essays and osteoblast cells essays. However, the best results in both kind of essays were achieved in the nanotubular coatings obtained at 20 V and heat treated at 350 °C. These coatings potentially have great potential in biomedical applications as implants; however, tribological and in vivo assays would be necessary for his future application as a biomedical device.

References

[1] M. Echeverry-Rendón, O. Galvis, R. Aguirre, S. Robledo, J. G. Castaño, and F. Echeverría, “Modification of titanium alloys surface properties by plasma electrolytic oxidation (PEO) and influence on biological response,” *J. Mater. Sci. Mater. Med.*, vol. 28, no. 11, 2017, doi: 10.1007/s10856-017-5972-x.

[2] M. Echeverry-rendón *et al.*, “Osseointegration improvement by plasma electrolytic oxidation of modified titanium alloys surfaces,” *J. Mater. Sci. Mater. Med.*, vol. 26, no. 2, pp. 1–18, 2015, doi: 10.1007/s10856-015-5408-4.

[3] R. Aguirre Ocampo and F. Echeverría Echeverría, “Effect of the anodization parameters on TiO2 nanotubes characteristics produced in aqueous electrolytes with CMC,” *Appl. Surf. Sci.*, vol. 469, pp. 994–1006, 2019, doi: 10.1016/j.apsusc.2018.11.097.

[4] S. Ferraris and S. Spriano, “Antibacterial titanium surfaces for medical implants,” *Mater. Sci. Eng. C*, vol. 61, pp. 965–978, 2016, doi: 10.1016/j.msec.2015.12.062.

[5] M. Kulkarni, Y. Patil-Sen, I. Junkar, C. V. Kulkarni, M. Lorenzetti, and A. Iglič, “Wettability studies of topologically distinct titanium surfaces,” *Colloids Surfaces B Biointerfaces*, vol. 129, pp. 47–53, 2015, doi: 10.1016/j.colsurfb.2015.03.024.

[6] T. Li, K. Gulati, N. Wang, Z. Zhang, and S. Ivanovski, “Understanding and augmenting the stability of therapeutic nanotubes on anodized titanium implants,” *Mater. Sci. Eng. C*, vol. 88, no. March, pp. 182–195, 2018, doi: 10.1016/j.msec.2018.03.007.

[7] J. Jakubowicz, “Formation of porous TiOx biomaterials in H3PO4 electrolytes,” *Electrochem. commun.*, vol. 10, no. 5, pp. 735–739, May 2008, doi: 10.1016/j.elecom.2008.02.027.

[8] K. Huo, B. Gao, J. Fu, L. Zhao, and P. K. Chu, “Fabrication, modification, and biomedical applications of anodized TiO2 nanotube arrays,” *RSC Adv.*, vol. 4, no. 33, p. 17300, 2014, doi: 10.1039/c4ra01458h.

[9] K. M. Kummer, E. N. Taylor, N. G. Durmas, K. M. Tarquinio, B. Ercan, and T. J. Webster, “Effects of different sterilization techniques and varying anodized TiO 2 nanotube dimensions on bacteria growth,” *J. Biomed. Mater. Res. - Part B Appl. Biomater.*, vol. 101 B, no. 5, pp. 677–688, 2013, doi: 10.1002/jbm.b.32870.

[10] X. Yan and X. Chen, “Titanium Dioxide Nanomaterials,” in *Encyclopedia of Inorganic and Bioinorganic Chemistry*, R. A. Scott, Ed. Chichester, UK: John Wiley & Sons, Ltd, 2011, pp. 1–38.

[11] G. K. Mor, O. K. Varghese, M. Paulose, K. Shankar, and C. a. Grimes, “A review on highly ordered, vertically oriented TiO2 nanotube arrays:

Fabrication, material properties, and solar energy applications," *Sol. Energy Mater. Sol. Cells*, vol. 90, no. 14, pp. 2011–2075, Sep. 2006, doi: 10.1016/j.solmat.2006.04.007.

[12] C. A. Grimes and G. K. Mor, *TiO2nanotube arrays: Synthesis, properties, and applications*. 2009.

[13] P. Roy, S. Berger, and P. Schmuki, "TiO2 nanotubes: synthesis and applications.," *Angew. Chem. Int. Ed. Engl.*, vol. 50, no. 13, pp. 2904–39, Mar. 2011, doi: 10.1002/anie.201001374.

[14] B. Chen, J. Hou, and K. Lu, "Formation Mechanism of TiO 2 Nanotubes and Their Applications in Photoelectrochemical Water Splitting and Supercapacitors," *Langmuir*, vol. 29, no. 19, p. 24061, May 2013, doi: 10.1021/la400586r.

[15] S. Minagar, C. C. Berndt, J. Wang, E. Ivanova, and C. Wen, "A review of the application of anodization for the fabrication of nanotubes on metal implant surfaces.," *Acta Biomater.*, vol. 8, no. 8, pp. 2875–88, Aug. 2012, doi: 10.1016/j.actbio.2012.04.005.

[16] D. Gong *et al.*, "Titanium oxide nanotube arrays prepared by anodic oxidation," *J. Mater. Res.*, vol. 16, no. 12, pp. 3331–3334, Jan. 2001, doi: 10.1557/JMR.2001.0457.

[17] S. Li, G. Zhang, D. Guo, L. Yu, and W. Zhang, "Anodization Fabrication of Highly Ordered TiO 2 Nanotubes," *Phys. Chem. C*, vol. 113, pp. 12759–12765, 2009.

[18] K. Shankar *et al.*, "Highly-ordered TiO 2 nanotube arrays up to 220 μm in length: use in water photoelectrolysis and dye-sensitized solar cells," *Nanotechnology*, vol. 18, no. 6, p. 065707, 2007, doi: 10.1088/0957-4484/18/6/065707.

[19] T. Kondo *et al.*, "Ideally ordered porous TiO2 prepared by anodization of pretextured Ti by nanoimprinting process," *Electrochem. commun.*, vol. 50, pp. 73–76, 2015, doi: 10.1016/j.elecom.2014.11.013.

[20] M. Kulkarni, A. Mazare, P. Schmuki, and A. Iglic, "Influence of anodization parameters on morphology of TiO2 nanostructured surfaces," *Adv. Mater. Lett.*, vol. 7, no. 1, pp. 23–28, 2016, doi: 10.5185/amlett.2016.6156.

[21] V. Zwilling, E. Darque-Ceretti, A. Boutry-Forveille, D. David, M. Y. Perrin, and M. Aucouturier, "Structure and Physicochemistry of Anodic Oxide Films on Titanium and TA6V Alloy," *Surf. Interface Anal.*, vol. 637, no. January, pp. 629–637, Jul. 1999, doi: 10.1002/(SICI)1096-9918(199907)27:7<629::AID-SIA551>3.0.CO;2-0.

[22] S. P. Albu, A. Ghicov, J. M. Macak, and P. Schmuki, "250 μm long anodic TiO2 nanotubes with hexagonal self-ordering," *Phys. Status Solidi - Rapid Res. Lett.*, vol. 1, no. 2, pp. 65–67, 2007, doi: 10.1002/pssr.200600069.

[23] M. Paulose *et al.*, “TiO 2 nanotube arrays of 1000 μm length by anodization of titanium foil: Phenol red diffusion,” *J. Phys. Chem. C*, vol. 111, no. 41, pp. 14992–14997, 2007, doi: 10.1021/jp075258r.

[24] D. Khudhair *et al.*, “Anodization parameters influencing the morphology and electrical properties of TiO2 nanotubes for living cell interfacing and investigations,” *Mater. Sci. Eng. C*, vol. 59, pp. 1125–1142, 2016, doi: 10.1016/j.msec.2015.10.042.

[25] K. Indira, U. K. Mudali, T. Nishimura, and N. Rajendran, “A Review on TiO2 Nanotubes: Influence of Anodization Parameters, Formation Mechanism, Properties, Corrosion Behavior, and Biomedical Applications,” *J. Bio- Tribo-Corrosion*, vol. 1, no. 4, p. 28, 2015, doi: 10.1007/s40735-015-0024-x.

[26] D. Regonini, C. R. Bowen, A. Jaroenworaluck, and R. Stevens, “A review of growt mechanism,structure and cristallinity of anodized TiO2 nanotubes,” *Mater. Sci. Eng. R*, vol. 74, pp. 377–406, 2013.

[27] T. W. Wong and N. A. Ramli, “Carboxymethylcellulose film for bacterial wound infection control and healing,” *Carbohydr. Polym.*, vol. 112, pp. 367–375, 2014, doi: 10.1016/j.carbpol.2014.06.002.

[28] J. G. Batelaan, C. G. Van Ginkel, and F. Balk, “Carboxymethylcellulose (CMC),” *Handb. Environ. Chem.*, vol. 3, pp. 329–336, 1992, doi: 10.1007/978-3-540-47108-0-11.

[29] A. Benchabane and K. Bekkour, “Rheological properties of carboxymethyl cellulose (CMC) solutions,” *Colloid Polym. Sci.*, vol. 286, no. 10, pp. 1173–1180, 2008, doi: 10.1007/s00396-008-1882-2.

[30] M. Edali, M. N. Esmail, and G. H. Vatistas, “Rheological properties of high concentrations of carboxymethyl cellulose solutions,” *J. Appl. Polym. Sci.*, vol. 79, no. 10, pp. 1787–1801, 2001, doi: 10.1002/1097-4628(20010307)79:10<1787::AID-APP70>3.0.CO;2-2.

[31] A. El Ruby and S. Rohani, “Synthesis of Titania nanotubes by anodization,” *AIDIC Conference Series*. pp. 121–129, 2009, doi: 10.3303/AC0S0909015.

[32] A. E. R. Mohamed, N. Kasemphaibulsuk, S. Rohani, and S. Barghi, “Fabrication of titania nanotube arrays in viscous electrolytes.,” *J. Nanosci. Nanotechnol.*, vol. 10, no. xx, pp. 1998–2008, 2010, doi: 10.1166/jnn.2010.2102.

[33] W. F. Oliveira *et al.*, “Staphylococcus aureus and Staphylococcus epidermidis infections on implants,” *J. Hosp. Infect.*, vol. 98, no. 2, pp. 111–117, 2018, doi: 10.1016/j.jhin.2017.11.008.

[34] W. Orapiriyakul, P. S. Young, L. Damiati, and P. M. Tsimbouri, “Antibacterial surface modification of titanium implants in orthopaedics,” *J. Tissue Eng.*, vol. 9, no. July, 2018, doi: 10.1177/2041731418789838.

[35] V. V. Divya Rani, L. Vinoth-Kumar, V. C. Anitha, K. Manzoor, M. Deepthy, and

V. N. Shantikumar, “Osteointegration of titanium implant is sensitive to specific nanostructure morphology,” *Acta Biomater.*, vol. 8, no. 5, pp. 1976–1989, 2012, doi: 10.1016/j.actbio.2012.01.021.

[36] K. Das, S. Bose, and A. Bandyopadhyay, “TiO2 nanotubes on Ti: Influence of nanoscale morphology on bone cell-materials interaction.,” *J. Biomed. Mater. Res. A*, vol. 90, no. 1, pp. 225–37, Jul. 2009, doi: 10.1002/jbm.a.32088.

[37] S. Oh, K. S. Brammer, K. S. Moon, J. M. Bae, and S. Jin, “Influence of sterilization methods on cell behavior and functionality of osteoblasts cultured on TiO2 nanotubes,” *Mater. Sci. Eng. C*, vol. 31, no. 5, pp. 873–879, 2011, doi: 10.1016/j.msec.2011.02.004.

[38] C. Von Wilmowsky *et al.*, “In Vivo Evaluation of Anodic TiO2 Nanotubes; An Experimental Study in the Pig,” *J. Biomed. Mater. Res. - Part B Appl. Biomater.*, vol. 89, no. 1, pp. 165–171, 2009, doi: 10.1002/jbm.b.31201.

[39] Y. Wang, C. Wen, P. Hodgson, and Y. Li, “Biocompatibility of TiO2 nanotubes with different topographies,” *J. Biomed. Mater. Res. - Part A*, vol. 102, no. 3, pp. 743–751, 2014, doi: 10.1002/jbm.a.34738.

[40] M. Kulkarni, A. Mazare, P. Schmuki, and A. Iglič, “Biomaterial surface modification of titanium and titanium alloys for medical applications,” in *Nanomedicine*, 2014, pp. 111–136.

[41] S. Chen *et al.*, “Tuning surface properties of bone biomaterials to manipulate osteoblastic cell adhesion and the signaling pathways for the enhancement of early osseointegration,” *Colloids Surfaces B Biointerfaces*, vol. 164, pp. 58–69, 2018, doi: 10.1016/j.colsurfb.2018.01.022.

[42] R. Aguirre *et al.*, “Formation of nanotubular TiO2 structures with varied surface characteristics for biomaterial applications,” *J. Biomed. Mater. Res. - Part A*, vol. 106, no. 5, 2018, doi: 10.1002/jbm.a.36331.

[43] A. Mazare, G. Totea, C. Burnei, P. Schmuki, I. Demetrescu, and D. Ionita, “Corrosion, antibacterial activity and haemocompatibility of TiO2 nanotubes as a function of their annealing temperature,” *Corros. Sci.*, vol. 103, pp. 215–222, 2016, doi: 10.1016/j.corsci.2015.11.021.

[44] C. Adlhart *et al.*, “Surface modifications for antimicrobial effects in the healthcare setting: a critical overview,” *J. Hosp. Infect.*, vol. 99, no. 3, pp. 239–249, 2018, doi: 10.1016/j.jhin.2018.01.018.

[45] D. Campoccia, L. Montanaro, and C. R. Arciola, “The significance of infection related to orthopedic devices and issues of antibiotic resistance,” *Biomaterials*, vol. 27, no. 11, pp. 2331–2339, 2006, doi: 10.1016/j.biomaterials.2005.11.044.

[46] N. Høiby, T. Bjarnsholt, M. Givskov, S. Molin, and O. Ciofu, “Antibiotic resistance of bacteria in biofilms,” *Int. J. Antimicrob. Agents*, vol. 35, pp. 322–332, 2010, doi: 10.1016/S0140-6736(01)05321-1.

[47] R. M. Donlan, “Biofilms and Device-Associated Infections,” vol. 7, no. 2, pp.

277–281, 2001.

[48] C. Lin *et al.*, “Effect of superhydrophobic surface of titanium on staphylococcus aureus adhesion,” *J. Nanomater.*, vol. 2011, 2011, doi: 10.1155/2011/178921.

[49] S. D. Puckett, E. Taylor, T. Raimondo, and T. J. Webster, “The relationship between the nanostructure of titanium surfaces and bacterial attachment,” *Biomaterials*, vol. 31, no. 4, pp. 706–713, 2010, doi: 10.1016/j.biomaterials.2009.09.081.

[50] H. Li, Q. Cui, B. Feng, J. Wang, X. Lu, and J. Weng, “Antibacterial activity of TiO 2 nanotubes : Influence of crystal phase , morphology and Ag deposition,” *Appl. Surf. Sci.*, vol. 284, pp. 2–6, 2013, doi: 10.1016/j.apsusc.2013.07.076.

[51] Z. Peng *et al.*, “Dual effects and mechanism of TiO2 nanotube arrays in reducing bacterial colonization and enhancing c3h10T1/2 cell adhesion,” *Int. J. Nanomedicine*, vol. 8, no. July, pp. 3093–3105, 2013, doi: 10.2147/IJN.S48084.

[52] M. F. Kunrath, B. F. Leal, R. Hubler, S. D. de Oliveira, and E. R. Teixeira, “Antibacterial potential associated with drug-delivery built TiO 2 nanotubes in biomedical implants,” *AMB Express*, vol. 9, no. 1, 2019, doi: 10.1186/s13568-019-0777-6.

[53] I. Horcas, R. Fernández, J. M. Gómez-Rodríguez, J. Colchero, J. Gómez-Herrero, and A. M. Baro, “WSXM: A software for scanning probe microscopy and a tool for nanotechnology,” *Rev. Sci. Instrum.*, vol. 78, no. 1, 2007, doi: 10.1063/1.2432410.

[54] D. R. G. Mitchell, “DiffTools: Electron diffraction software tools for DigitalMicrograph TM,” *Microsc. Res. Tech.*, vol. 71, no. 8, pp. 588–593, 2008, doi: 10.1002/jemt.20591.

[55] M. Klinger and A. Jäger, “Crystallographic Tool Box (CrysTBox): Automated tools for transmission electron microscopists and crystallographers,” *J. Appl. Crystallogr.*, vol. 48, no. 2015, pp. 2012–2018, 2015, doi: 10.1107/S1600576715017252.

[56] M. Klinger, “More features, more tools, more CrysTBox,” *J. Appl. Crystallogr.*, vol. 50, pp. 1226–1234, 2017, doi: 10.1107/S1600576717006793.

[57] M. E. Bowden, G. V White, I. W. M. Brown, M. J. Ryan, and G. J. Gainsford, “Improved powder diffraction patterns for the titanium suboxides,” vol. 11, no. October 1995, pp. 60–68, 1996.

[58] D. Nečas and P. Klapetek, “Gwyddion: An open-source software for SPM data analysis,” *Cent. Eur. J. Phys.*, vol. 10, no. 1, pp. 181–188, 2012, doi: 10.2478/s11534-011-0096-2.

[59] S. Metwally and U. Stachewicz, “Surface potential and charges impact on cell responses on biomaterials interfaces for medical applications,” *Mater. Sci. Eng. C*, vol. 104, no. February, 2019, doi: 10.1016/j.msec.2019.109883.

[60] J. Hudzicki, “Kirby-Bauer Disk Diffusion Susceptibility Test Protocol Author Information,” *Am. Soc. Microbiol.*, no. December 2009, pp. 1–13, 2012.

[61] D. J. LeClere *et al.*, “Tracer Investigation of Pore Formation in Anodic Titania,” *J. Electrochem. Soc.*, vol. 155, no. 9, p. C487, 2008, doi: 10.1149/1.2946727.

[62] D. Yu, Y. Song, X. Zhu, R. Yang, and A. Han, “Morphological evolution of TiO2 nanotube arrays with lotus-root-shaped nanostructure,” *Appl. Surf. Sci.*, vol. 276, pp. 711–716, 2013, doi: 10.1016/j.apsusc.2013.03.158.

[63] Y. Tang, J. Tao, Y. Zhang, T. Wu, H. Tao, and Y. Zhu, “Preparation of TiO2 nanotube on glass by anodization of Ti films at room temperature,” *Trans. Nonferrous Met. Soc. China*, vol. 19, no. 1, pp. 192–198, Feb. 2009, doi: 10.1016/S1003-6326(08)60251-4.

[64] Y. Zhang *et al.*, “Growth of anodic TiO2 nanotubes in mixed electrolytes and novel method to extend nanotube diameter,” *Electrochim. Acta*, vol. 160, pp. 33–42, 2015, doi: 10.1016/j.electacta.2015.02.058.

[65] G. K. Mor, O. K. Varghese, M. Paulose, N. Mukherjee, and C. a. Grimes, “Fabrication of tapered, conical-shaped titania nanotubes,” *J. Mater. Res.*, vol. 18, no. 11, pp. 2588–2593, 2011, doi: 10.1557/JMR.2003.0362.

[66] G. K. Mor, O. K. Varghese, M. Paulose, and C. a. Grimes, “Transparent Highly Ordered TiO2 Nanotube Arrays via Anodization of Titanium Thin Films,” *Adv. Funct. Mater.*, vol. 15, no. 8, pp. 1291–1296, Aug. 2005, doi: 10.1002/adfm.200500096.

[67] J. Bai *et al.*, “The formation mechanism of titania nanotube arrays in hydrofluoric acid electrolyte,” *J. Mater. Sci.*, vol. 43, no. 6, pp. 1880–1884, 2008, doi: 10.1007/s10853-007-2418-8.

[68] J. Zhao, X. Wang, R. Chen, and L. Li, “Fabrication of titanium oxide nanotube arrays by anodic oxidation,” *Solid State Commun.*, vol. 134, no. 10, pp. 705–710, 2005, doi: 10.1016/j.ssc.2005.02.028.

[69] J. M. Macak, K. Sirotna, and P. Schmuki, “Self-organized porous titanium oxide prepared in Na2SO4/NaF electrolytes,” *Electrochim. Acta*, vol. 50, no. 18, pp. 3679–3684, Jun. 2005, doi: 10.1016/j.electacta.2005.01.014.

[70] S. H. Kang, J.-Y. Kim, H. S. Kim, and Y.-E. Sung, “Formation and mechanistic study of self-ordered TiO2 nanotubes on Ti substrate,” *J. Ind. Eng. Chem.*, vol. 14, no. 1, pp. 52–59, Jan. 2008, doi: 10.1016/j.jiec.2007.06.004.

[71] H. Tsuchiya *et al.*, “Self-organized TiO2 nanotubes prepared in ammonium fluoride containing acetic acid electrolytes,” *Electrochem. commun.*, vol. 7, no. 6, pp. 576–580, Jun. 2005, doi: 10.1016/j.elecom.2005.04.008.

[72] P. Kar, A. Pandey, J. J. Greer, and K. Shankar, “Ultrahigh sensitivity assays for human cardiac troponin I using TiO2 nanotube arrays.,” *Lab Chip*, vol. 12, no. 4, pp. 821–8, 2012, doi: 10.1039/c2lc20892j.

[73] S. Yoriya, M. Paulose, O. K. Varghese, G. K. Mor, and C. A. Grimes, “Fabrication of Vertically Oriented TiO 2 Nanotube Arrays Using Dimethyl Sulfoxide Electrolytes,” *J. Phys. Chem. C*, vol. 111, no. 37, pp. 13770–13776, 2007, doi: 10.1021/jp074655z.

[74] N. K. Allam and C. A. Grimes, “Formation of Vertically Oriented TiO 2 Nanotube Arrays using a Fluoride Free HCl Aqueous Electrolyte,” pp. 13028–13032, 2007.

[75] L. Aïnouche, L. Hamadou, A. Kadri, N. Benbrahim, and D. Bradai, “Interfacial barrier layer properties of three generations of TiO2 nanotube arrays,” *Electrochim. Acta*, vol. 133, pp. 597–609, 2014, doi: 10.1016/j.electacta.2014.04.086.

[76] Y. L. Cheong, F. K. Yam, S. W. Ng, Z. Hassan, S. S. Ng, and I. M. Low, “Fabrication of titanium dioxide nanotubes in fluoride-free electrolyte via rapid breakdown anodization,” *J. Porous Mater.*, vol. 22, no. 6, pp. 1437–1444, Dec. 2015, doi: 10.1007/s10934-015-0024-8.

[77] R. Hahn, H. Lee, D. Kim, S. Narayanan, S. Berger, and P. Schmuki, “Self-organized Anodic TiO2-nanotubes in Fluoride Free Electrolytes,” in *ECS Transactions*, 2008, vol. 16, no. 3, pp. 369–373, doi: 10.1149/1.2982577.

[78] T. Manovah David, P. Wilson, C. Ramesh, and P. Sagayaraj, “A comparative study on the morphological features of highly ordered titania nanotube arrays prepared via galvanostatic and potentiostatic modes,” *Curr. Appl. Phys.*, vol. 14, no. 6, pp. 868–875, 2014, doi: 10.1016/j.cap.2014.04.002.

[79] M. R. Sturgeon, P. Lai, and M. Z. Hu, “A comparative study of anodized titania nanotube architectures in aqueous and nonaqueous solutions,” *J. Mater. Res.*, vol. 26, no. 20, pp. 2612–2623, Oct. 2011, doi: 10.1557/jmr.2011.243.

[80] A. Haring, A. Morris, and M. Hu, “Controlling morphological parameters of anodized titania nanotubes for optimized solar energy applications,” *Materials (Basel).*, 2012, doi: 10.3390/ma5101890.

[81] Q. Zhang, L. Ma, Q. Zhao, Z. Li, and X. Xu, “Mophology-modulations of TiO 2 nanostructures for enhanced photocatalytic performance,” *Appl. Surf. Sci.*, vol. 332, pp. 224–228, 2015.

[82] J. Wu, H. Xu, and W. Yan, “Photoelectrocatalytic degradation Rhodamine B over highly ordered TiO2 nanotube arrays photoelectrode,” *Appl. Surf. Sci.*, vol. 386, pp. 1–13, 2016, doi: 10.1016/j.apsusc.2016.05.155.

[83] R. Zhang *et al.*, “Guided proliferation and bone-forming functionality on highly ordered large diameter TiO2 nanotube arrays,” *Mater. Sci. Eng. C*, vol. 53, pp. 272–279, 2015, doi: 10.1016/j.msec.2015.04.046.

[84] J. Wan, X. Yan, J. Ding, M. Wang, and K. Hu, “Self-organized highly ordered TiO2 nanotubes in organic aqueous system,” *Mater. Charact.*, vol. 60, no. 12, pp. 1534–1540, 2009, doi: 10.1016/j.matchar.2009.09.002.

[85] S. So, K. Lee, and P. Schmuki, “Ultrafast growth of highly ordered anodic TiO2 nanotubes in lactic acid electrolytes.,” *J. Am. Chem. Soc.*, vol. 134, no. 28, pp. 11316–8, 2012, doi: 10.1021/ja301892g.

[86] S. Sreekantan, K. A. Saharudin, Z. Lockman, and T. W. Tzu, “Fast-rate formation of TiO2 nanotube arrays in an organic bath and their applications in photocatalysis.,” *Nanotechnology*, vol. 21, no. 36, p. 365603, 2010, doi: 10.1088/0957-4484/21/36/365603.

[87] R. Narayanan, T. Y. Kwon, and K. H. Kim, “TiO2 nanotubes from stirred glycerol/NH4F electrolyte: Roughness, wetting behavior and adhesion for implant applications,” *Mater. Chem. Phys.*, vol. 117, no. 2–3, pp. 460–464, 2009, doi: 10.1016/j.matchemphys.2009.06.023.

[88] S. Bauer, S. Kleber, and P. Schmuki, “TiO2 nanotubes: Tailoring the geometry in H3PO4/HF electrolytes,” *Electrochem. commun.*, vol. 8, no. 8, pp. 1321–1325, Aug. 2006, doi: 10.1016/j.elecom.2006.05.030.

[89] J. Park, S. Bauer, K. Von Der Mark, and P. Schmuki, “Nanosize and vitality: TiO2 nanotube diameter directs cell fate,” *Nano Lett.*, vol. 7, no. 6, pp. 1686–1691, 2007, doi: 10.1021/nl070678d.

[90] J. Park, S. Bauer, K. A. Schlegel, F. W. Neukam, K. von der Mark, and P. Schmuki, “TiO2 nanotube surfaces: 15 nm--an optimal length scale of surface topography for cell adhesion and differentiation.,” *Small*, vol. 5, no. 6, pp. 666–71, Mar. 2009, doi: 10.1002/smll.200801476.

[91] S. Sreekantan, Z. Lockman, R. Hazan, M. Tasbihi, L. K. Tong, and A. R. Mohamed, “Influence of electrolyte pH on TiO2 nanotube formation by Ti anodization,” *J. Alloys Compd.*, vol. 485, no. 1–2, pp. 478–483, Oct. 2009, doi: 10.1016/j.jallcom.2009.05.152.

[92] C. W. Lai and S. Sreekantan, “Photoelectrochemical properties of TiO 2 nanotube arrays: effect of electrolyte pH and annealing temperature,” *J. Exp. Nanosci.*, vol. 9, no. 3, pp. 230–239, May 2012, doi: 10.1080/17458080.2011.654276.

[93] M.-Y. Hsu, W.-C. Yang, H. Teng, and J. Leu, “Microstructure and Composition of TiO[sub 2] Nanotube Arrays Fabricated with HF and NH[sub 4]F Electrolytes and Their Evolution during Annealing,” *J. Electrochem. Soc.*, vol. 158, no. May, p. K81, 2011, doi: 10.1149/1.3533388.

[94] R. Aguirre O. and F. Echeverría E., “Effects of fluoride source on the characteristics of titanium dioxide nanotubes,” *Appl. Surf. Sci.*, vol. 445, pp. 308–319, 2018, doi: 10.1016/j.apsusc.2018.03.139.

[95] W. Zhu, X. Liu, H. Liu, D. Tong, J. Yang, and J. Peng, “An efficient approach to control the morphology and the adhesion properties of anodized TiO2 nanotube arrays for improved photoconversion efficiency,” *Electrochim. Acta*, vol. 56, no. 6, pp. 2618–2626, Feb. 2011, doi: 10.1016/j.electacta.2010.11.012.

[96] S. Yoriya, W. Kittimeteeworakul, and N. Punprasert, “Effect of Anodization Parameters on Morphologies of TiO 2 Nanotube Arrays and Their Surface Properties,” *J. Chem. Chem. Eng*, vol. 6, pp. 686–691, 2012, doi: 10.1016/j.jmst.2015.07.012.

[97] H. Sopha, L. Hromadko, K. Nechvilova, and J. M. Macak, “Effect of electrolyte age and potential changes on the morphology of TiO2 nanotubes,” *J. Electroanal. Chem.*, vol. 759, pp. 122–128, 2015, doi: 10.1016/j.jelechem.2015.11.002.

[98] F. M. B. Hassan, H. Nanjo, M. Kanakubo, I. Ishikawa, and M. Nishioka, “Effect of Ultrasonic Waves on the Formation of TiO2 Nanotubes by Electrochemical Anodization of Titanium in Glycerol and NH4F,” *eJournal Surf. Sci. Nanotechnol.*, vol. 7, no. February, pp. 84–88, 2009, doi: 10.1380/ejssnt.2009.84.

[99] Q. Chen, D. Xu, Z. Wu, and Z. Liu, “Free-standing TiO(2) nanotube arrays made by anodic oxidation and ultrasonic splitting.,” *Nanotechnology*, vol. 19, no. 36, p. 365708, 2008, doi: 10.1088/0957-4484/19/36/365708.

[100] G. D. Sulka, J. Kapusta-Kołodziej, A. Brzózka, and J. Marian, “Anodic growth of TiO2 nanopore arrays at various temperatures,” *Electrochim. Acta*, no. 104, pp. 526–535, 2013.

[101] S. P. Albu, A. Ghicov, J. M. Macak, R. Hahn, and P. Schmuki, “Nanotube Membrane for Flow-through Photocatalytic Applications,” pp. 5–8, 2007, doi: 10.1021/nl070264k.

[102] C.-J. Lin, W.-Y. Yu, Y.-T. Lu, and S.-H. Chien, “Fabrication of open-ended high aspect-ratio anodic TiO2 nanotube films for photocatalytic and photoelectrocatalytic applications,” *Chem. Commun.*, no. 45, pp. 6031–6033, 2008, doi: 10.1039/b813937g.

[103] F. Zhang, S. Chen, Y. Yin, C. Lin, and C. Xue, “Anodic formation of ordered and bamboo-type TiO2 anotubes arrays with different electrolytes,” *J. Alloys Compd.*, vol. 490, no. 1–2, pp. 247–252, 2010, doi: 10.1016/j.jallcom.2009.09.169.

[104] N. Vaenas, T. Stergiopoulos, A. G. Kontos, V. Likodimos, and P. Falaras, “Influence of controlled-charge anodization processes on the morphology of TiO2 nanotubes and their efficiency in dye-sensitized solar cells,” *Electrochim. Acta*, vol. 113, pp. 490–496, 2013, doi: 10.1016/j.electacta.2013.09.118.

[105] F. Mura, A. Masci, M. Pasquali, and A. Pozio, “Effect of a galvanostatic treatment on the preparation of highly ordered TiO2 nanotubes,” *Electrochim. Acta*, vol. 54, no. 14, pp. 3794–3798, 2009, doi: 10.1016/j.electacta.2009.01.073.

[106] K. S. Brammer, S. Oh, J. O. Gallagher, and S. Jin, “Enhanced cellular mobility guided by TiO2 nanotube surfaces,” *Nano Lett.*, vol. 8, no. 3, pp. 786–793, 2008, doi: 10.1021/nl072572o.

[107] A. Roguska *et al.*, “Improvement of the bio-functional properties of TiO2 nanotubes,” *Appl. Surf. Sci.*, vol. 388, pp. 775–785, 2016, doi: 10.1016/j.apsusc.2016.03.128.

[108] W. Yu, C. Qian, X. Jiang, F. Zhang, and W. Weng, “Mechanisms of stem cell osteogenic differentiation on TiO2 nanotubes,” *Colloids Surfaces B Biointerfaces*, vol. 136, pp. 779–785, 2015, doi: 10.1016/j.colsurfb.2015.10.019.

[109] B. Ercan, E. Taylor, E. Alpaslan, and T. J. Webster, “Diameter of titanium nanotubes influences anti-bacterial efficacy.,” *Nanotechnology*, vol. 22, no. 29, p. 295102, 2011, doi: 10.1088/0957-4484/22/29/295102.

[110] Z. Lewandowska, P. Piszczek, A. Radtke, T. Jedrzejewski, W. Kozak, and B. Sadowska, “The evaluation of the impact of titania nanotube covers morphology and crystal phase on their biological properties,” *J. Mater. Sci. Mater. Med.*, vol. 26, no. 4, pp. 1–12, 2015, doi: 10.1007/s10856-015-5495-2.

[111] S.-H. An, R. Narayanan, T. Matsumoto, H.-J. Lee, T.-Y. Kwon, and K.-H. Kim, “Crystallinity of anodic TiO2 nanotubes and bioactivity.,” *J. Nanosci. Nanotechnol.*, vol. 11, no. 6, pp. 4910–4918, 2011, doi: 10.1166/jnn.2011.4114.

[112] S. Oh and S. Jin, “Titanium oxide nanotubes with controlled morphology for enhanced bone growth,” *Mater. Sci. Eng. C*, vol. 26, no. 8, pp. 1301–1306, Sep. 2006, doi: 10.1016/j.msec.2005.08.014.

[113] X. Shi, Q. Xu, and A. Tian, “Antibacterial Activities of TiO2 Nanotubes on Porphyromonas gingivalis,” 2015.

[114] A. Mazare, M. Dilea, D. Ionita, I. Titorencu, V. Trusca, and E. Vasile, “Changing bioperformance of TiO 2 amorphous nanotubes as an effect of inducing crystallinity,” *Bioelectrochemistry*, vol. 87, no. April 2016, pp. 124–131, 2012, doi: 10.1016/j.bioelechem.2012.01.002.

[115] S. Oh, Chiara Daraio, L.-H. Chen, T. R. Pisanic, R. R. Fiñones, and S. Jin, “Significantly accelerated osteoblast cell growth on aligned TiO2 nanotubes,” *J. Biomed. Mater. Res. A*, vol. 78 A, no. 1, pp. 97–103, 2006, doi: 10.1002/jbm.a.

[116] K. D. Yun *et al.*, “Effect of nanotubular-micro-roughened titanium surface on cell response in vitro and osseointegration in vivo,” *Mater. Sci. Eng. C*, vol. 30, no. 1, pp. 27–33, 2010, doi: 10.1016/j.msec.2009.08.004.

[117] H. H. Park *et al.*, “Bioactive and electrochemical characterization of TiO2 nanotubes on titanium via anodic oxidation,” *Electrochim. Acta*, vol. 55, no. 20, pp. 6109–6114, Aug. 2010, doi: 10.1016/j.electacta.2010.05.082.

[118] L. M. Bjursten, L. Rasmusson, S. Oh, G. C. Smith, K. S. Brammer, and S. Jin, “Titanium dioxide nanotubes enhance bone bonding in vivo,” *J. Biomed. Mater. Res. - Part A*, vol. 92, no. 3, pp. 1218–1224, 2010, doi:

10.1002/jbm.a.32463.

[119] K. S. Brammer, S. Oh, C. J. Cobb, L. M. Bjursten, H. van der Heyde, and S. Jin, “Improved bone-forming functionality on diameter-controlled TiO(2) nanotube surface.,” *Acta Biomater.*, vol. 5, no. 8, pp. 3215–23, 2009, doi: 10.1016/j.actbio.2009.05.008.

[120] H. J. A. Y.Q. Haoa, S.J. Lib, Y.L. Haob, Y.K. Zhaoc, Y. L. Y. Q. Hao, S. J. Li, Y. L. Y. Q. Hao, Y. K. Zhao, and H. J. Ai, “Effect of nanotube diameters on bioactivity of a multifunctional titanium alloy,” *Appl. Surf. Sci.*, vol. 268, pp. 44–51, Mar. 2013, doi: 10.1016/j.apsusc.2012.11.142.

[121] E. Gongadze, D. Kabaso, S. Bauer, J. Park, P. Schmuki, and A. Iglič, “Adhesion of osteoblasts to a vertically aligned TiO2 nanotube surface.,” *Mini Rev. Med. Chem.*, vol. 13, no. 2, pp. 194–200, 2013.

[122] H. Zhang, S. Yang, N. Masako, D. J. Lee, L. F. Cooper, and C.-C. Ko, “Proliferation of preosteoblasts on TiO 2 nanotubes is FAK/RhoA related,” *RSC Adv.*, vol. 5, no. 48, pp. 38117–38124, 2015, doi: 10.1039/C4RA16803H.

[123] C. Von Wilmowsky, S. Bauer, S. Roedl, F. W. Neukam, P. Schmuki, and K. A. Schlegel, “The diameter of anodic TiO 2 nanotubes affects bone formation and correlates with the bone morphogenetic protein-2 expression in vivo,” *Clin. Oral Implants Res.*, vol. 23, no. 3, pp. 359–366, 2012, doi: 10.1111/j.1600-0501.2010.02139.x.

[124] S. Bauer, J. Park, J. Faltenbacher, S. Berger, K. von der Mark, and P. Schmuki, “Size selective behavior of mesenchymal stem cells on ZrO(2) and TiO(2) nanotube arrays.,” *Integr. Biol. (Camb).*, vol. 1, no. 8–9, pp. 525–532, 2009, doi: 10.1039/b908196h.

[125] S. Oh *et al.*, “Stem cell fate dictated solely by altered nanotube dimension,” *Proc. Natl. Acad. Sci. U. S. A.*, vol. 106, no. 7, pp. 2130–2135, 2009, doi: 10.1073/pnas.0813200106.

[126] N. Wang *et al.*, “Effects of TiO2 nanotubes with different diameters on gene expression and osseointegration of implants in minipigs,” *Biomaterials*, vol. 32, no. 29, pp. 6900–6911, 2011, doi: 10.1016/j.biomaterials.2011.06.023.

[127] J. M. Macak, S. Aldabergerova, A. Ghicov, and P. Schmuki, “Smooth anodic TiO 2 nanotubes: Annealing and structure,” *Phys. Status Solidi Appl. Mater. Sci.*, vol. 203, no. 10, pp. 67–69, 2006, doi: 10.1002/pssa.200622214.

[128] D. Fang, Z. Luo, K. Huang, and D. C. Lagoudas, “Effect of heat treatment on morphology, crystalline structure and photocatalysis properties of TiO2 nanotubes on Ti substrate and freestanding membrane,” *Appl. Surf. Sci.*, vol. 257, no. 15, pp. 6451–6461, 2011, doi: 10.1016/j.apsusc.2011.02.037.

[129] M. Jarosz *et al.*, “Heat treatment effect on crystalline structure and photoelectrochemical properties of anodic TiO2 nanotube arrays formed in ethylene glycol and glycerol based electrolytes,” *J. Phys. Chem. C*, vol. 119,

no. 42, pp. 24182–24191, 2015, doi: 10.1021/acs.jpcc.5b08403.

[130] Y. Yang, X. Wang, and L. Li, “Crystallization and phase transition of titanium oxide nanotube arrays,” *J. Am. Ceram. Soc.*, vol. 91, no. 2, pp. 632–635, 2008, doi: 10.1111/j.1551-2916.2007.02133.x.

[131] a. Jaroenworaluck, D. Regonini, C. R. R. Bowen, and R. Stevens, “A microscopy study of the effect of heat treatment on the structure and properties of anodised TiO2 nanotubes,” *Appl. Surf. Sci.*, vol. 256, no. 9, pp. 2672–2679, Feb. 2010, doi: 10.1016/j.apsusc.2009.09.078.

[132] W. Q. Yu, Y. L. Zhang, X. Q. Jiang, and F. Q. Zhang, “In vitro behavior of MC3T3-E1 preosteoblast with different annealing temperature titania nanotubes,” *Oral Dis.*, vol. 16, no. 7, pp. 624–630, 2010, doi: 10.1111/j.1601-0825.2009.01643.x.

[133] J. S. Suwandi, R. E. M. Toes, T. Nikolic, and B. O. Roep, “Inducing tissue specific tolerance in autoimmune disease with tolerogenic dendritic cells,” *Clin. Exp. Rheumatol.*, vol. 33, pp. 97–103, 2015, doi: 10.1002/jbm.a.

[134] Y. Bai *et al.*, “The effect of annealing temperatures on surface properties, hydroxyapatite growth and cell behaviors of TiO2 nanotubes,” *Surf. Interface Anal.*, vol. 43, no. 6, pp. 998–1005, 2011, doi: 10.1002/sia.3683.

[135] C. Yue, R. Kuijer, H. J. Kaper, H. C. Van der Mei, and H. J. Busscher, “Simultaneous interaction of bacteria and tissue cells with photocatalytically activated, anodized titanium surfaces,” *Biomaterials*, vol. 35, no. 9, pp. 2580–2587, 2014, doi: 10.1016/j.biomaterials.2013.12.036.

[136] C. Dumitriu, M. Popescu, C. Ungureanu, and C. Pirvu, “Antibacterial efficiencies of TiO2 nanostructured layers prepared in organic viscous electrolytes,” *Appl. Surf. Sci.*, vol. 341, pp. 157–165, 2015, doi: 10.1016/j.apsusc.2015.02.183.

[137] K. Narendrakumara *et al.*, “Adherence of Oral Streptococci to nanostructured titanium surfaces,” *Dent. Mater.*, vol. 31, no. 12, pp. 1460–1468, 2015.

[138] K. Koch and W. Barthlott, “Superhydrophobic and superhydrophilic plant surfaces: An inspiration for biomimetic materials,” *Philos. Trans. R. Soc. A Math. Phys. Eng. Sci.*, vol. 367, no. 1893, pp. 1487–1509, 2009, doi: 10.1098/rsta.2009.0022.

[139] E. Matykina, I. Garcia, J. J. de Damborenea, and M. a. Arenas, “Comparative determination of TiO2 surface free energies for adhesive bonding application,” *Int. J. Adhes. Adhes.*, vol. 31, no. 8, pp. 832–839, Dec. 2011, doi: 10.1016/j.ijadhadh.2011.08.003.

[140] M. Żenkiewicz, “Comparative study on the surface free energy of a solid calculated by different methods,” *Polym. Test.*, vol. 26, no. 1, pp. 14–19, Feb. 2007, doi: 10.1016/j.polymertesting.2006.08.005.

[141] L. Yang *et al.*, “Effect of annealing temperature on wettability of TiO2 nanotube

array films.," *Nanoscale Res. Lett.*, vol. 9, no. 1, p. 621, Jan. 2014, doi: 10.1186/1556-276X-9-621.

[142] G. Liu, K. Du, and K. Wang, "Surface wettability of TiO2 nanotube arrays prepared by electrochemical anodization," *Appl. Surf. Sci.*, vol. 388, pp. 313–320, 2016, doi: 10.1016/j.apsusc.2016.01.010.

[143] Y. Sun *et al.*, "Effect of heat treatment on surface hydrophilicity-retaining ability of titanium dioxide nanotubes," *Appl. Surf. Sci.*, vol. 440, no. 400, pp. 440–447, 2018, doi: 10.1016/j.apsusc.2018.01.136.

[144] L. Lin *et al.*, "Enhanced osteointegration of medical titanium implant with surface modifications in micro/nanoscale structures," *J. Orthop. Transl.*, vol. 2, no. 1, pp. 35–42, 2014, doi: 10.1016/j.jot.2013.08.001.

[145] S. Lin, S. Huang, S. Chen, L. U. Vinzons, J. Ciou, and P. Wong, "Investigation of the Interfacial E ff ects of Small Chemical-Modi fi ed TiO 2 Nanotubes on 3T3 Fibroblast Responses," 2014.

[146] Roshasnorlyza Hazan, Srimala Sreekantan, Adilah Abdul Khalil, Ira Maya Sophia Nordin, and Ishak Mat, "Surface Engineering of Titania for Excellent Fibroblast 3T3 Cell-Metal Interaction," *J. Phys. Sci.*, vol. 20, no. 1, pp. 35–47, 2009.

[147] S. Bauer, J. Park, K. von der Mark, and P. Schmuki, "Improved attachment of mesenchymal stem cells on super-hydrophobic TiO2 nanotubes," *Acta Biomater.*, vol. 4, no. 5, pp. 1576–1582, 2008, doi: 10.1016/j.actbio.2008.04.004.

[148] J. a Sorkin, S. Hughes, P. Soares, and K. C. Popat, "Titania nanotube arrays as interfaces for neural prostheses.," *Mater. Sci. Eng. C. Mater. Biol. Appl.*, vol. 49, pp. 735–45, Apr. 2015, doi: 10.1016/j.msec.2015.01.077.

[149] F. Shen *et al.*, "Vascular cell responses to ECM produced by smooth muscle cells on TiO2 nanotubes," *Appl. Surf. Sci.*, vol. 349, pp. 589–598, 2015, doi: 10.1016/j.apsusc.2015.05.042.

[150] N.-S. S. Peighambardoust and F. Nasirpouri, "Manipulating morphology, pore geometry and ordering degree of TiO2 nanotube arrays by anodic oxidation," *Surf. Coatings Technol.*, vol. 235, pp. 727–734, Nov. 2013, doi: 10.1016/j.surfcoat.2013.08.058.

[151] R. Beranek, H. Hildebrand, and P. Schmuki, "Self-Organized Porous Titanium Oxide Prepared in H[sub 2]SO[sub 4]/HF Electrolytes," *Electrochem. Solid-State Lett.*, vol. 6, no. 3, p. B12, 2003, doi: 10.1149/1.1545192.

[152] a. Apolinário *et al.*, "The role of the Ti surface roughness in the self-ordering of TiO2 nanotubes: a detailed study of the growth mechanism," *J. Mater. Chem. A*, vol. 2, no. 24, p. 9067, 2014, doi: 10.1039/c4ta00871e.

[153] A. Apolinário *et al.*, "Modeling the Growth Kinetics of Anodic TiO2 Nanotubes.," *J. Phys. Chem. Lett.*, vol. 6, no. 5, pp. 845–51, 2015, doi: 10.1021/jz502380b.

[154] D. Regonini and F. J. Clemens, “Anodized TiO2nanotubes: Effect of anodizing time on film length, morphology and photoelectrochemical properties,” *Mater. Lett.*, vol. 142, pp. 97–101, 2015, doi: 10.1016/j.matlet.2014.11.145.

[155] K. S. Raja, T. Gandhi, and M. Misra, “Effect of water content of ethylene glycol as electrolyte for synthesis of ordered titania nanotubes,” *Electrochem. commun.*, vol. 9, no. 5, pp. 1069–1076, May 2007, doi: 10.1016/j.elecom.2006.12.024.

[156] R. G. Freitas, M. A. Santanna, and E. C. Pereira, “Dependence of TiO2 nanotube microstructural and electronic properties on water splitting,” *J. Power Sources*, vol. 251, pp. 178–186, 2014, doi: 10.1016/j.jpowsour.2013.11.067.

[157] M. Dubey and H. He, “Morphological and Photovoltaic Studies of TiO2 NTs for High Efficiency Solar Cells,” in *Scanning Electron Microscopy*, InTech, 2012.

[158] G. Ali, C. Chen, S. H. Yoo, J. M. Kum, and S. O. Cho, “Fabrication of complete titania nanoporous structures via electrochemical anodization of Ti.,” *Nanoscale Res. Lett.*, vol. 6, no. 1, p. 332, 2011, doi: 10.1186/1556-276X-6-332.

[159] Y. Ye, Y. Liu, and T. Guo, “Effect of H2O content in electrolyte on synthesis and field emission property of anodized TiO2 nanotubes,” *Surf. Coatings Technol.*, vol. 245, pp. 28–33, Apr. 2014, doi: 10.1016/j.surfcoat.2014.02.027.

[160] H. Xu, Q. Zhang, C. Zheng, W. Yan, and W. Chu, “Application of ultrasonic wave to clean the surface of the TiO2 nanotubes prepared by the electrochemical anodization,” *Appl. Surf. Sci.*, vol. 257, no. 20, pp. 8478–8480, 2011, doi: 10.1016/j.apsusc.2011.04.135.

[161] D. G. Li, D. R. Chen, J. D. Wang, and P. Liang, “Effect of acid solution, fluoride ions, anodic potential and time on the microstructure and electronic properties of self-ordered TiO2nanotube arrays,” *Electrochim. Acta*, vol. 207, pp. 152–163, 2016, doi: 10.1016/j.electacta.2016.04.002.

[162] W. J. St??pniowski, J. Choi, H. Yoo, M. Michalska-Doma??ska, P. Chilimoniuk, and T. Czujko, “Quantitative fast Fourier transform based arrangement analysis of porous anodic oxide formed by self-organized anodization of FeAl intermetallic alloy,” *Mater. Lett.*, vol. 164, no. December, pp. 176–179, 2016, doi: 10.1016/j.matlet.2015.10.168.

[163] M. Michalska-doman, “Characterization of nanopores arrangement of anodic alumina layers synthesized on low- (AA1050) and high-purity aluminum by two-step anodizing in sulfuric acid with addition of ethylene glycol at low temperature,” 2016, doi: 10.1007/s10934-016-0316-7.

[164] W. J. Stępniowski, M. Michalska-Domańska, M. Norek, and T. Czujko, “Fast Fourier transform based arrangement analysis of poorly organized alumina nanopores formed via self-organized anodization in chromic acid,” *Mater. Lett.*, vol. 117, no. December, pp. 69–73, 2014, doi:

10.1016/j.matlet.2013.11.099.

[165] A. Nowak-Stepniowska, “A Review of Quantitative Arragement Analysis Methods Applied to Nanostructured Anodic Oxides Charaterization,” *Curr. Nanosci.*, vol. 11, pp. 581–592, 2015.

[166] L. Zaraska, W. J. St??pniowski, E. Ciepiela, and G. D. Sulka, “The effect of anodizing temperature on structural features and hexagonal arrangement of nanopores in alumina synthesized by two-step anodizing in oxalic acid,” *Thin Solid Films*, vol. 534, pp. 155–161, 2013, doi: 10.1016/j.tsf.2013.02.056.

[167] W. J. Stepniowski *et al.*, “Anodization of cold deformed technical purity aluminum (AA1050) in oxalic acid,” *Surf. Coatings Technol.*, vol. 258, no. January, pp. 268–274, 2014, doi: 10.1016/j.surfcoat.2014.09.013.

[168] J. Kapusta-Kołodziej, O. Tynkevych, A. Pawlik, M. Jarosz, J. Mech, and G. D. Sulka, “Electrochemical growth of porous titanium dioxide in a glycerol-based electrolyte at different temperatures,” *Electrochim. Acta*, vol. 144, pp. 127–135, Oct. 2014, doi: 10.1016/j.electacta.2014.08.055.

[169] K. Lee, D. Kim, and P. Schmuki, “Highly self-ordered nanochannel TiO2 structures by anodization in a hot glycerol electrolyte,” *Chem. Commun.*, vol. 47, no. 20, pp. 5789–5791, 2011, doi: 10.1039/c1cc11160d.

[170] J. Wang and Z. Lin, “Anodic Formation of Ordered TiO 2 Nanotube Arrays : Effects of Electrolyte Temperature and Anodization Potential,” *J. Phys. Chem. C*, pp. 4026–4030, 2009.

[171] J. M. Macak and P. Schmuki, “Anodic growth of self-organized anodic TiO2 nanotubes in viscous electrolytes,” *Electrochim. Acta*, vol. 52, no. 3, pp. 1258–1264, Nov. 2006, doi: 10.1016/j.electacta.2006.07.021.

[172] Y. C. Lim, Z. Zainal, W. T. Tan, and M. Z. Hussein, “Anodization parameters influencing the growth of titania nanotubes and their photoelectrochemical response,” *Int. J. Photoenergy*, vol. 2012, 2012, doi: 10.1155/2012/638017.

[173] G. K. Mor, K. Shankar, M. Paulose, O. K. Varghese, and C. a. Grimes, “Enhanced photocleavage of water using titania nanotube arrays,” *Nano Lett.*, vol. 5, no. 1, pp. 191–195, 2005, doi: 10.1021/nl048301k.

[174] V. M. Prida, E. Manova, V. Vega, M. Hernandez-velez, P. Aranda, and K. R. Pirota, “Temperature influence on the anodic growth of self-aligned Titanium dioxide nanotube arrays,” *J. Magn. Magn. Mater.*, vol. 316, pp. 110–113, 2007, doi: 10.1016/j.jmmm.2007.02.021.

[175] X. H. Yang and W. L. Zhu, “Viscosity properties of sodium carboxymethylcellulose solutions,” *Cellulose*, vol. 14, no. 5, pp. 409–417, 2007, doi: 10.1007/s10570-007-9137-9.

[176] H. Sopha, L. Hromadko, K. Nechvilova, and J. M. Macak, “Effect of electrolyte age and potential changes on the morphology of TiO 2 nanotubes,” *Jeac*, vol. 759, pp. 122–128, 2015, doi: 10.1016/j.jelechem.2015.11.002.

[177] K. Lee, H. Kim, Y. Lee, and Y. Tak, “Effect of Electrolyte Conductivity on the Formation of a Nanotubular TiO 2 Photoanode for a Dye-Sensitized Solar Cell,” *J. Korean Phys. Soc.*, vol. 54, no. 3, pp. 1027–1031, 2009, doi: 10.3938/jkps.54.1027.

[178] T. H. Kim, J. W. Lee, B. S. Kim, H. Cha, and Y. C. Nah, “Morphological investigation of anodized TiO 2 nanotubes fabricated using different voltage conditions,” *Microporous Mesoporous Mater.*, vol. 196, pp. 41–45, 2014, doi: 10.1016/j.micromeso.2014.04.056.

[179] M. Jarosz, A. Pawlik, J. Kapusta-Kołodziej, M. Jaskuła, and G. D. Sulka, “Effect of the previous usage of electrolyte on growth of anodic titanium dioxide (ATO) in a glycerol-based electrolyte,” *Electrochim. Acta*, vol. 136, pp. 412–421, Aug. 2014, doi: 10.1016/j.electacta.2014.05.077.

[180] Y. Tang, J. Tao, Z. Dong, J. T. Oh, and Z. Chen, “The formation of micrometer-long TiO2 nanotube arrays by anodization of titanium film on conducting glass substrate,” *Adv. Nat. Sci. Nanosci. Nanotechnol.*, vol. 2, no. 4, 2011, doi: 10.1088/2043-6262/2/4/045002.

[181] D. Regonini, a. Satka, a. Jaroenworaluck, D. W. E. Allsopp, C. R. Bowen, and R. Stevens, “Factors influencing surface morphology of anodized TiO2 nanotubes,” *Electrochim. Acta*, vol. 74, pp. 244–253, Jul. 2012, doi: 10.1016/j.electacta.2012.04.076.

[182] D. Regonini and F. J. Clemens, “Anodized TiO2 nanotubes: Effect of anodizing time on film length, morphology and photoelectrochemical properties,” *Mater. Lett.*, vol. 142, pp. 97–101, 2015, doi: 10.1016/j.matlet.2014.11.145.

[183] H. Omidvar, S. Goodarzi, A. Seif, and A. R. Azadmehr, “Influence of anodization parameters on the morphology of TiO2 nanotube arrays,” *Superlattices Microstruct.*, vol. 50, no. 1, pp. 26–39, 2011, doi: 10.1016/j.spmi.2011.04.006.

[184] X. Wang, Y. Li, H. Song, Y. Huang, R. Su, and F. Besenbacher, “Fluoride concentration controlled TiO2 nanotubes: the interplay of microstructure and photocatalytic performance,” *RSC Adv.*, vol. 6, no. 22, pp. 18333–18339, 2016, doi: 10.1039/C5RA24732B.

[185] P. Acevedo-Peña, L. Lartundo-Rojas, and I. González, “Effect of water and fluoride content on morphology and barrier layer properties of TiO2 nanotubes grown in ethylene glycol-based electrolytes,” *J. Solid State Electrochem.*, vol. 17, no. 11, pp. 2939–2947, 2013, doi: 10.1007/s10008-013-2212-2.

[186] B. G. LEE, J. W. CHOI, S. E. LEE, Y. S. JEONG, H. J. OH, and C. S. CHI, “Formation behavior of anodic TiO2nanotubes in fluoride containing electrolytes,” *Trans. Nonferrous Met. Soc. China (English Ed.*, vol. 19, no. 4, pp. 842–845, 2009, doi: 10.1016/S1003-6326(08)60361-1.

[187] L. V. Taveira, J. M. Macák, H. Tsuchiya, L. F. P. Dick, and P. Schmuki, “Initiation and Growth of Self-Organized TiO2 Nanotubes Anodically Formed

in NH4F⁄(NH 4)2SO4 Electrolytes," *J. Electrochem. Soc.*, vol. 152, no. 10, p. B405, 2005, doi: 10.1149/1.2008980.

[188] Y. C. Nah, N. K. Shrestha, D. Kim, S. P. Albu, I. Paramasivam, and P. Schmuki, "Voltage induced self-peeling of initiation layers on self-organized TiO2-WO3 nanotubes and formation of oxide nanosheet rolls," *Electrochem. Solid-State Lett.*, vol. 13, no. 8, pp. 2–6, 2010, doi: 10.1149/1.3428513.

[189] J. M. Macák, H. Tsuchiya, and P. Schmuki, "High-aspect-ratio TiO2 nanotubes by anodization of titanium.," *Angew. Chem. Int. Ed. Engl.*, vol. 44, no. 14, pp. 2100–2, Mar. 2005, doi: 10.1002/anie.200462459.

[190] C. Dumitriu, C. Pirvu, and I. Demetrescu, "The Electrochemical Formation and Shielding Mechanism of TiO2 Nanotubes in Organic Electrolytes with Different Viscosity," *J. Electrochem. Soc.*, vol. 160, no. 2, pp. G55–G60, 2012, doi: 10.1149/2.035302jes.

[191] W. L. Lü, N. Wang, P. Gao, C. Y. Li, H. S. Zhao, and Z. T. Zhang, "Effects of anodic titanium dioxide nanotubes of different diameters on macrophage secretion and expression of cytokines and chemokines," *Cell Prolif.*, vol. 48, no. 1, pp. 95–104, 2015, doi: 10.1111/cpr.12149.

[192] M.-Y. Lan and S. Lee, "Diameter Selective behavior of human nasal ephitelial cell on Ag-coated TiO2 nanotubes," *Ceram. Int.*, vol. 40, pp. 4745–4751, 2014.

[193] D. Guan, P. J. Hymel, and Y. Wang, "Growth mechanism and morphology control of double-layer and bamboo-type TiO 2 nanotube arrays by anodic oxidation," *Electrochim. Acta*, vol. 83, pp. 420–429, 2012, doi: 10.1016/j.electacta.2012.08.036.

[194] C. Moseke, F. Hage, E. Vorndran, and U. Gbureck, "TiO 2 nanotube arrays deposited on Ti substrate by anodic oxidation and their potential as a long-term drug delivery system for antimicrobial agents," *Appl. Surf. Sci.*, vol. 258, no. 14, pp. 5399–5404, 2012, doi: 10.1016/j.apsusc.2012.02.022.

[195] M. Norek, W. J. Stępniowski, and D. Siemiaszko, "Effect of ethylene glycol on morphology of anodic alumina prepared in hard anodization," *J. Electroanal. Chem.*, vol. 762, no. December 2015, pp. 20–28, 2016, doi: 10.1016/j.jelechem.2015.12.026.

[196] W. J. Stępniowski, A. Nowak-Stępniowska, M. Michalska-domańska, M. Norek, T. Czujko, and Z. Bojar, "Fabrication and geometric characterization of highly-ordered hexagonally arranged arrays of nanoporous anodic alumina," *Polish J. Chem. Technol.*, vol. 16, no. 1, pp. 63–69, 2014, doi: 10.2478/pjct-2014-0011.

[197] L. Zaraska, G. D. Sulka, and M. Jaskuła, "The effect of n-alcohols on porous anodic alumina formed by self-organized two-step anodizing of aluminum in phosphoric acid," *Surf. Coatings Technol.*, vol. 204, no. 11, pp. 1729–1737, 2010, doi: 10.1016/j.surfcoat.2009.10.051.

[198] W. J. Stępniowski, A. Nowak-Stępniowska, A. Presz, T. Czujko, and R. A. Varin, “The effects of time and temperature on the arrangement of anodic aluminum oxide nanopores,” *Mater. Charact.*, vol. 91, no. April, pp. 1–9, 2014, doi: 10.1016/j.matchar.2014.01.030.

[199] D. C. Leitao *et al.*, “Nanoscale topography: A tool to enhance pore order and pore size distribution in anodic aluminum oxide,” *J. Phys. Chem. C*, vol. 115, no. 17, pp. 8567–8572, 2011, doi: 10.1021/jp202336j.

[200] G. D. Sulka, J. Kapusta-Kołodziej, A. Brzózka, and M. Jaskuła, “Fabrication of nanoporous TiO2 by electrochemical anodization,” *Electrochim. Acta*, vol. 55, no. 14, pp. 4359–4367, May 2010, doi: 10.1016/j.electacta.2009.12.053.

[201] M. Jarosz, J. Kapusta-Kołodziej, M. Jaskuła, and G. D. Sulka, “Effect of different polishing methods on anodic titanium dioxide formation,” *J. Nanomater.*, vol. 2015, 2015, doi: 10.1155/2015/295126.

[202] V. Asgari, M. Noormohammadi, A. Ramazani, and M. A. Kashi, “A facile method to form highly-ordered TiO2nanotubes at a stable growth rate of 1000 nm min-1under 60 v using an organic electrolyte for improved photovoltaic properties,” *J. Phys. D. Appl. Phys.*, vol. 50, no. 37, 2017, doi: 10.1088/1361-6463/aa812a.

[203] S. Farsinezhad, A. N. Dalrymple, and K. Shankar, “Toward single-step anodic fabrication of monodisperse TiO2 nanotube arrays on non-native substrates,” *Phys. Status Solidi Appl. Mater. Sci.*, vol. 211, no. 5, pp. 1113–1121, 2014, doi: 10.1002/pssa.201330649.

[204] Q. Cai, M. Paulose, O. K. Varghese, and C. A. Grimes, “The Effect of Electrolyte Composition on the Fabrication of Self-Organized Titanium Oxide Nanotube Arrays by Anodic Oxidation,” *J. Mater. Res.*, vol. 20, no. 01, pp. 230–236, 2005, doi: 10.1557/JMR.2005.0020.

[205] J. M. Macák, H. Tsuchiya, and P. Schmuki, “High-Aspect-Ratio TiO 2 Nanotubes by Anodization of Titanium,” *nanopo*, pp. 2100–2102, 2005, doi: 10.1002/anie.200462459.

[206] N. Liu, K. Lee, and P. Schmuki, “Small diameter TiO2 nanotubes vs. nanopores in dye sensitized solar cells,” *Electrochem. commun.*, vol. 15, no. 1, pp. 1–4, 2012, doi: 10.1016/j.elecom.2011.11.003.

[207] K. Shankar, G. K. Mor, A. Fitzgerald, and C. A. Grimes, “Cation effect on the electrochemical formation of very high aspect ratio TiO2nanotube arrays in formamide-water mixtures,” *J. Phys. Chem. C*, vol. 111, no. 1, pp. 21–26, 2007, doi: 10.1021/jp066352v.

[208] G. Liu, N. Hoivik, and K. Wang, “Small diameter TiO2nanotubes with enhanced photoresponsivity,” *Electrochem. commun.*, vol. 28, pp. 107–110, 2013, doi: 10.1016/j.elecom.2012.12.020.

[209] F. Mohammadpour, F. Behzadi, and M. Moradi, “Fast anodically growth of

long, small diameter TiO2 nanotubes by electropolishing of Ti foils in an ethanol-containing solution," *Mater. Lett.*, vol. 150, no. February, pp. 81–83, 2015, doi: 10.1016/j.matlet.2015.02.081.

[210] X. Wang, L. Sun, S. Zhang, and X. Wang, "Ultralong, small-diameter TiO2 nanotubes achieved by an optimized two-step anodization for efficient dye-sensitized solar cells," *ACS Appl. Mater. Interfaces*, vol. 6, no. 3, pp. 1361–1365, 2014, doi: 10.1021/am404966e.

[211] P. Quitério, A. Apolinário, C. T. Sousa, J. D. Costa, J. Ventura, and J. P. Araújo, "The cyclic nature of porosity in anodic TiO2 nanotube arrays," *J. Mater. Chem. A*, vol. 3, no. January 2015, pp. 3692–3698, 2015, doi: 10.1039/C4TA04607B.

[212] C. C. Raj and L. Neelakantan, "Electrochemical Investigation on the Inhibitive Nature of Barrier Layer on the Growth Rate of TiO $_2$ Nanotube Arrays," *J. Electrochem. Soc.*, vol. 165, no. 10, pp. E521–E526, 2018, doi: 10.1149/2.0021811jes.

[213] J. E. Carrera-crespo, F. González, I. González, and P. Acevedo-pe, "Electrochimica Acta Effect of heat treatment on the crystal phase composition , semiconducting properties and photoelectrocatalytic color removal efficiency of TiO 2 nanotubes arrays," vol. 140, pp. 564–571, 2014, doi: 10.1016/j.electacta.2014.06.056.

[214] Y. C. Lim, Z. Zainal, M. Z. Hussein, and W. T. Tan, "The effect of heat treatment on phase transformation, morphology and photoelectrochemical response of short TiO2 nanotubes," *Dig. J. Nanomater. Biostructures*, vol. 8, no. 1, pp. 167–176, 2012.

[215] J. Yu and B. Wang, "Effect of calcination temperature on morphology and photoelectrochemical properties of anodized titanium dioxide nanotube arrays," *Appl. Catal. B Environ.*, vol. 94, no. 3–4, pp. 295–302, Feb. 2010, doi: 10.1016/j.apcatb.2009.12.003.

[216] H.-C. Liang and X.-Z. Li, "Effects of structure of anodic TiO(2) nanotube arrays on photocatalytic activity for the degradation of 2,3-dichlorophenol in aqueous solution.," *J. Hazard. Mater.*, vol. 162, no. 2–3, pp. 1415–22, Mar. 2009, doi: 10.1016/j.jhazmat.2008.06.033.

[217] O. K. Varghese, D. Gong, M. Paulose, C. a. Grimes, and E. C. Dickey, "Crystallization and high-temperature structural stability of titanium oxide nanotube arrays," *J. Mater. Res.*, vol. 18, no. 01, pp. 156–165, 2003, doi: 10.1557/JMR.2003.0022.

[218] A. Shivaram, S. Bose, and A. Bandyopadhyay, "Thermal degradation of TiO2 nanotubes on titanium," *Appl. Surf. Sci.*, vol. 317, pp. 573–580, 2014, doi: 10.1016/j.apsusc.2014.08.107.

[219] S. P. Albu, H. Tsuchiya, S. Fujimoto, and P. Schmuki, "TiO2 nanotubes - Annealing effects on detailed morphology and structure," *Eur. J. Inorg. Chem.*,

no. 27, pp. 4351–4356, 2010, doi: 10.1002/ejic.201000608.

[220] F. Hardcastle, “Raman Spectroscopy of Titania (TiO2) Nanotubular Water-Splitting Catalysts,” *J. Ark. Acad. Sci.*, vol. 65, pp. 43–48, 2011.

[221] S. Bauer, A. Pittrof, H. Tsuchiya, and P. Schmuki, “Size-effects in TiO2 nanotubes: Diameter dependent anatase/rutile stabilization,” *Electrochem. commun.*, vol. 13, no. 6, pp. 538–541, 2011, doi: 10.1016/j.elecom.2011.03.003.

[222] F. A. Scaramuzzo, A. Dell’Era, G. Tarquini, R. Caminiti, P. Ballirano, and M. Pasquali, “Phase transition of TiO2 nanotubes: An X-ray study as a function of temperature,” *J. Phys. Chem. C*, vol. 121, no. 39, pp. 24871–24876, 2017, doi: 10.1021/acs.jpcc.7b08297.

[223] J. Zhang, M. Li, Z. Feng, J. Chen, and C. Li, “UV Raman Spectroscopic Study on TiO_2. I. Phase Transformation at the Surface and in the Bulk,” *J. Phys. Chem. B*, vol. 110, no. 2, pp. 927–935, 2006, doi: 10.1021/jp0552473.

[224] A. A. Valeeva *et al.*, “Nonstoichiometric titanium dioxide nanotubes with enhanced catalytical activity under visible light,” *Sci. Rep.*, vol. 8, no. 1, pp. 1–10, 2018, doi: 10.1038/s41598-018-28045-1.

[225] S. Y. Kim, Y. K. Kim, I. S. Park, G. C. Jin, T. S. Bae, and M. H. Lee, “Effect of alkali and heat treatments for bioactivity of TiO2 nanotubes,” *Appl. Surf. Sci.*, vol. 321, pp. 412–419, 2014, doi: 10.1016/j.apsusc.2014.09.177.

[226] V. H. Castrejón-Sánchez, E. Camps, and M. Camacho-López, “Quantification of phase content in TiO2 thin films by Raman spectroscopy,” *Superf. y Vacio*, vol. 27, no. 3, pp. 88–92, 2014.

[227] A. Niilisk *et al.*, “Structural study of TiO2 thin films by micro-Raman spectroscopy,” *Cent. Eur. J. Phys.*, vol. 4, no. 1, pp. 105–116, 2006, doi: 10.1007/s11534-005-0009-3.

[228] S. W. Lu, C. Harris, S. Walck, and M. Arbab, “Phase sensitivity of Raman spectroscopy analysis of CVD titania thin films,” *J. Mater. Sci.*, vol. 44, no. 2, pp. 541–544, 2009, doi: 10.1007/s10853-008-3086-z.

[229] Q. Dou, P. Shrotriya, W. Li, and K. R. Hebert, “Stress-generating electrochemical reactions during the initial growth of anodic titanium dioxide nanotube layers,” *Electrochim. Acta*, vol. 295, pp. 418–426, 2019, doi: 10.1016/j.electacta.2018.10.094.

[230] Q. Dou, P. Shrotriya, W. Li, and K. R. Hebert, “Roles of mechanical stress and lower-valent oxide in the formation of anodic titanium dioxide nanotube layers,” *Electrochim. Acta*, vol. 292, pp. 676–684, 2018, doi: 10.1016/j.electacta.2018.09.182.

[231] X. Wang, J. Zhao, X. Wang, and J. Zhou, “Causes for the formation of titania nanotubes during anodization,” *IEEE Trans. Nanotechnol.*, vol. 14, no. 1, pp. 113–117, 2015, doi: 10.1109/TNANO.2014.2370041.

[232] D. I. Petukhov *et al.*, “Formation mechanism and packing options in tubular anodic titania films,” *Microporous Mesoporous Mater.*, vol. 114, no. 1–3, pp. 440–447, Sep. 2008, doi: 10.1016/j.micromeso.2008.01.033.

[233] T. Ioroi, H. Senoh, S. Yamazaki, Z. Siroma, N. Fujiwara, and K. Yasuda, “Stability of Corrosion-Resistant Magnéli-Phase Ti4O7-Supported PEMFC Catalysts at High Potentials,” *J. Electrochem. Soc.*, vol. 155, no. 4, p. B321, 2008, doi: 10.1149/1.2833310.

[234] S. Harada, K. Tanaka, and H. Inui, “Thermoelectric properties and crystallographic shear structures in titanium oxides of the Magnli phases,” *J. Appl. Phys.*, vol. 108, no. 8, 2010, doi: 10.1063/1.3498801.

[235] Y. Lu, Y. Matsuda, K. Sagara, L. Hao, T. Otomitsu, and H. Yoshida, “Fabrication and Thermoelectric Properties of Magneli Phases by Adding Ti into TiO_2,” *Adv. Mater. Res.*, vol. 415–417, pp. 1291–1296, 2011, doi: 10.4028/www.scientific.net/AMR.415-417.1291.

[236] A. Jemec Kokalj *et al.*, “The first comprehensive safety study of Magnéli phase titanium suboxides reveals no acute environmental hazard,” *Environ. Sci. Nano*, 2019, doi: 10.1039/c8en01119b.

[237] C. C. Chen, W. C. Say, S. J. Hsieh, and E. W. G. Diau, “A mechanism for the formation of annealed compact oxide layers at the interface between anodic titania nanotube arrays and Ti foil,” *Appl. Phys. A Mater. Sci. Process.*, vol. 95, no. 3, pp. 889–898, 2009, doi: 10.1007/s00339-009-5093-6.

[238] M. J. Hÿtch, “Geometric Phase Analysis of High Resolution Electron Microscope Images,” *Scanning Microsc.*, vol. 11, pp. 53–66, 1997, doi: 10.1177/0013916508328610.

[239] “CrysTBox - gpaGUI step by step.” [Online]. Available: https://www.fzu.cz/crystbox_gpaGUI_stepByStep.

[240] C. G. Jothi Prakash, C. Clement Raj, and R. Prasanth, “Fabrication of zero contact angle ultra-super hydrophilic surfaces,” *J. Colloid Interface Sci.*, vol. 496, pp. 300–310, 2017, doi: 10.1016/j.jcis.2017.01.007.

[241] V. C. Anitha, J.-H. Lee, J. Lee, A. Narayan Banerjee, S. Woo Joo, and B. Ki Min, “Biofilm formation on a TiO2 nanotube with controlled pore diameter and surface wettability.,” *Nanotechnology*, vol. 26, no. 6, p. 065102, Feb. 2015, doi: 10.1088/0957-4484/26/6/065102.

[242] D. H. Shin, T. Shokuhfar, C. K. Choi, S. H. Lee, and C. Friedrich, “Wettability changes of TiO2 nanotube surfaces,” *Nanotechnology*, vol. 22, no. 31, 2011, doi: 10.1088/0957-4484/22/31/315704.

[243] M. Y. Lan, C. P. Liu, H. H. Huang, J. K. Chang, and S. W. Lee, “Diameter-sensitive biocompatibility of anodic TiO2 nanotubes treated with supercritical CO2 fluid,” *Nanoscale Res. Lett.*, vol. 8, no. 1, pp. 1–8, 2013, doi: 10.1186/1556-276X-8-150.

[244] J. Xue, Z. Wang, W. Hu, Q. Shen, X. Liu, and H. Jia, “The surface wettability of TiO2 nanotube arrays: which is more important—morphology or chemical composition?,” *J. Porous Mater.*, vol. 26, no. 1, pp. 1–8, 2018, doi: 10.1007/s10934-018-0616-1.

[245] E. Balaur, J. M. Macak, H. Tsuchiya, and P. Schmuki, “Wetting behaviour of layers of TiO2 nanotubes with different diameters,” *J. Mater. Chem.*, vol. 15, no. 42, pp. 4488–4491, 2005, doi: 10.1039/b509672c.

[246] A. Hamlekhan *et al.*, “Fabrication of anti-aging TiO2 nanotubes on biomedical Ti alloys,” *PLoS One*, vol. 9, no. 5, pp. 1–10, 2014, doi: 10.1371/journal.pone.0096213.

[247] Y. Luan *et al.*, “Bacterial interactions with nanostructured surfaces,” *Curr. Opin. Colloid Interface Sci.*, vol. 38, pp. 170–189, 2018, doi: 10.1016/j.cocis.2018.10.007.

[248] W. Yang, Q. Peng, R. Chen, Y. Wen, and B. Shan, “Correlation between Hydrophilicity and Surface Aggregation in Anodized TiO2 Nanotube Arrays,” *Phys. Procedia*, vol. 48, pp. 220–227, Jan. 2013, doi: 10.1016/j.phpro.2013.07.035.

[249] Z.-Y. Luo, K.-X. Chen, D.-C. Mo, and S.-S. Lyu, “A New Route for Surface Modification: Fluorine-Induced Superhydrophilicity,” *J. Phys. Chem. C*, vol. 120, no. 22, pp. 11882–11888, Jun. 2016, doi: 10.1021/acs.jpcc.6b00820.

[250] Z.-Y. Luo, D.-C. Mo, and S.-S. Lyu, “FLUORINE-INDUCED SUPERHYDROPHILIC TIO2 NANOTUBE ARRAYS,” in *Proceedings of the ASME 2016 5th International Conference on Micro/Nanoscale Heat and Mass Transfer MNHMT2016 January 4-6, 2016, Biopolis, Singapore MNHMT2016-6328*, 2016, pp. 4–9.

[251] G. A. Pankey and L. D. Sabath, “Clinical Relevance of Bacteriostatic versus Bactericidal Activity in the Treatment of Gram-Positive Bacterial Infections,” *Clin. Infect. Dis.*, vol. 39, no. 5, pp. 755–756, 2004, doi: 10.1086/422881.

[252] A. Elbourne, J. Chapman, A. Gelmi, D. Cozzolino, R. J. Crawford, and V. K. Truong, “Bacterial-nanostructure interactions: The role of cell elasticity and adhesion forces,” *J. Colloid Interface Sci.*, vol. 546, pp. 192–210, 2019, doi: 10.1016/j.jcis.2019.03.050.

[253] A. Roosjen, H. J. Busscher, W. Norde, and H. C. Van der Mei, “Bacterial factors influencing adhesion of Pseudomonas aeruginosa strains to a poly(ethylene oxide) brush,” *Microbiology*, vol. 152, no. 9, pp. 2673–2682, 2006, doi: 10.1099/mic.0.29005-0.

[254] P. B. J. Vermeltfoort, T. G. Van Kooten, G. M. Bruinsma, A. M. M. Hooymans, H. C. Van Der Mei, and H. J. Busscher, “Bacterial transmission from contact lenses to porcine corneas: An ex vivo study,” *Investig. Ophthalmol. Vis. Sci.*, vol. 46, no. 6, pp. 2042–2046, 2005, doi: 10.1167/iovs.04-1401.

[255] N. Gusnaniar *et al.*, “Physico-chemistry of bacterial transmission versus adhesion,” *Adv. Colloid Interface Sci.*, vol. 250, pp. 15–24, 2017, doi: 10.1016/j.cis.2017.11.002.

[256] G. M. Bruinsma, H. C. Van Der Mei, and H. J. Busscher, “Bacterial adhesion to surface hydrophilic and hydrophobic contact lenses,” *Biomaterials*, vol. 22, no. 24, pp. 3217–3224, 2001, doi: 10.1016/S0142-9612(01)00159-4.

[257] G. Lerebour, S. Cupferman, and M. N. Bellon-Fontaine, “Adhesion of Staphylococcus aureus and Staphylococcus epidermidis to the Episkin® reconstructed epidermis model and to an inert 304 stainless steel substrate,” *J. Appl. Microbiol.*, vol. 97, no. 1, pp. 7–16, 2004, doi: 10.1111/j.1365-2672.2004.02181.x.

[258] O. Habimana, A. J. C. Semião, and E. Casey, “The role of cell-surface interactions in bacterial initial adhesion and consequent biofilm formation on nanofiltration/reverse osmosis membranes,” *J. Memb. Sci.*, vol. 454, pp. 82–96, 2014, doi: 10.1016/j.memsci.2013.11.043.

[259] E. Birkenhauer and S. Neethirajan, “Characterization of electrical surface properties of mono- and co-cultures of Pseudomonas aeruginosa and methicillin-resistant Staphylococcus aureus using Kelvin probe force microscopy,” *RSC Adv.*, vol. 4, no. 80, pp. 42432–42440, 2014, doi: 10.1039/c4ra07446g.

[260] J. Ng, X. Zhang, T. Zhang, J. H. Pan, J. H. A. Du, and D. D. Sun, “Construction of self-organized free-standing TiO2 nanotube arrays for effective disinfection of drinking water,” *J. Chem. Technol. Biotechnol.*, vol. 85, no. 8, pp. 1061–1066, 2010, doi: 10.1002/jctb.2395.

[261] J. Podporska-Carroll, E. Panaitescu, B. Quilty, L. Wang, L. Menon, and S. C. Pillai, “Antimicrobial properties of highly efficient photocatalytic TiO2 nanotubes,” *Appl. Catal. B Environ.*, vol. 176–177, pp. 70–75, 2015, doi: 10.1016/j.apcatb.2015.03.029.

[262] C. M. N. Chan *et al.*, “Antibacterial and photocatalytic activities of TiO2 nanotubes,” *J. Exp. Nanosci.*, vol. 8, no. 6, pp. 695–703, 2013, doi: 10.1080/17458080.2011.616540.

[263] H. Zhang, S. Komasa, C. Mashimo, T. Sekino, and J. Okazaki, “Effect of ultraviolet treatment on bacterial attachment and osteogenic activity to alkali-treated titanium with nanonetwork structures,” *Int. J. Nanomedicine*, vol. 12, pp. 4633–4646, 2017, doi: 10.2147/IJN.S136273.

[264] A. M. Gallardo-Moreno, M. A. Pacha-Olivenza, M. C. Fernández-Calderón, C. Pérez-Giraldo, J. M. Bruque, and M. L. González-Martín, “Bactericidal behaviour of Ti6Al4V surfaces after exposure to UV-C light,” *Biomaterials*, vol. 31, no. 19, pp. 5159–5168, 2010, doi: 10.1016/j.biomaterials.2010.03.005.

[265] H. Yang, S. Mei, L. Zhao, and Y. Zhang, “Effects of Ultraviolet Irradiation on the Antibacterial Activity of TiO2 Nanotubes,” *Nanosci. Nanotechnol. Lett.*, vol.

8, no. 6, pp. 498–504, Jun. 2016, doi: 10.1166/nnl.2016.2135.

[266] W. Liu *et al.*, “Antibacterial and osteogenic stem cell differentiation properties of photoinduced,” *Nanomedicine*, vol. 10, pp. 713–723, 2015.

[267] M. Motola *et al.*, “UV light-induced photocatalytic, antimicrobial, and antibiofilm performance of anodic TiO 2 nanotube layers prepared on titanium mesh and Ti sputtered on silicon,” *Chem. Pap.*, vol. 73, no. 5, pp. 1163–1172, 2019, doi: 10.1007/s11696-018-0667-4.

[268] Y. Liao *et al.*, “Photocatalytic generation of multiple ROS types using low-temperature crystallized anodic TiO2 nanotube arrays,” *J. Hazard. Mater.*, vol. 260, pp. 434–441, 2013, doi: 10.1016/j.jhazmat.2013.05.047.

[269] B. Del Curto *et al.*, “Decreased bacterial adhesion to surface-treated titanium,” *Int. J. Artif. Organs*, vol. 28, no. 7, pp. 718–730, 2005, doi: 10.1177/039139880502800711.

[270] S. Arango-Santander, A. Pelaez-Vargas, S. C. Freitas, and C. García, “A novel approach to create an antibacterial surface using titanium dioxide and a combination of dip-pen nanolithography and soft lithography,” *Sci. Rep.*, vol. 8, no. 1, pp. 1–10, 2018, doi: 10.1038/s41598-018-34198-w.

[271] M. Li, J. J. Yin, W. G. Wamer, and Y. M. Lo, “Mechanistic characterization of titanium dioxide nanoparticle-induced toxicity using electron spin resonance,” *J. Food Drug Anal.*, vol. 22, no. 1, pp. 76–85, 2014, doi: 10.1016/j.jfda.2014.01.006.

[272] Y. Kakuma, A. Y. Nosaka, and Y. Nosaka, “Difference in TiO2 photocatalytic mechanism between rutile and anatase studied by the detection of active oxygen and surface species in water,” *Phys. Chem. Chem. Phys.*, vol. 17, no. 28, pp. 18691–18698, 2015, doi: 10.1039/c5cp02004b.

[273] Y. Nosaka and A. Y. Nosaka, “Generation and Detection of Reactive Oxygen Species in Photocatalysis,” *Chem. Rev.*, vol. 117, no. 17, pp. 11302–11336, 2017, doi: 10.1021/acs.chemrev.7b00161.

[274] Y. Guo *et al.*, “Detection of reactive oxygen species (ROS) generated by TiO2(R), TiO2(R/A) and TiO2(A) under ultrasonic and solar light irradiation and application in degradation of organic dyes,” *J. Hazard. Mater.*, vol. 192, no. 2, pp. 786–793, 2011, doi: 10.1016/j.jhazmat.2011.05.084.

[275] S. Daviosdóttir, K. Dirscherl, S. Canulescu, R. Shabadi, and R. Ambat, “Nanoscale surface potential imaging of the photocatalytic TiO2 films on aluminum,” *RSC Adv.*, vol. 3, no. 45, pp. 23296–23302, 2013, doi: 10.1039/c3ra43082k.

[276] A. Lipovsky, L. Levitski, Z. Tzitrinovich, A. Gedanken, and R. Lubart, “The different behavior of rutile and anatase nanoparticles in forming oxy radicals upon illumination with visible light: An EPR study,” *Photochem. Photobiol.*, vol. 88, no. 1, pp. 14–20, 2012, doi: 10.1111/j.1751-1097.2011.01015.x.

[277] C. M. Bhadra *et al.*, “Antibacterial titanium nano-patterned arrays inspired by dragonfly wings,” *Sci. Rep.*, vol. 5, no. November, 2015, doi: 10.1038/srep16817.

[278] L. Damiati *et al.*, “Impact of surface topography and coating on osteogenesis and bacterial attachment on titanium implants,” *J. Tissue Eng.*, vol. 9, 2018, doi: 10.1177/2041731418790694.

[279] L. C. Hsu, J. Fang, D. A. Borca-Tasciuc, R. W. Worobo, and C. I. Moraru, “Effect of Micro- and Nanoscale Topography on the Adhesion of Bacterial Cells to Solid Surfaces,” *Appl. Environ. Microbiol.*, vol. 79, no. 8, pp. 2703–2712, 2013, doi: 10.1128/aem.03436-12.

[280] E. P. Ivanova *et al.*, “Differential attraction and repulsion of Staphylococcus aureus and Pseudomonas aeruginosa on molecularly smooth titanium films,” *Sci. Rep.*, vol. 1, pp. 1–8, 2011, doi: 10.1038/srep00165.

[281] E. P. Ivanova *et al.*, “Impact of nanoscale roughness of titanium thin film surfaces on bacterial Retention,” *Langmuir*, vol. 26, no. 3, pp. 1973–1982, 2010, doi: 10.1021/la902623c.

[282] V. K. Truong *et al.*, “The influence of nano-scale surface roughness on bacterial adhesion to ultrafine-grained titanium,” *Biomaterials*, vol. 31, no. 13, pp. 3674–3683, 2010, doi: 10.1016/j.biomaterials.2010.01.071.

[283] S. Lavenus, P. Pilet, J. Guicheux, P. Weiss, G. Louarn, and P. Layrolle, “Behaviour of mesenchymal stem cells, fibroblasts and osteoblasts on smooth surfaces,” *Acta Biomater.*, vol. 7, no. 4, pp. 1525–1534, 2011, doi: 10.1016/j.actbio.2010.12.033.

[284] R. Fu *et al.*, “Spreading area and shape regulate apoptosis and differentiation of osteoblasts,” *Biomed. Mater.*, vol. 8, no. 5, 2013, doi: 10.1088/1748-6041/8/5/055005.

[285] S. Lavenus, M. Berreur, V. Trichet, P. Pilet, G. Louarn, and P. Layrolle, “Adhesion and osteogenic differentiation of human mesenchymal stem cells on titanium nanopores,” *Eur. Cells Mater.*, vol. 22, no. 0, pp. 84–96, 2011, doi: 10.22203/eCM.v022a07.

[286] R. M. do Nascimento *et al.*, “Optimized-Surface Wettability: A New Experimental 3D Modeling Approach Predicting Favorable Biomaterial–Cell Interactions,” *Adv. Theory Simulations*, vol. 2, no. 7, p. 1900079, 2019, doi: 10.1002/adts.201900079.

[287] A. Obata, T. Ogasawara, and T. Kasuga, “Combinatorial effects of inorganic ions on adhesion and proliferation of osteoblast-like cells,” *J. Biomed. Mater. Res. - Part A*, vol. 107, no. 5, pp. 1042–1051, 2019, doi: 10.1002/jbm.a.36623.

[288] K. S. Brammer, C. J. Frandsen, and S. Jin, “TiO 2 nanotubes for bone regeneration,” *Trends Biotechnol.*, vol. 30, no. 6, pp. 315–322, 2012, doi: 10.1016/j.tibtech.2012.02.005.

[289] M. Kulkarni *et al.*, “Titanium nanostructures for biomedical applications,” *Nanotechnology*, vol. 26, no. April 2016, pp. 62002 (1–18), 2015, doi: 10.1088/0957-4484/26/6/062002.

[290] E. Gongadze *et al.*, “Adhesion of osteoblasts to a nanorough titanium implant surface.,” *Int. J. Nanomedicine*, vol. 6, pp. 1801–1816, 2011, doi: 10.2147/IJN.S21755.

[291] C. Wang, C. Qiao, W. Song, and H. Sun, “Ultrafast Spreading Effect Induced Rapid Cell Trapping into Porous Scaffold with Superhydrophilic Surface,” *ACS Appl. Mater. Interfaces*, vol. 7, no. 32, pp. 17545–17551, 2015, doi: 10.1021/acsami.5b04009.

[292] Y. H. Wang, Y. Liu, P. Maye, and D. W. Rowe, “Examination of mineralized nodule formation in living osteoblastic cultures using fluorescent dyes,” *Biotechnol. Prog.*, vol. 22, no. 6, pp. 1697–1701, 2006, doi: 10.1021/bp060274b.

[293] M. Nakamura *et al.*, “Surface electric fields increase osteoblast adhesion through improved wettability on hydroxyapatite electret,” *ACS Appl. Mater. Interfaces*, vol. 1, no. 10, pp. 2181–2189, 2009, doi: 10.1021/am900341v.

[294] M. Kulkarni *et al.*, “Protein interactions with layers of TiO2 nanotube and nanopore arrays: Morphology and surface charge influence,” *Acta Biomater.*, vol. 45, pp. 357–366, 2016, doi: 10.1016/j.actbio.2016.08.050.

[295] L. Zhang, J. Shao, and Y. Han, “Ultraviolet-enhanced wettability and bioactivity of self-organized TiO 2 nanotube layer,” *J. Nanosci. Nanotechnol.*, vol. 11, no. 12, pp. 10908–10912, 2011, doi: 10.1166/jnn.2011.3941.

[296] L. Zhao, S. Mei, W. Wang, P. K. Chu, Z. Wu, and Y. Zhang, “The role of sterilization in the cytocompatibility of titania nanotubes,” *Biomaterials*, vol. 31, no. 8, pp. 2055–2063, 2010, doi: 10.1016/j.biomaterials.2009.11.103.

[297] J. Wu, L. Zhou, X. Ding, Y. Gao, and X. Liu, “Biological Effect of Ultraviolet Photocatalysis on Nanoscale Titanium with a Focus on Physicochemical Mechanism,” *Langmuir*, vol. 31, no. 36, pp. 10037–10046, 2015, doi: 10.1021/acs.langmuir.5b01850.

[298] L. Chu *et al.*, “Preferential colonization of osteoblasts over co-cultured bacteria on a bifunctional biomaterial surface,” *Front. Microbiol.*, vol. 9, no. OCT, pp. 1–13, 2018, doi: 10.3389/fmicb.2018.02219.

[299] G. Subbiahdoss, R. Kuijer, D. W. Grijpma, H. C. van der Mei, and H. J. Busscher, “Microbial biofilm growth vs. tissue integration: ‘The race for the surface’ experimentally studied,” *Acta Biomater.*, vol. 5, no. 5, pp. 1399–1404, 2009, doi: 10.1016/j.actbio.2008.12.011.

[300] J. W. Lee, K. B. Lee, H. S. Jeon, and H. K. Park, “Effects of surface Nano-Topography on human osteoblast filopodia,” *Anal. Sci.*, vol. 27, no. 4, pp. 369–374, 2011, doi: 10.2116/analsci.27.369.

[301] J. Albuschies and V. Vogel, “The role of filopodia in the recognition of nanotopographies,” *Sci. Rep.*, vol. 3, 2013, doi: 10.1038/srep01658.

[302] H. C. Blair *et al.*, “Osteoblast differentiation and bone matrix formation in vivo and in vitro,” *Tissue Eng. - Part B Rev.*, vol. 23, no. 3, pp. 268–280, 2017, doi: 10.1089/ten.teb.2016.0454.

[303] J. Y. Lim, M. C. Shaughnessy, Z. Zhou, H. Noh, E. A. Vogler, and H. J. Donahue, “Surface energy effects on osteoblast spatial growth and mineralization,” *Biomaterials*, vol. 29, no. 12, pp. 1776–1784, 2008, doi: 10.1016/j.biomaterials.2007.12.026.

[304] A. Bassi, J. Gough, M. Zakikhani, and S. Downes, “Bone tissue regeneration,” in *Electrospinning for Tissue Regeneration*, 2011, pp. 93–110.

[305] N. J. Hickok and I. M. Shapiro, “Immobilized antibiotics to prevent orthopaedic implant infections,” *Adv. Drug Deliv. Rev.*, vol. 64, no. 12, pp. 1165–1176, 2012, doi: 10.1016/j.addr.2012.03.015.

[306] R. Pokrowiecki *et al.*, “In vitro studies of nanosilver-doped titanium implants for oral and maxillofacial surgery,” *Int. J. Nanomedicine*, vol. 12, pp. 4285–4297, 2017, doi: 10.2147/IJN.S131163.

[307] E. P. Su *et al.*, “Effects of titanium nanotubes on the osseointegration, cell differentiation, mineralisation and antibacterial properties of orthopaedic implant surfaces,” *Bone Jt. J.*, vol. 100B, no. 1, pp. 9–16, 2018, doi: 10.1302/0301-620X.100B1.BJJ-2017-0551.R1.

[308] K. Bartlet, S. Movafaghi, L. P. Dasi, A. K. Kota, and K. C. Popat, “Antibacterial activity on superhydrophobic titania nanotube arrays,” *Colloids Surfaces B Biointerfaces*, vol. 166, pp. 179–186, 2018, doi: 10.1016/j.colsurfb.2018.03.019.

[309] M. Y. Lan, C. P. Liu, H. H. Huang, and S. W. Lee, “Both Enhanced Biocompatibility and Antibacterial Activity in Ag-Decorated TiO2 Nanotubes,” *PLoS One*, vol. 8, no. 10, pp. 4–11, 2013, doi: 10.1371/journal.pone.0075364.

[310] H. Zhu, Z. Guo, and W. Liu, “Adhesion behaviors on superhydrophobic surfaces,” *Chem. Commun.*, vol. 50, no. 30, pp. 3900–3913, 2014, doi: 10.1039/c3cc47818a.

[311] S. M. Oliveira, W. Song, N. M. Alves, and J. F. Mano, “Chemical modification of bioinspired superhydrophobic polystyrene surfaces to control cell attachment/proliferation,” *Soft Matter*, vol. 7, no. 19, pp. 8932–8941, Oct. 2011, doi: 10.1039/c1sm05943b.